Gold Nanoparticle Synthesis for Surface Enhanced Raman Spectroscopically Active Substrate

by

Tim Wei-Ting Chen

A thesis
presented to the University of Waterloo
in fulfillment of the
thesis requirement for the degree of
Master of Applied Science
in
Chemical Engineering

Waterloo, Ontario, Canada, 2010

I hereby declare that I am the sole author of this thesis. This is a true copy of the thesis, including any required final revisions, as accepted by my examiners.

I understand that my thesis may be made electronically available to the public.

Abstract

Large and small nanospheres, large and small nanoplates, nanorods and nanostars have been synthesized and fabricated into SERS substrates consisting of sandwiched and aggregated structure. Using 633 nm laser as excitation, individual SERS spectra of each labeling molecules, benzenethiol, 4-nitrobenzenethiol and 4-quinolinethiol, have been successfully obtained and the combination of these three molecules have the least amount of overlapping and can all be identified from the reference multiplexed spectra. Among all the substrates that have analyzed, the substrate made from nanospheres with sandwiched structure is able to produce multiplexed SERS spectra with more details and higher reproducibility. Although multiplexed SERS spectra can also be observed from substrates made from small nanoplates, nanostars and nanorods substrates with sandwiched structures, the unique peaks representing the labeling molecules are less consistent in their intensity. In addition, substrates with micro sized plates in sandwiched configuration are found to exhibit much lower SERS activities and this can be due to the size of the plate being much greater than the light source, restraining the surface plasmon resonance effect. Most of the substrates fabricated with aggregated nanoparticles have very low reproducibilities and saturated signals with 633 nm excitation. The spectra peaks are much easier to identify and are much more reproducible when 785 nm excitation have been adopted. This can be due to the size of the aggregated nanoparticles are much bulkier which a deeper penetrating light source is required to induce more molecules labels to exhibit SERS activities. A novel SERS substrate has been fabricated with nanoparticle-thiol-microplate sandwiched configuration by using a double ended thiol molecules, benzenedithiol, to strongly connect nanospheres and the plates together. However, the measurement of the SERS activity is limited by the overpowering of the light source, which has frequently melted and evaporated the plate samples once they have been exposed to the excitation radiation. In addition, instead of spreading evenly on the microplate surfaces, the nanoparticles have appeared to be aggregated which may have increased the difficulty in obtaining SERS activity.

Acknowledgements

I would like to thank Curtis Woodford, Eric Jervis, Dale Henneke, Ting Tsui, Shirley Tang, Dale Weber and all the ones who made this project possible.

Dedication

This is dedicated to the ones I love.

Contents

List of Tables

List of Figures

Chapter 1

Introduction

1.1 Notes on Nanotechnology

A nanometer is one billionth of a meter, which is almost the same magnitude as the size of an atom and nanotechnology involves the construction, production or manipulation of materials at a very small scale, usually within a hundred nanometers.[64] At this dimension, objects and matter are invisible to naked eye. Nevertheless, it is hard to ignore the properties that they exhibit are different from their bulk sizes. In recent years, engineers and scientists have been intensely investigated the unique properties that nanomaterials and nanostructures possess. These properties serve as a foundation for developing new applications and devices. Nanotechnology is not only bridging the understanding of a solids' properties from its bulk state to the atomic level, but also revolutionizing how things are being manufactured. Rather than the conventional top-down fabrication technique, engineers and scientists can fabricate materials from the bottom and up. With the ability to construct materials at the atomic level, they can create materials with customized functionality, such as enhanced hardness, plasticity, conductivity, hydrophobicity, reactivity or even reflectivity. Compared to microtechnology, nanotechnology is far more versatile. It not only can be adapted to the traditional electrical and semiconductor sectors but also has also found a place in the optical and biotechnology industries. For instance, a growing number of studies have emerged from biotechnology laboratories claiming the use of gold nanoparticles as biosensoers and drug carriers. The establishment of nanotechnology fundamentals for medical and biological applications cannot be overlooked when considering

their potential to treat diseases. Nevertheless, due to the complexity of the technology, there are still limits that prevent these ideas from being transformed into practice. A tremendous amount of time and effort are still required to overcome the barriers.

1.2 Fabrication of Nanomaterials and Nanoparticles

The fabrication of nanoparticles can generally be divided into two main categories: top-down and bottom-up approaches. Top-down fabrication usually involves reducing bulk size materials into nanomaterials by the means of physical, chemical and mechanical processes. On the other hand, the bottom-up approaches consist of constructing materials starting from the atomic level. Some examples of the top-down and bottom-up fabrication methods are enlisted in Table 1.1 and 1.2, respectively. It is not uncommon to have a manufacturing process that involves both top-down and bottom-up fabrication, such as the coating of nanofilms which usually involves evaporation of melted bulk metal and condensation of the gaseous metal on a substrate. In order to fabricate materials that retain a set of functionalities, the bottom-up fabrication techniques are usually implemented; for instances, a majority of biological nanomaterials are made from the bottom up approaches since their functionalities are made to adapt to the complexity of the living environment. Lithography is a major top-down fabrication method that has been widely applied in the high-tech industries. It generally involves processes such as depositing, masking, etching and stripping to create fine patterns on a flat semiconductor substrate.[30] However, due to the trend of shrinking product sizes, top-down lithography fabrication techniques are beginning to face technical challenges raised by the small size effect. Therefore, the advancement in bottom-up lithography methods is slowly taking over the current status of the top-down lithography fabrications. Lithography itself is a fabrication process that can be further classified into many subcategories, but due to the scope of this study, it is not listed.

Table 1.1: Top-Down Fabrication Methods.[30]

Mechanical	Thermal	High Energy	Chemical
Ball Milling	Annealing	Arc Discharge	Chemical Etching
Rolling/Beating	Electrospinning	Laser Ablation	Chemical-Mechanical Polishing
Extrusion	Electrohydrodynamic Atomization	Solar Energy Vaporization	Electropolishing
Mechanical Machining	Sublimation	RF Sputtering	Anodizing
Compaction	Template Synthesis Evaporation	Electron Beam Evaporation	Combustion
Atomization	Evaporation	Reactive Ion Etching	
	Chill Block Melt Spinning	Pyrolysis	
	Liquid Dynamic Compaction	High-Energy Sonication	
	Combustion	Ion Milling	
	Thermolysis and pyrolysis		
	Carbonization of Copolymers		

Table 1.2: Bottom-Up Fabrication Methods.[30]

Gas-Phase	Nonbiological Liquid Phase	Biological and Inorganic
Chemical Vapor Deposition	Molecular Self-Assembly	Protein Synthesis
Atomic Layer Deposition	Supramolecular Chemistry	Nucleic Acid Synthesis
Combustion	Nucleation and Sol-Gel Processes	Membrane Syntehsis
Thermolysis and Pyrolysis	Reduction of Metal Salts	Inorganic Biological Structures
Molecular Beam Epitaxy	Single Crystal Growth	Crystal Formation Methods
Ion Implantation	Electrodeposition Electroplating	
Gas Phase Condensation	Electroless Deposition	
Solid Template Synthesis	Anodizing	
MOCVD	Electrolysis in Molten Salt Solution	
	Solid Template Synthesis	
	Liquid Template Synthesis	
	Super Critial Fluid Expansion	

1.3 Properties of Nanoparticles

1.3.1 High Surface to Volume Ratio

One of the main focuses of nanotechnology is to synthesize metal and semiconductor nanoparticles, then observe their physical nature, such as the shape, volume and surface area. In general, a high surface to volume ratio is one of the physical properties that is found in nanoparticles. Assuming a spherical nanoparticle, its surface to volume ratio can be derived as:

$$\frac{S}{V} = \frac{4\pi r^2}{\frac{4}{3}\pi r^3} = \frac{3}{r} \tag{1.1}$$

where S is the surface area of the nanoparticle, V is its volume and r is the particle radius. From this relationship, it can be observed that the surface to volume ratio can increase significantly as the radius of the nanoparticle decreases, as shown in Figure 1.1. A larger surface areas leads to an increase in the interactions with other materials and this can have a great impact on applications where surface area is of great importance, such as catalysis and electroplating. According to Ichinose et al., 1 cm^3 of 1 nm particles can

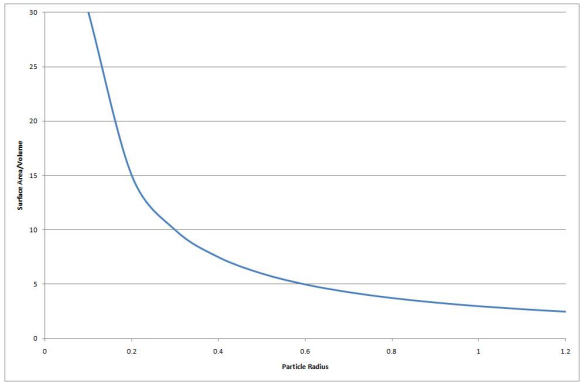

Figure 1.1: The variation of a spherical particle's surface to volume ratio as the radius increases.

have an estimated of 100 m^2 active surface area.[67] In addition, nanoparticles are gaining attention in biological applications since their large surface to volume ratio are able to provide more loadings for drug delivery.

1.3.2 Surface Energy, Agglomeration and Surfactants

The lotus effect is one of the most famous surface energy phenomena in nature. A lotus leaf's has millions of nanostructures that are low in surface energy. These structures make the surface water repellent, causing the water droplets to remove dirt and other debris as they roll off the leaf.[30] This self-cleaning mechanism has lead to extensive research and many industrial products have been developed utilizing this principle, such as self-cleaning paint, waterproof films and coatings.

The particle's surface energy is dependent on the increase of surface area and the decrease of radius. A bulk material's surface is usually made of two to three layers of atoms and since these surface atoms are exposing to the atmosphere, they usually have fewer bonding neighboring atoms. According to thermodynamic principles, the atoms at the outer layers would have less boundary to hold off energy from the inner atoms and would exhibit lower stability and hence, the surface energy increases as the particle becomes smaller.[30] As a particle becomes smaller in size, an increase of its surface energy has an effect on several physical properties such as wettability and melting points.[56, 31]

In addition, high surface energies induce instability in nanoparticles; in order to achieve the minimum energy state, nanoparticles have a tendency to fuse together. This phenomenon is known as agglomeration. In general, high energy nanoparticle surfaces can be stabilized by electrostatic, chemisorption and steric stabilization processes, which can create physical and chemical barriers on the particle's surface.

Agglomeration of nanoparticles is a subject widely studied by scientists and engineers. In many cases, it is overcome by introducing a capping agent during the synthesis of nanoparticles. The capping agents are usually chemical substances that can minimize the surface energy of phase boundaries. Often these capping agents are surfactants. Surfactants consists of a polar or ionic hydrophilic end which interacts strongly with aqueous phases and a nonpolar hydrophobic portion that interacts strongly with organic phases. In systems where the concentration of the surfactant is over the critical micelle concentration, the surfactants may aggregate and self-assemble, forming membrane like micelle layers. This effect can influence the nanoparticle's functionality. Surfactants are commonly used to modify the interfacial tension of two or multi phase systems and have a wide range of industrial applications, such as detergents, emulsifier, paints, adhesives, cosmetics, plastics and pharmaceuticals. One of main reasons that surfactants are introduced in the synthesis of nanoparticles is to create 'caps' around the particles to prevent newly formed nanoparticles from fusing together. These 'capped' nanoparticles may still attract each other forming island like structures with a steric barrier preventing the nanoparticle surfacs from contacting. This phenomenon is known as flocculation.

1.3.3 Quantum Confinement Effect and Surface Plasmon Resonance

A bulk metal particle normally has a tight filling of electrons where its valence and conduction bands may overlap each other, forming a continuous-like electron shell packing. As the particle is reduced in size, particularly to the nanoscale regime, the motion of the electrons surrounding itself are being constrained by the quantum confinement effect, so the energy bandgap between the highest valence band and the lowest conduction band becomes wider, transforming the electronic energy levels to a discrete state. As a result, the particle's electrical and optical properties deviate, corresponding to the particle's size.[7] With a bigger increase of the energy level bandgap, smaller nanoparticles are able to absorb higher energy

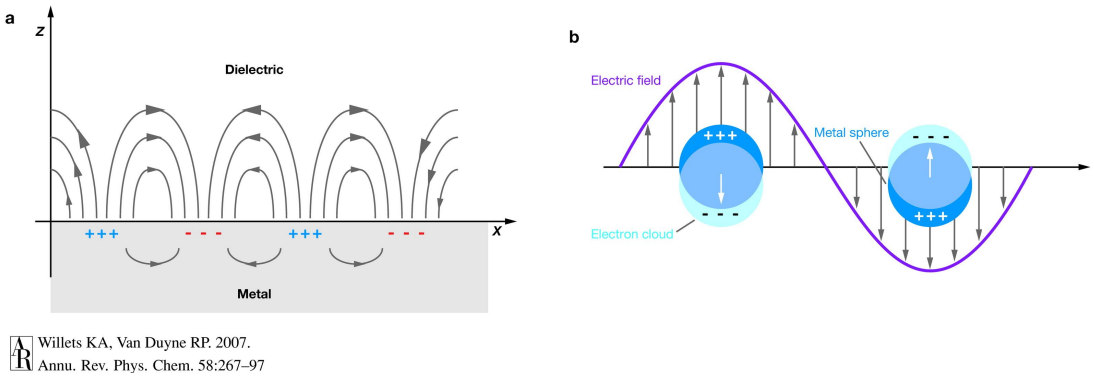

Willets KA, Van Duyne RP. 2007.
Annu. Rev. Phys. Chem. 58:267–97

Figure 1.2: Surface plasmon resonance behavior on a flat surface and around metal nanospheres.[87]

and fluoresce at a lower wavelength, causing a blue-shift to the nanoparticles. In contrast, a red-shift occurs with larger nanopaticles, since they have a lower increase of the energy bandgaps. This makes them more capable of absorbing lower energy and fluorescing at a higher wavelength.[30] The optical properties of nanoparticles are important to many industrial applications; for example, sensors, lasers, pigments, and optical filters.

Surface plasmon resonance is associated with the excitation of a metal surface by electromagnetic radiation or light waves forming a collective of conduction electrons coherently oscillating and propagating between the interface of the dielectric and conductive medium. A similar phenomenon can be observed at a narrower scope; where a high magnitude radiation interacts with particles that are much smaller in dimension, leads to the formation of localized surface resonance, as shown in Figure 1.2.[30, 87] Upon exposure of electromagnetic radiation, the particle creates a polarized field oscillating locally around the particles, resulting in an internal depolarization field. Once the frequency of the incident radiation is coherent with the oscillating conduction electrons, a strong absorption of the optical spectrum results. In addition, a complex phenomenon known as light scattering also arises when the radiation interacts with the particle. Localized surface plasmon resonance is a useful property for tuning the optical properties of metal nanoparticles. This dependents on their dielectric constant, size, shape, orientation, and the surrounding medium. The phenomenon plays a key role in developing optical applications such as plasmonics and Surface Enhanced Raman Spectroscopy (SERS).

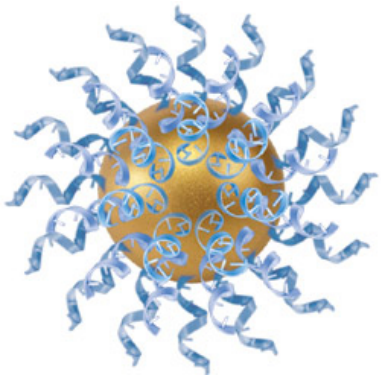

Figure 1.3: A illustrative sample of a gold sphere attached with thiol molecules.[59]

1.4 The Choice of Gold

For a long time, gold has been known to be inert in the human body. It is widely used in cosmetics, dental fillings and medicines. In recent nanotechnology development, gold nanoparticles have been extensively studied due to their potential of becoming next generation drug carriers and biosensors. Many of the studies have proposed using chemical synthesis strategies, such as nucleation in sol-gels and the reduction of salt metal ions in surfactant mediums, to tailor the size and shape of the gold nanoparticles while examining the particle's practical application value. Aside from the properties that have been mentioned in the last section, gold nanoparticles have a natural affinity to sulphur bonds, which allows sulphur containing compounds, such as thiols, to bind and form self assembled monolayers on their surfaces, as shown in Figure 1.3. Once the thiol groups are attached to the gold surface, the terminal ends of the thiols can be modified to assign the nanoparticle's functionality, such as connecting drug molecules or acting as anchors to connect to proteins. Other than being drug carriers, the gold nanoparticles can also be great candidates for biosensor applications due to their metallic nature. The surface plasmon resonance exhibited from the nanoparticles is one of the key properties in determining the particles' optical and electrical behavior, which allows the particles to be detectable by optical probes based on the phenomenon, such as fluorescence and SERS. The detection of gold nanoparticles by using such probes not only can detect where the location of the nanoparticles are, but also gather information such as the vibrational modes and light scattering wavelength from the bonds of the labeling molecules to the gold surfaces. When the

labeled particle is exposed to radiation, each labeling molecule has its unique set of Raman signals due to the differences in the structure and vibration modes of the labeling molecules that can cause the incident light to scatter at different frequencies. Therefore, SERS detection is capable of detecting multiple labels at one time because there are distinctive signal outputs. Compared to the other labeling detection techniques, the main advantages of SERS are its non-destructive nature, the degree of sensitivity, the functionality from visible to near-infrared region and the ability of multiplexing capacity; as a result, SERS is one of the sensor techniques widely studied in the biotechnology industry and the number of publications related to SERS has grown rapidly over the years.

1.5 Brief History of the Project

Since 2008, the Jervis Lab from the University of Waterloo has outlined an investigation on tracking stem cells in body tissues. The preliminary experimental technique involves the combinatorial methods of Woodford et al., which is approached by attaching stem cell morphogens and extracellular matrix proteins to 5 um microspheres containing biomolcular labels and mixed in random.[88] As the cell culture progressed, the cells would interact with the biomolecules on the microspheres and be stained with those biomarkers at the end of the culture. Once labeled, the cells' spatial position and the biomolecules that they interacted with can be determined through fluorescence imaging. Nevertheless, there are limitations for this labeling technique due to the excess cost and complexity, the limitation of multiple labels that can be applied at once and the fluorescence based detection techniques can interfere cell staining at the end of the culture. These constrains are then overshadowed by the methods published by Fenniri et al., who have published a series of paper that mentioned the development of 630 combinations of bar codes with polystrene copolymer microbeads and with the use of Raman spectroscopy. The encoding of such methods are distinctive and simple because the code combination can be generated from the same labeling molecules in variant molecular structures. However, the downside of the methodology is its slow acquisition process, which may take up to 30 minutes to acquire the signals from each spot. As a results, SERS with gold nanoparticles has emerged to have the highest potential for purpose of detecting cells with multiplexed labels. Since compared to the conventional Raman spectroscopy, surfaced enhanced Raman spectroscopy not only can provide shorter spectrum acquisition time and higher spectra intensity outputs but

also have a lower impact on the sample during detection. Nevertheless, SERS is reported to be less consistent due to the high dependency on the construction of the substrates, such as surface roughness and spacings between the particles.

1.6 Overview and Objectives

Among all the synthesis routes, reduction of gold ions in surfactant mediums is the one of the most reported methods to synthesize gold nanoparticles for SERS application. Based on similar mechanisms but with different environment condition, solvents, surfactants and reducing agents, the synthesis is able to customize nanoparticles to achieve the required size, shape and functionality. The synthetic route is also accustomed to modifications, such as additional growing steps and separation processes, to obtain a more uniform and higher yield production. In this report, gold nanoparticles, nanorods, nanoplates and nanostars are synthesized due to their vast publicity. Once synthesized, the particles are characterized by the transmitted electron microscope and the scanning electron microscope to evaluate the production consistency of the synthesis. Then, the gold nanoparticles are employed in the sandwiched construction of the gold nanoparticle-thiol-gold layers for SERS measurement. Multiplexing ability of the thiol labels are also investigated while investigating the effect of the shapes and sizes of gold nanoparticles on the sandwiched SERS substrate. At last, the potential for the application of a portable SERS substrate consisted of gold nanoparticle-thiol-gold plates is evaluated. A summary of the proposed objectives for this report are:

- To synthesize and characterize gold nanoparticles with different sizes and shapes
- To assemble gold nanoparticles onto gold coated substrates decorated with thiol labels and form sandwiched structure consisting of gold particles-thiol-gold layers
- To obtain and analyze SERS activities from each of the sandwiched substrates and evaluate multiplexing capabilities
- To evaluate SERS activities obtained from sandwiched substrates consisting of gold particles-thiol-gold nanoplates

Chapter 2

Background

2.1 Raman Spectroscopy

Light scattering is a natural physical phenomenon that when an incident light interacts with the medium that it passes through, it forces a change in energy state or a deviation in trajectory between the excitation light and the scattered light. A majority of light scattering process is in a form of elastic scattering where the incident photons are redirected but their energy is conserved. Mie and Rayleigh scattering are often referred to elastic scattering processes that occur in a medium consisting of particles that are on the order of the same magnitude or smaller than the wavelength of the incident light, respectively. Raman scattering is an inelastic scattering process that energy transfer occurs during the interaction of the incident radiation and molecules in a medium, causing the scattered photons to shift in frequency. The process of phenomenon was first reported by C.V. Raman and K.S. Krishnan in 1928. Two years later, Raman was awarded the Nobel Prize in Chemistry and the effect was named after him in honor of his contribution.[78, 30] Analytical instruments rely primarily on the inelastic scattering process to gather sample information such as vibrational modes of molecular bonds. However, compared to Rayleigh scattering, the phenomenon of Raman scattering have weak natural occurrences since only approximately 1 in 10^6-10^8 of the scattered photons possesses Raman effect, making it hard to observe without the use of steady and powerful light sources and sensitive detectors. Despite the fact that Raman spectroscopy has low reliability in the early days, modern instrumentation has greatly enhanced the detection efficiency of Raman effects and Raman analysis

has evolved into various types, such as SERS, transmission Raman, resonance Raman and polarized Raman. Table 2.1 shown is a few examples of various Raman spectroscopy techniques that are being developed. Utilization of these Raman spectrometer techniques is

Table 2.1: Examples of various types of Raman spectroscopy.

Type	Description
SERS	Typically studied with silver and gold colloids or substrates. Once the surface plasmons of the silver and gold are excited by an incident light, the electric fields surrounding the metal increases. Raman intensities are proportional to the electric field and the magnitude of enhancement can be up to 10^{11}.
Resonance Raman Scattering	The vibrational modes corresponding to the excited electronic state can be enhanced by matching the excitation wavelength with the electronic transition state of the molecules and crystals.
Coherent Anti-Stokes Raman Scattering	A technique that uses two incident light beams to generate a coherent anti-Stokes frequency beam and can be enhanced by resonance.
Surface-Enhanced Resonance Raman Spectroscopy	A combination of SERS and resonance Raman spectroscopy technique to produce intense Raman signals from a substrate surface and usually, the excitation wavelength is matched with maximum absorbance of the analyte.
Transmission Raman	A technique that can be used to analyze significant bulk of a turbid material, such as powders, capsules and living tissues. Has a great application potential be used in medical diagnostics.

growing rapidly in the field of chemical engineering, pharmaceuticals, forensic applications, material sciences, semiconductor sectors and environmental studies.

2.1.1 Raman Scattering Process

Light scattering process is dependent on the interaction of the incident electromagnetic waves with a sample's molecular structures or bonds. When an incident electromagnetic wave with electrical vector $\overline{E}$ interacts with molecular with molecular polarizability α, it induces a dipole moment around the molecule and the strength of the induced electric dipole moment can be represented as:

$$P = \alpha \overline{E} \tag{2.1}$$

The strength of the electric field of the incident electromagnetic wave can be expressed as,

$$\overline{E} = E_0 cos(2\pi\nu_0 t) \tag{2.2}$$

where E_0 is the maximum amplitude of the electric field and ν_0 is the frequency of the incident electromagnetic wave and by substituting Equation 2.2 into Equation 2.1 forms,

$$P = \alpha E_0 cos(2\pi\nu_0 t) \tag{2.3}$$

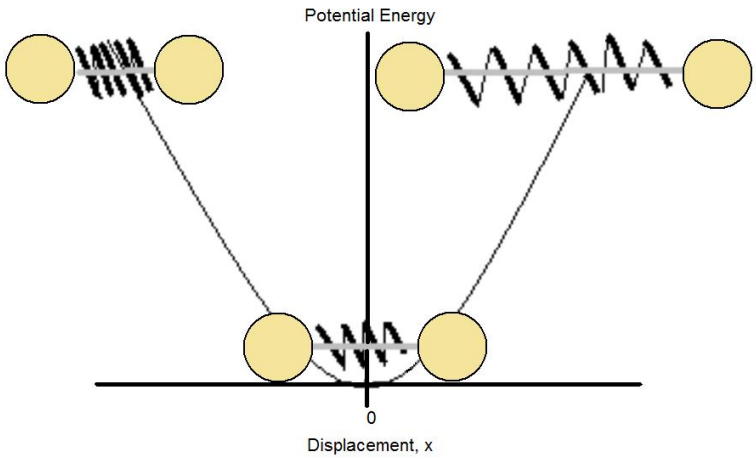

Figure 2.1: A schematic showing oscillation motion of two atoms about equilibrium and the respective potential energy at expansion and compression.[86]

The equation describes that the induced dipole moment is time-dependent and it coincides with the polarizability of the electron clouds from the molecular stretch, which varies with the instantaneous movement and displacement position of constituent atoms. Consider the simplest model of vibrational movements for diatomic molecules, where two atoms are connected by stretchable molecular bonds that behave as springs, as shown in Figure 2.1 When the bond between the atoms is stretched and released, the two atoms will oscillate about their average separation distance and reach for their equilibrium. The frequency of this oscillation can be described as,

$$\nu_{vib} = \frac{1}{2\pi}\sqrt{\frac{k}{\mu}} \tag{2.4}$$

where k, the force constant, denotes the stiffness of the bond and μ is the reduced mass of harmonic oscillator. However, from a quantum mechanics perspective, the simplest form to approximate the vibrational energy of diatomic molecules is the quantum harmonic oscillator function:

$$E_{vib} = (j + 1/2)h\nu_{vib} \tag{2.5}$$

where j is the vibrational quantum number and h is the Planck constant. The equation refers to a model of potential well for diatomic molecules that is divided into discrete energy levels and for each of the energy level, a vibrational quantum number is given

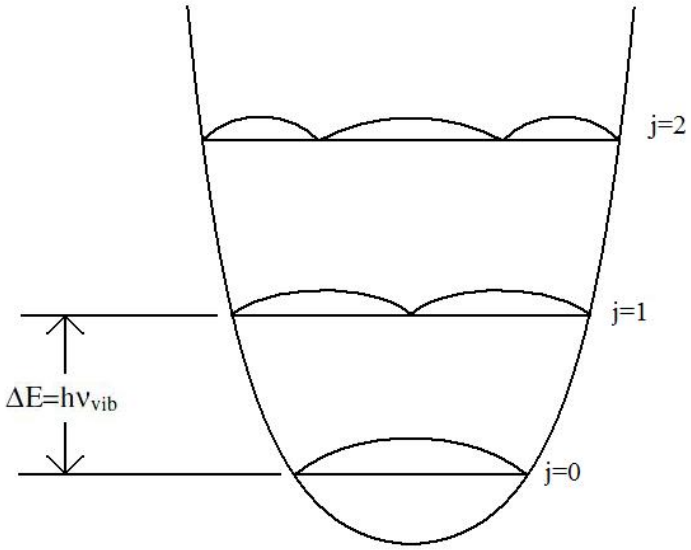

Figure 2.2: A representation of discrete energy levels from a potential well.

as a reference, as shown in Figure 2.2. At low to moderate temperatures, a majority of atoms will vibrate at the ground level or zero-point energy state and the probability of finding atoms vibrating at other energy levels is governed by the Boltzmann distribution. Throughout all the energy levels, the molecules are vibrating in a harmonic motion at the fundamental frequency, ν_{vib}, and a difference in one quantum number is equivalent to the shift of energy state to the next adjacent level, where $\Delta E_{vib} = h\nu_{vib}$. For atoms vibrating at a particular energy level, the instantaneous vibrational displacement of atoms about their equilibrium position can be written as,

$$dQ = Q_0 cos(2\pi\nu_{vib}t) \tag{2.6}$$

where Q_0 is the amplitude of the atoms' maximum displacement from their equilibrium position. However, since the distance of vibrational displacement is usually very small for typical diatomic molecular bonds, their polarizability can be approximated by using the Taylor series expansion,

$$\alpha = \alpha_0 + \frac{\partial\alpha}{\partial Q}dQ \tag{2.7}$$

where α_0 is the polarizability of molecular stretch at the equilibrium position and the instantaneous displacement of atoms, dQ, can be substituted with Equation 2.6 to obtain:

$$\alpha = \alpha_0 + \frac{\partial \alpha}{\partial Q} Q_0 cos(2\pi \nu_{vib} t) \tag{2.8}$$

and Equation 2.8 can be further substituted into Equation 2.3 to yield,

$$P = \alpha_0 E_0 cos(2\pi \nu_0 t) + \frac{\partial \alpha}{\partial Q} Q_0 E_0 cos(2\pi \nu_0 t) cos(2\pi \nu_{vib} t) \tag{2.9}$$

By using the trigonometry relationship, the equation can be expanded to:

$$P = \alpha_0 E_0 cos(2\pi \nu_0 t) + \left(\frac{\partial \alpha}{\partial Q} \frac{Q_0 E_0}{2} \right) \{ cos\left[2\pi(\nu_0 - \nu_{vib})t\right] + cos\left[2\pi(\nu_0 + \nu_{vib})t\right] \} \tag{2.10}$$

From the observation of the equation indicates that the vibrational displacement of atoms corresponds to the poliarizability of the system and in oder for light scattering to occur, the term $\partial\alpha/\partial Q$ must be non-zero. In addition, the induced dipole moment of a molecular bond is produced at three different frequencies, namely ν_0, $(\nu_0 - \nu_{vib})$ and $(\nu_0 + \nu_{vib})$, and from which the effects of Rayleigh, Stokes and anti-Stokes scattering are observed, respectively.

Figure 2.3 shown is a simple illustration of incident light interacts with a molecule in between gold nanoparticles and produces scattering light at different frequencies. An interpretation of this effect is that during the interaction of the incident radiation with the molecular bonds, it induces a dipole moment where the molecular system is excited from the ground state to an energy level that is much higher than any particular vibrational energy levels, known as the virtual energy state. Once relaxed, the molecules will simultaneously undergo either the elastical Rayleigh scattering effect or the inelastical Raman scattering effect, which can be further divided into the Stokes and anti-Stokes scattering. For a population of molecules, a majority of them are expected to experience Rayleigh scattering effects, where the molecules are dropped back down to the original energy state and emit photon energy that have the same magnitude and frequency as the incident radiation. Nevertheless, the remaining molecules may endure a transfer of energy either in and out of the incident radiation, making them to emit light at different frequencies and end up resting at an energy level different from their initial state, as shown in Figure 2.4. Stokes scattering occurs when the molecule is shifted from the lower energy state to a higher energy state while emitting light that has a lower frequency and longer wavelength than

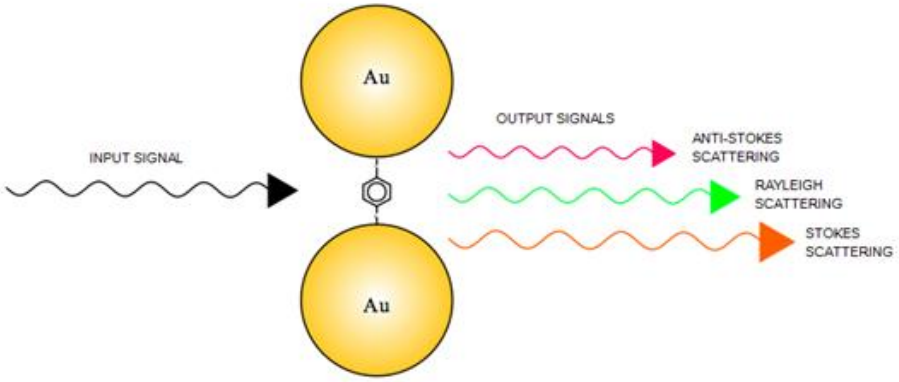

Figure 2.3: The SERS effect and the respective wavelengths of anti-Stokes, Rayleigh and Stokes scattering.

the incident radiation frequency. In contrast, anti-Stokes scattering happens during the shift of molecule from a higher energy state to a lower energy state and emits light that has higher frequency and shorter wavelength than the excitation radiation. Nevertheless, despite the low natural occurrence of Raman scattering, the effect is predominated by the Stokes scattering because according to the Boltzmann distribution from Equation 2.11, the molecules have a higher probably to vibrate at their ground energy state at low to moderate temperatures and are more readily to be promoted to a higher energy state.

$$\frac{I_{Anti-Stokes}}{I_{Stokes}} = \left(\frac{\nu_0 - \nu_{vib}}{\nu_0 + \nu_{vib}}\right)^4 e^{-\frac{h\nu_0}{kT}} \tag{2.11}$$

Therefore, in practice, it is common only the Stokes scattering spectra are recorded for sample analysis since they provide stronger signals.[26]

Fluorescence is another effect which can occur simultaneously with Raman scattering during the interaction of the light and the molecular bonds. Despite having similar origins, Raman scattering and fluorescence are two completely different processes. Fluorescence process involves the excitation of a molecule into the excited state and remains excited for a certain resonance time while enduring inter-molecular process. In the end, it relaxes back to the lower energy levels and emits a photon at longer wavelength than the incident photon. Normally, a photon with low energy is unable to provide enough excitation for the fluorescence effect to occur. However, fluorescence can be problematic if does occur

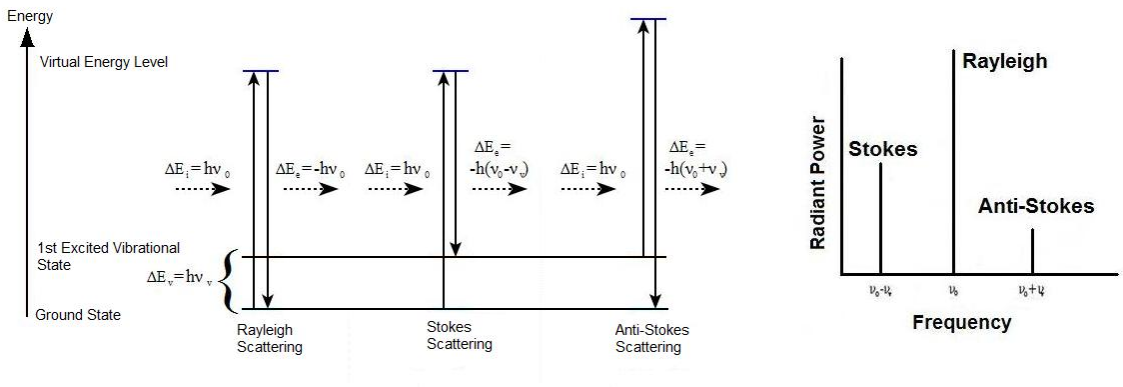

Figure 2.4: The energy states and the occurrence frequency of anti-Stokes, Rayleigh and Stokes scattering

because it is usually very intense and can cause interference with the more informative Raman signals.

2.1.2 Characteristics of Raman Spectroscopy

Infrared and Raman spectroscopy are similar analytical methods that can characterize nanomaterials based on the vibrational, rotational and other low frequency modes of molecular bonds in a system. However, the detection of the infrared methods are based on asymmetrical(dipolar) vibrational modes mechanisms and in contrast, Raman methods rely on symmetrical(polarizable) vibration modes. In general, the information obtained from the two methods are complementary to each other.[30] Nevertheless, utilization of Raman spectroscopies offers a number of advantages. For instance, the analysis can be done without any direct contact to liquid, solid or gaseous samples and requires only the minimal preparation. The spectroscopy also holds a key advantage for the analysis of biological materials, where water is a good solvent to use for the spectroscopy because it is a weak scatterer and does not perturb with other species in aqueous systems. Moreover, the spectroscopy can be utilized with low power light sources, ranging from visible to near-infrared regimes, which are cheaper and safer to operate and are less harmful on the samples.

One of the biggest drawbacks of Raman spectroscopy is its weakness in signal detection.

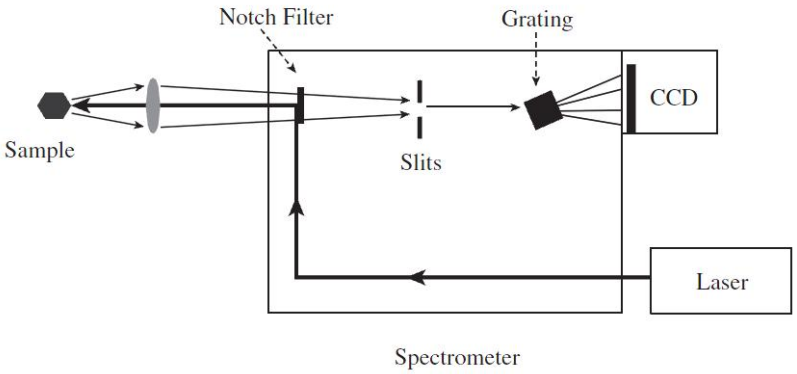

Figure 2.5: A simple schematic of a Raman spectrometer set-up.[78]

Consider Raman line intensity I_r, which can be expressed as:

$$I_r = \nu^4 \sigma I exp(-E_i/kT)C \tag{2.12}$$

where ν and I is the frequency and intensity of the incident radiation respectively, σ is the Raman cross-section, C is the analyte concentration and the whole exponential term represents the Boltsmann factor of state i. Typically, the cross section of the Raman scattering effect is in between 10^{-30} - 10^{-25} cm^2 per molecule and in comparison, fluorescence cross section are roughly 10^{-16} cm^2 per molecule.[48] Nevertheless, by applying excitation light source that has wavelength in resonance with the absorption band of the molecule produces surface enhanced resonance Raman scattering (SERRS) and this can improve the value of effective Raman cross section. Another disadvantage of SERS is the interference with fluorescence and the effect becomes more apparent when a shorter wavelength light source is selected.[77] Therefore, for a specific measurement, choosing a light source with the correct wavelength can be critical.

A modern Raman spectroscopy consists of lasers, microscopy lenses, notch or edge filters, monochromators or laser-line filters and charge-coupled device (CCD) detectors. Figure 2.5 shown is a simple schematic of a typical Raman spectroscopy set-up. Historically, mercury arc lamps were used as the light sources and photon-counting photomultiplier tubes (PMT) were used as detectors for the spectroscopy but the weakness in the light source and long acquisition time to obtain Raman signals had limited the usage of the

instrument. The development of lasers has later transformed Raman spectroscopy into a more practical tool since they are the ideal monochromatic light sources that is capable of producing more intensity so that they can allow improved spatial resolution and higher signal to noise ratio on the output signal. In addition, lasers today can be generated in a number of wavelengths, providing more options to achieve the best detection scenario. The invention of CCD detectors has also improved the sensitivity of spectroscopy and has shortened signal detection time into a matter of seconds. Monochromators and laser-line filters are optical devices that enable light to pass through, while narrowing the range of wavelength and rejecting unwanted noise signals. The purpose of notch and edge filters is to reject elastically scattered light from the sample prior to entering the spectrometer. Raman spectroscopy can often be applied with microscopic and computer analysis systems to provide more versatile functionalities. With the advancement in manufacturing technology nowadays, even portable Raman systems have become commercially available, extending the application to new areas, such as marine ecological studies and identification of explosives.

2.2 Surface Enhanced Raman Spectroscopy

SERS is one of the specialized techniques of Raman spectroscopy. It is capable of providing very sensitive Raman scattering measurements for molecules in low concentration adsorbed on rough metal surfaces. It was first discovered in the 1970s by Fleischmann and his coworkers in experimental work, where pyridine adsorbed on roughened silver electrode surfaces was able to produce an enhancement output six orders of magnitude greater than bulk pyridine. Jeanmaire and Van Duyne later found that the enhancement cannot be contributed by the increase of surface area alone and have proposed the electromagnetic enhancement mechanism.[37] Albrecht and Creighton also recognized effect and had proposed a theory based on chemical effect.[1] Although many other enhancement theories have been proposed, these are the two primary mechanisms that are most often discussed. Although the exact SERS enhancement mechanism in modern studies still remains as a focus of debate, electromagnetic enhancement refers to the excitation of localized plasmon resonance depending on surface roughness or curvature. Chemical enhancement is the less understood effect, which depends on the polarizability of molecules forming a charge-transfer complex between the chemisorbed species and the metal surface.[16] All SERS

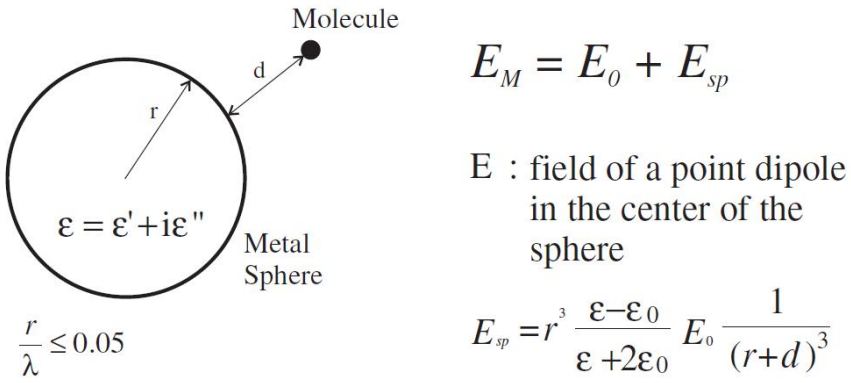

Figure 2.6: An illustration to describe the electromagnetic field strength and dieletric constant around a metal sphere.[47]

measurements should have both enhancement effects, but it is difficult to impossible to separate the individual effects, making the understanding of enhancement more challenging. However, among the two effects, electromagnetic enhancement is usually thought to be the more dominate, since its contribution factor is on the order of 10^4-10^7, where chemical enhancement is only on the order of less than 10^2.[6] Although conventional enhancement factors are normally reported to be on the order of 10^6, in optimum cases the enhancement factor can be as high as 10^{14}.

2.2.1 Electromagnetic Enhancement

The electromagnetic enhancement mechanism for SERS is generally described as a two step process. First, the electromagnetic field of the incident radiation is enhanced due to the additional field initiated by the polarization of metal particles. Then, if the Raman field emitted by the molecules are in resonance with the polarization of the metal particle, it is further polarized by the metal particle, hence resulting in amplified Raman signals.[2] A review article by Kneipp et al. has also provided a simplified description of the SERS enhancement concept and an illustration is shown in Figure 2.6. Consider a small metallic sphere with the complex dielectric constant $\varepsilon(\nu)$ surrounded in a medium with a dielectric constant, ε_0. The diameter of the sphere, 2r, is assumed to be small compared to the wavelength of light and is constrained within the Rayleigh limit. The field enhancement

factor $A(\nu)$ is the ratio of the field at the position of the molecule and the incoming field can be represented as

$$A(\nu) = \frac{E_M(\nu)}{E_0(\nu)} \sim \frac{\varepsilon - \varepsilon_0}{\varepsilon + 2\varepsilon_0} \left(\frac{r}{r+d} \right)^3 \tag{2.13}$$

where $A(\nu)$ is at maximum when the real part of $\varepsilon(\nu)$ is close or equal to -$2\varepsilon_0$ and at this condition, surface plasmons of the metal sphere is in resonant excitation. The difference in dielectric constant between the roughened surface and the surrounding media results in sharp points on the surface that have a more concentrated electric field density.[85][66] and generally, the imaginary part of the dielectric constant needs to be small in order to favor strong electromagnetic enhancements.[47] Similar with the laser field, the scattered Stokes or anti-Stokes will also be enhanced if they are resonating with the surface plasmons of the metal sphere. Considering the enhancement effect of the laser and the Stokes field, the electromagnetic enhancement factor for the Stokes signal power, $G(\nu_S)$, can be represented as:

$$G_{em}(\nu_S) = |A(\nu_L)|^2 |A(\nu_S)|^2 \sim \left| \frac{\varepsilon(\nu_L) - \varepsilon_0}{\varepsilon(\nu_L) + 2\varepsilon_0} \right|^2 \left| \frac{\varepsilon(\nu_S) - \varepsilon_0}{\varepsilon(\nu_S) + 2\varepsilon_0} \right|^2 \left(\frac{r}{r+d} \right)^{12} \tag{2.14}$$

Although this formula is based on a simple model, it is capable of describing some of the important properties of SERS enhancement. For instance, the enhancement reaches a maximum when the excitation and scattered fields are in resonance with the surface plasmons and it scales roughly to the forth power of the local field of the metallic nanstructure. However, the equation also addresses the issue that the enhancement is more effective for lower frequency Raman modes and the scattering power of different Raman bands in a spectrum decreases as the vibrational energy increases. Electromagnetic enhancement of SERS does not require direct contact of the molecule to the metal sphere, but its strength decreases with respect to the distance with the decay of dipole field over the distance of $[1/d]^3$ and overall to the fourth power, $[1/d]^{12}$.[47] Molecules closest to the surface usually exhibit the largest enhancement, but the enhancement can be long-ranged, extending tens of nanometers away from the surface, depending on the substrate morphology.

2.2.2 Chemical Enhancement

Although early evidence for the existence of chemical enhancement was thought to be inferential, more experimental observations have indicated that the effect can also take a part

in SERS enhancement. For instance, the electromagnetic enhancement is a non-selective Raman scattering effect for all kinds of molecules on a particular surface, the enhancement factor for CO and N_2 can differ by a factor of 200 under the same experimental conditions. This phenomenon is hard to explain by only electromagnetic enhancement effects.[6] Other findings suggest the existence of other mechanisms, where the electromagnetic effect is believed to be minimal, there are dependent on the electrode potential.[47] The chemical enhancement effect, is sometimes called the first layer effect, since it requires a direct contact of the metal surfaces to the molecules. The interaction of the molecule to the surface can be described in several ways. When an analyte molecule is adsorbed onto the metal surface, it creates a bond which allows free electrons at the metal surface into the analyte. Interactions, such as electronic coupling between molecules and metals, or the formation of adsorbate-surface complex, can result in increased Raman cross section of the adsorbed molecules.[47] The mechanism can also be explained by the resonance Raman effect, where the electronic states of the analyte are shifted and broadened, due to the interaction with the surface or the new electronic stats that arise from chemisorption. This can be regarded as resonant intermediates states for Raman scattering. This is uncommon when the highest occupied molecular orbital (HOMO) and the lowest unoccupied molecular orbital (LUMO) of the adsorbate are approximated symmetrical with respect to the Fermi level of the metal. The charge transfer excitation can occur by employing light having half the energy.[6] Figure 2.7 is a typical energy band gap diagram of a molecule adsorbed on a metal surface. Paths a), b), c) and d) resemble the possible resonant Raman processes involving metal, molecular and molecular-metallic states. Path a) represents the electron is excited within the metal and path b) involves the excitation of intramolecular electron by incident light. Path c) describes the surface electron of the metal is excited to the adsorbed molecule and for path d) the intramolecular electron is excited from the molecule to an empty orbital of the surface metal. The potential-dependent SERS enhancement can be due to the change in resonance condition for paths c) and d) when the Fermi level is shifted.[89, 47] Some other reviews have described the photo driven dynamical charge transfer effect is consisted of a set of steps. In brief, when a photon is annihilated, its energy is transferred to excite an electron close to the metal surface forming a hot-electron state. Then, the hot electron is tunneled out of the surface and transferred into the LUMO of the analyte molecule. The electron then undergoes a interaction process with the LUMO where the normal coordinates of the internal molecular vibrations may be effected. After

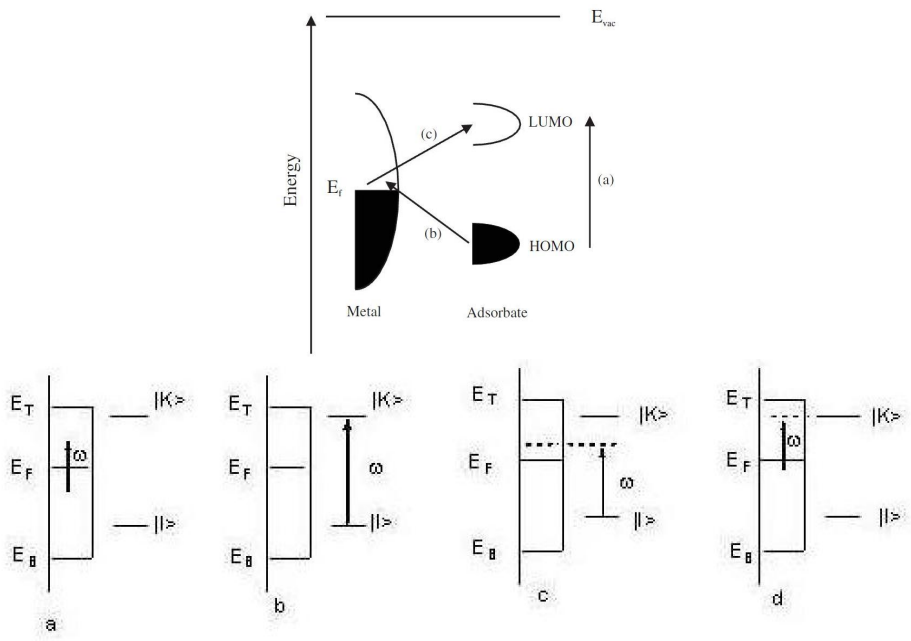

Figure 2.7: The chemisorption mechanism for a molecule adsorbing on a metal surface.[6][81]

the interaction, the electron relaxes and releases Raman shifted photons while returning to its initial state. [47][89]

2.2.3 Characteristics of SERS

Since SERS is an advanced technique of normal Raman spectroscopy, it inherits the feature of providing non-destructive, *in situ* measurements for liquid, solid or gaseous samples. However, overtone and combination bands are not common for SERS spectrum and the intensity of the bands usually decreases as the vibrational frequency increases.[6] Although most of spectra obtained from SERS are very similar to the non-enhanced spectra, there are often slight differences in the number of modes presented, when compared to each other. Some peaks found in traditional Raman can be strongly presented, but in SERS spectrum those peaks can become very weak or even disappear. Selection rules for Raman spectroscopy are visible for symmetric vibrational modes but the rules are sometimes relaxed for SERS since the symmetry of system can be lightly altered when molecules are adsorbed onto a surface.[57] The symmetry of the molecule is largely dependent on the orientation that the molecule is attached to the surface, and in some cases, the concentration of the analyte is also a factor. One of the classic examples is the measurement of pyridine. When pyridine is well below the concentration to provide monolayer surface coverage, pyridine rings are usually found laying parallel to plane of the surface and therefore, the resulting spectrum is very weak. However, as the concentration increases, the pyridine ring is forced to be oriented perpendicularly to the surface plane, providing dense packing, hence the SERS intensity rapidly increases. Since the exclusion rules are less applicable in SERS spectrum, symmetric vibrational modes, lost due the adsorption to the surfaces, can sometimes be retrieved via infrared spectrum. Nevertheless, the rules can become even more complicated than breaking of symmetry because some types of bands are naturally more intense in SERS than the ones found in normal Raman scattering.[77] To better illustrate the effect of molecular orientation and symmetry, the study by Emory et al. compared the SERS spectra of R6G observed from a single silver nanoparticle where the molecule is polarized in different directions using polarization-scrambled laser excitation and dichroic sheet polarizer, as shown in Figure 2.8. It can be seen that the enhancement is much stronger when the molecule is polarized along the long molecular axis and the peaks at 1657, 1578, 1514, 1365, 1310 and 1184 cm^{-1} are referenced to the symmetric modes of

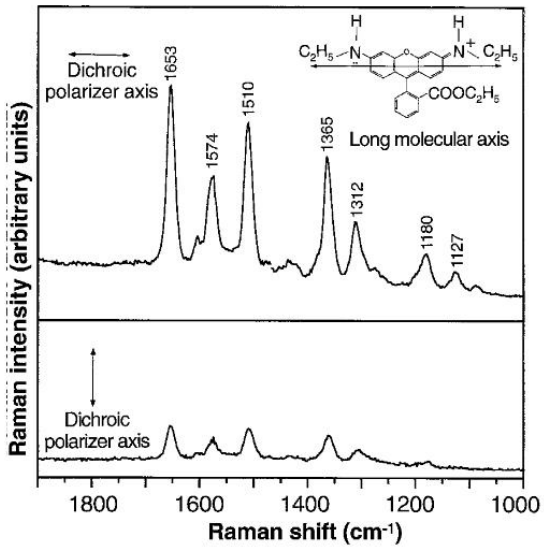

Figure 2.8: Raman intensities of a R6G molecule polarized in different axis.[62]

in-plane C-C stretching vibrations.[62]

SERS is one of the most sensitive analytical methods to study surface phenomena, but the real application for SERS has never reached its expectation due to several barriers.[81] For instance, the materials commonly used for studying SERS enhancement factors are limited to silver, gold and copper because of their plasmon resonance frequencies can correspond to the light wavelengths that falls within visible to near IR range in order to provide the maximum enhancement. SERS effects also have been explored on other types of metals, such as rhodium, platinum, ruthenium, palladium, aluminum, iron, cobalt, and nickel; however, there are few publications on these other materials.[22][79] Another barrier for SERS development is that the surfaces of the substrate are required to be flat for many fundamental researches of surface sciences, but SERS enhancement effects usually have been explored on platforms featuring high surface roughness.[81] Surface roughness, usually on the order of 10-100 nm, is speculated to be one of the key aspects for obtaining strong SERS signals. Atomic roughness featuring adatoms, adclusters, steps, kinks and segregation can further increase the enhancement.[6][81] Nevertheless, SERS signals commonly have reproducibility issues, since consistent surface roughness is hard to tailor and a simple, unified approach to produce SERS active substrate is still lacking.[90][60] The

third and key barrier is the difficulty to separate electromagnetism and chemical effects in order to understand the exact mechanism to contribute major SERS enhancement. Confronted by these difficulties, the advancement of SERS stalled from the mid 80s to the mid 90s.[2] It was not until Nie and Emory made a remarkable discovery that SERS from a single rhodamine 6G molecule adsorbed onto a selected silver nanoparticle can produce an enhancement up to an order of 10^{14}[62] Another study done by Kneipp and coworkers also reported the detection of SERS from a single molecule by using NIR laser excitation to obtain enhancement with similar magnitude.[49][48] Their findings have become the turning point for SERS and the development of nanotechnologies and instrumentations, has been revived. Although the understanding of the exact enhancement mechanism still remains unknown, the development of SERS is progressing rapidly due to the advancements in nanotechnology.

2.3 SERS Active Substrates

Many of the current SERS studies are involved in the fabrication SERS active substrates to achieve the desired properties. To design the optimum substrate, there are several factors to considerate; for instance, ease of fabrication and utilization, stability over time, robustness, free of background noises, customizable surface functionalities, and tunable enhancement levels. The first generation of SERS active substrates consist of adsorption of pyridine molecules on electrochemically roughened silver electrodes. Surface roughness has been found as the key component in making quality SERS active substrate. Since then a number of fabrication methods have been reported to produce SERS promoting substrates; for instance, rough surfaces fabricated by sputtering, metal-vapour condention, oxidation-reduction cycling (ORC) or current-controlled ORC on electrodes, film deposition, and chemical etching by halide ions, nitric acid and CrO_3/H_2SO_4 mixtures.[3]

A majority of SERS active substrates are employed with metallic nanoparticles, since they can be easily prepared through chemical, thermal and photoinduced reduction of many readily available metal salts. By carefully controlling the synthesis parameters, metal colloids can be made into uniform sizes and can be prepared at low cost. More importantly, nanoparticles can lead to the formation of aggregates on substrate surface featuring roughness and fractal morphology that can promote intense Raman spectra.[2] One of the most

well-known SERS active substrate assemblies is produced by drop casting nanoparticle solution onto a pretreated substrate. Once the solution is evaporated, the nanoparticles self-assemble and form randomly packed aggregates.[50] Although the presence of those unpacked, isolated nanoparticles can also provide electromagnetic enhancement, it is rare for them to exhibit large SERS enhancement. SERS enhancement is usually found to be the greatest within a localized volume called a "hot-spot", where the particles form aggregates or are in close proximity to each other. Due to the electromagnetic interactions exhibit intense localized plasmon resonance, aggregated nanoparticles with narrow interparticle gaps are more likely to produce enhancement effects than individual particles. It is reported that the enhancement factor can be greater by a magnitude of five to six orders.[3] Since the effect of SERS is closely related to the density and strength of electromagnetic fields and plasmon resonance, SERS active substrates generally require fine-tuning of size and size distribution of nanoparticles, surface state, surrounding environment, shape and the nature of the substrate structures. Systems employing nanoparticles with sizes ranged 5 to 100 nm possess SERS activity, where the strongest enhancements are produced by particles ranging from 20 to 70 nm. However, if the nanoparticles' size becomes too small, the electrical conductivity for the particle decreases and the electronic scattering of the surface becomes dominate, so that the particle loses polarizability and quality of plasomon resonance; the ability to produce SERS enhancement is reduced.[50]

Many reports have claimed to adjust the size and shape of the nanoparticles in order to achieve surface plasmon resonance with respect to the source frequency, maximizing electric field enhancement. Emory et al. have observed a direct SERS enhancement relationship between the sizes of individual silver nanoparticle respect to the excitation wavelength.[14] They employed AFM measurements to categorize the sizes of nanoparticles and excited each particle with three different excitation wavelengths. They reported that the excitation profile has an approximate linear relationship between the excitation wavelength and particle size, where the incident laser with wavelengths of 488 nm, 568 nm and 647 nm can efficiently excite particles with sizes of 70 nm, 140 nm and 200 nm, respectively. Nevertheless, they also have claimed that the degree of variation in the slope is not only effected by the uniformality in the particle sizes but the shape also has to be considered. In comparison with spherical particles, Xia et al. reported an observation of SERS enhancement obtained from sharp and truncated silver nancubes with a size range of 60 to 100 nm. They showed that the surface plasmon resonance band is much broader for large

silver nanocubes compared to smaller ones. This could create more coherence in the overlapping of surface plamon band with the excitation source, producing stronger scattering intensities but the corners and the edges of the nanocubes may have also contributed to the boarding of the plasmon band.[55] Tian et. al. examined the SERS intensity of pyridine by drop casting a batch of 70±3 nm, 83±3 nm, 95±4 nm and 105±5 nm of gold core-palladium shell nanocubes on smooth glassy carbon electrode surfaces. By using UV-vis spectroscopy, they have measured the respective absorbance peaks for each nanocube sizes which are 568 nm, 591 nm, 603 nm and 620 nm, respectively. The excitation wavelength used in the experiment is 632 nm but the maximum SERS is subjected to particle size of 83 nm where the deviation of particle sizes and broadening of absorbance peak my have caused a shift in plasmon resonance.[74] A similar observation is also reported from Suh et al. who reported a series of SERS enhancement by employing a laser with a wavelength of 632 nm onto silver nanorods with uniform diameters, but different length. Typically, nanorods have a characteristic of exhibiting two absorption bands indicating the dipolar resonance along the transverse and longitudinal axis where the modes are dependent on the width and length of the nanorods, respectively. By tuning the length of the rods, Suh's group is able to observe the largest SERS enhancement occurs when the longitudinal mode of the nanorods are in correspondence to the excitation wavelength.[25]

The absorption peaks of the synthesized nanoparticles are widely accepted to provided valuable information when the excitation wavelength is matched to the maximum absorption peak, SERS enhancement can be maximized. Nevertheless, Etchegoin et. al. has pointed out that the relationship between the absorption maximum and SERS enhancement is rather indirect and misleading, since the effect of SERS is very dependent on the spatial localization of the nanoparticles, where a collection of factors can be influential, such as gap distances, dipole-dipole interactions from neighboring particles, alignment geometry and incident ray angle. The absorption maximum is like a bulk effect, and on the other hand, the enhancement maximum is a surface-like effect which is exhibited in particular gap spaces and hot spots. Systems that are more in spatial averaging and complexity in geometry with collective resonances would experience a weaker connection in between the absorption maximum and SERS enhancement.[71] Interestingly, Van Duyne et al. have applied a wavelength scanning technique to explore SERS enhancement from benzenethiol by fabricating nanoparticles with simple nanoparticle arrays using nanosphere lithography. Their findings have shown an agreement with the elecrtomgnetic mechanism that the

maximum SERS occurs when the incident photons and the scattered ones from the localized surface plasmon are both enhanced.[54] Therefore, it is important to understand the connection between the absorption maximum and SERS enhancement and the maximum absorption peaks can be regarded as good reference parameters for achieving maximum SERS enhancement. Other than shapes and sizes of nanoparticles, the structure, surface coverage, spacing, geometry, positioning and alignment of particles on the substrate surface can also effect the surface plasmon and the degree of SERS enhancement and the number of publications focused on these areas has grown rapidly in recent years. For instance, Nogami et al. reported a simple technique to link silver nanoparticles together and forms chains, as shown in Figure 2.9. From their observation, the chained nanoparticles exhibit optical properties similar to rod nanoparticles where their plasmon absorbance can also be tuned with the increase in the chain length. Typically, chained nanoparticles can achieve higher SERS enhancement than isolated nanoparticles, as shown in Figure 2.10 and Figure 2.11.[91] Murphy et al. fabricated sandwiched substrates consisting of 47 nm gold nanocubes, 4-mercaptobenzoic acid self-assembled monolayers and flat gold substrate to examine the relationship of SERS intensity and the surface coverage of nanoparticles. Figure 2.12 shows their scanning electron micrographs of the substrates that have surface coverage of 5.5 cubes/μm^2 and 22 cubes/μm^2 and Figure 2.13 is the Raman spectra taken from substrates consisting surface coverage of a)0, b)5.5,c) 8.6, d)15 and e)22 cubes/μm^2 taken with 785 nm and 632.8 nm excitation. The relationship between the maximum SERS intensity with respect to surface coverage 5.5, 8.6, 15 and 22 cubes/μm^2 taken with 785 nm and 632.8 nm excitation is shown Figure 2.14. It can be seen that SERS intensity can be approximated linearly as the surface coverage of nanocubes increases.[36]

Kim et al. observed SERS enhancement of benzenethiol from layered assemblies of close-packed gold nanoparticles fabricated by the Langmuir-Blodgett method, which is based on entrapping nanoparticles on a flat substrate via the interface of water and a nonpolar solvent. They found that SERS intensity increases along with the increase of nanoparticle layer thickness, since the increment layers of particles provide more spacing and roughness to the surface. They also claimed that the 30 nm gold nanoparticle film produces higher enhancement than the 5.5 nm particle film, due to the favoring of gap structures.[39] Halas et al. also studied SERS enhancement of *p*-mercaptoaniline from substrates fabricated with periodic 50 nm gold nanoparticle arrays with sub-10 nm interparticle spacings. From their observation, nanoparticles arranged with sub-10 nm gaps

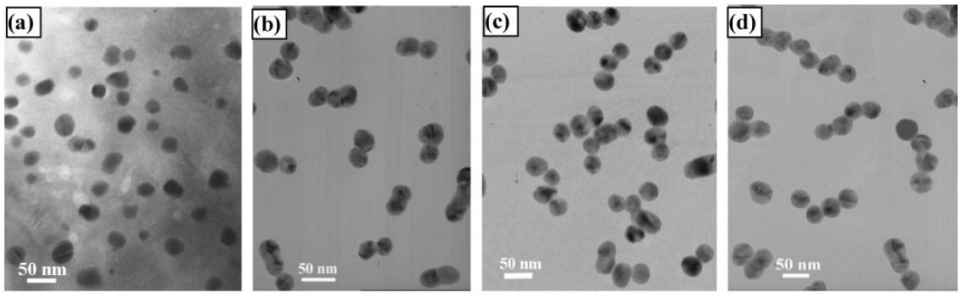

Figure 2.9: TEM images of chained silver nanoparticles with lengths of a)sol-1, b)sol-2, c)sol-3 and d)sol-4.[91]

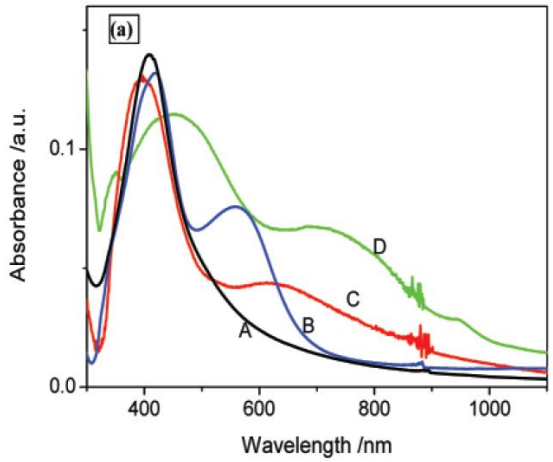

Figure 2.10: UV-vis-NIR absorbance spectra of chained silver nanoparticles with lengths of a)sol-1, b)sol-2, c)sol-3 and d)sol-4.[91]

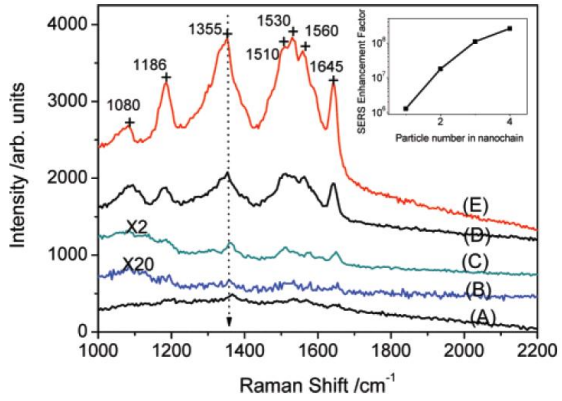

Figure 2.11: SERS spectra of 100 mM R6G absorbed on a)glass, and chained silver nanoparticles with lengths of b)sol-1, c)sol-2, d)sol-3 and e)sol-4.[91]

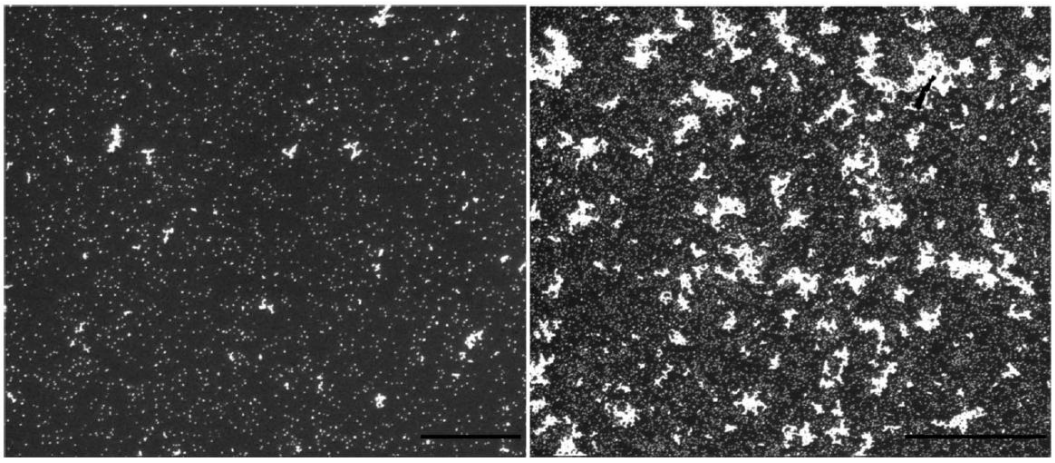

Figure 2.12: Surface coverage of 5.5 cubes/m^2 and 22 cubes/m^2.[36]

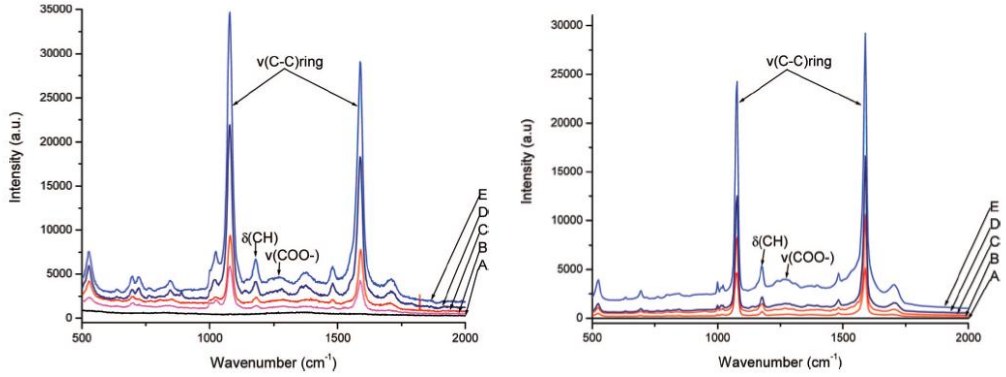

Figure 2.13: Raman spectra taken from substrates consisting surface coverage of a)0, b)5.5,c) 8.6, d)15 and e)22 cubes/μm^2 taken with 785 nm and 632.8 nm excitation.[36]

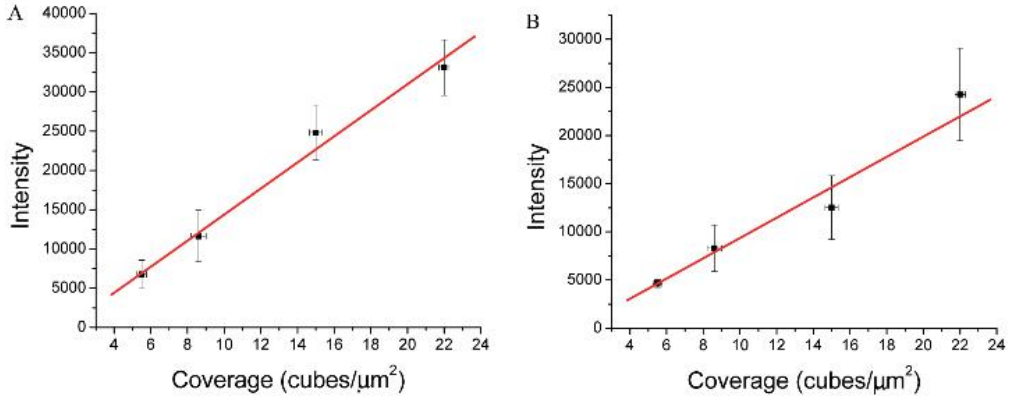

Figure 2.14: The maximum SERS intensity with respect to surface coverage 5.5, 8.6, 15 and 22 cubes/μm^2 taken with 785 nm and 632.8 nm excitation.[36]

can boost the enhancement to an order of 10^8, due to the hybridized plasmons formed by adjacent nanoparticles.[83] In addition, Moskovits et al. examined the physical nano-geometry effect on SERS intensity by fabricating a series of silver nanowires arrays in porous aluminum oxide. They also observed that SERS intensity is increased when the gaps between the nanowire arrays are decreased from 35 to 10 nm.[52] One of the studies by Emory et al. mentioned that the orientation of the nanoparticle and the dependence of polarization direction has a significant effect on SERS signals. Figure 2.15 shows is the comparison of the SERS spectra of R6G obtained from the expected positions of two nanoparticles aligned parallel or perpendicular to the plane of incident light. According to electromagnetic theories of surface plasmon resonance, the particles are in orthogonal orientations and the overall polarization is contributed by the preferential excitation of an oriented nanoparticle, while the other is from similar but Raman polarizability tensor of an oriented molecule.[62]

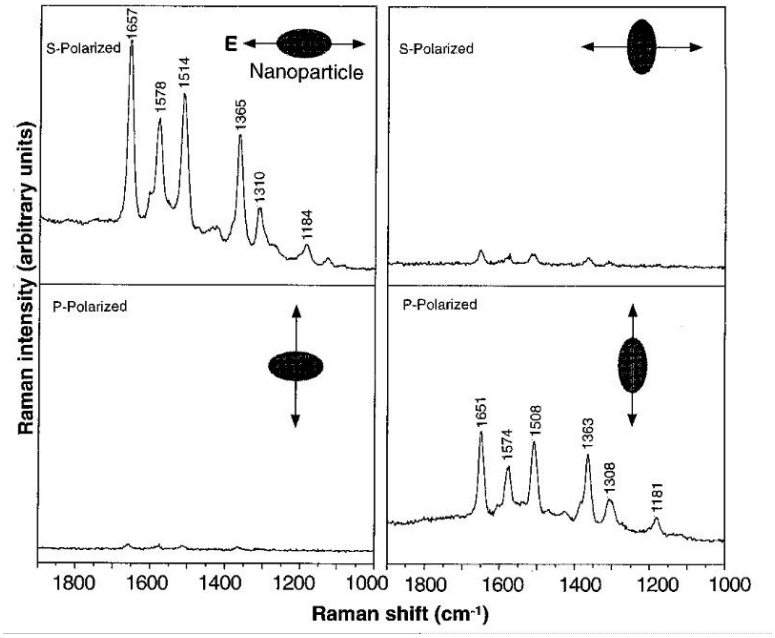

Figure 2.15: SERS intensity of R6G polarized within two nanoparticles aligned parallel and perpendicular to the incident light.[62]

Spectra reproducibility is a known issue in a number of SERS studies employing nanoparticles. Since SERS requires a precise control in a number of factors, such as the na-

ture of surface metal, particle sizes and shapes, and the degree of particle aggregation.[80] Although nanoparticles are one of the most utilized SERS active substrates, they are rather difficult to synthesize in a consistent manner because every preparation procedure requires special attention, even down to the narrowest details where the parameters become difficult to measure, such as the extend of mixing, method of reduction, cleanliness of glassware, and addition rate of chemicals. In addition, the stability of nanoparticles can also be short-lived depending on the storage condition and the nature of the colloidal solution. Factors, such as the surrounding temperature, ionic strength, the pH of the solvent, the surfactant used, aggregation, precipitation, and even exposure to light, can influence the particles' deterioration rate. With regards to these difficulties, it is not surprising to find that SERS enhancement measured with the nanoparticles produced in one laboratory is different from another.[3] Compared to standard substrate fabrication techniques, lithography has the advantage of fabricating nanoparticle arrays with more precision, such that the randomness for the spacing, alignment and geometry of nanoparticle can be minimize. This gives the substrates higher reproducibility. The study by Yan et al. demonstrated a method of constructing gold nanoparticle cluster arrays with varying binding diameter sizes. Figure 2.16 shows the SEM images of the nanocluster arrays with edge-to-edge separation of 200 nm and e-beam defined binding diameter sizes of a)50, b)80, c)100, d)130 and e)200 nm. This group has made a direct comparison of SERS enhancement factors using nanocluster arrays, unpatterned colloids and nanodisk arrays. From their experimental results, shown in Figure 2.17, it is clear that nanocluster arrays are capable of producing the highest SERS enhancement among the three, while exhibiting high reproducibility. The standard deviation from 12 random measurements from each substrate and the standard deviation as the percentage value of the mean is also shown in the figure.[90] There are some studies that already have utilized lithography fabrication to explore and control the assembling parameters that is capable of effecting SERS activity. For instance, Mirkin et al. have designed and fabricated gold nanodisks arrays with on-wire lithography and with the precision in assembling the substrate. The group is able to systematically tune the disk' gap distance between from 5 nm to 8 μm^2 and the disk thickness from 20 nm to several micrometers. They have found that the maximum SERS for the disk array system occurs with 30 nm of gap spaces and 120 nm of disk thickness. This finding is contrary to the beliefs others, who think that the optimal SERS enhancement occurs in small structures and gap spaces with 10 nm or less. They believed that the effect of gap size is in relation

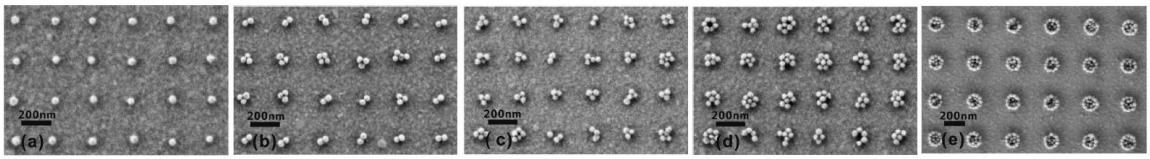

Figure 2.16: Nanoparticle arrays with 200 nm separation and binding diamter sizes of a)50, b)80, c)100, d)130 and e)200 nm.[90]

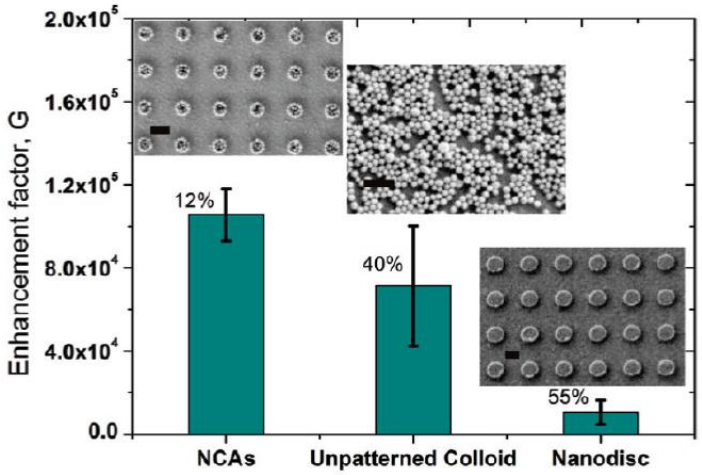

Figure 2.17: Comparison of SERS enhancement factors using nanocluster arrays, unpatterned colloids and nanodisk arrays.[90]

to the red-shift of dipole plasmon wavelength, while the particle size is associated with the amount of light penetration confined by the gap structures. Figure 2.18 shows a) the gold nanodisks arrays with 120 nm thick and 30 nm gap separation, b) the corresponding confocal Raman microscopic images and c) the three-dimensional Raman intensity images.[70] Since lithography fabricated SERS substrates have shown promising results in producing high SERS enhancement, recent SERS substrate development are not only focusing on two dimensional structures, rather three dimensional substrates are also evolving. Fan et al. have fabricated highly ordered treelike Si/ZnO hierarchical nanostructures, where there are branches growing from the nanopillars, as shown in Figure 2.19. In order to fully functionalize the three dimensional structure, silver nanoparticles are decorated on the branches to create close interdistances or "hot-spots" between the silver nanoparticle and the pillar branches. Figure 2.20 shows the SERS spectra of R6G molecules from 15 randomly se-

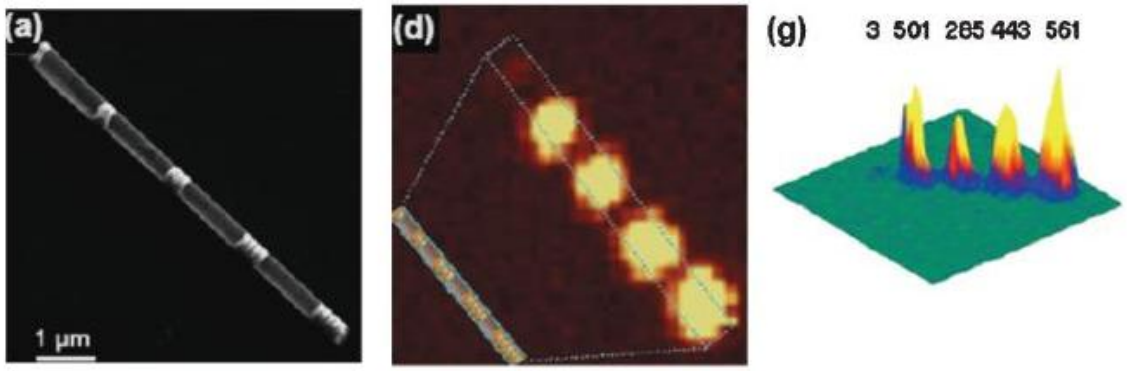

Figure 2.18: One dimensional structure of nanodisk arrays with 30 nm gaps and the SERS intensity of the structure.[70]

lected positions on the substrate under identical experimental conditions. Similar to other lithography substrates, the SERS intensity obtained from the substrate is reproducible with slight fluctuation. These fluctuations may be caused by the ununiform deposition of nanopartilces and the R6G molecules. They also have made a SERS measurement comparison with plain Si/ZnO nanotree arrays, sputtering fabricated silver nanoparticle substrate and silver nanoparticle decorated Si/ZnO nanotrees. The silver nanoparticle decorated substrate has shown the greatest enhancement among all three, as shown in Figure 2.21.[9] Although lithography fabricated substrates may have been a promising solution for many analytical and research applications, the strict production environment and the high fabrication cost has restrained them from actual practice.[17] Therefore, by evaluating the constraints of the lithography method and the degree of success from various reports using other alternative fabrication methods, this paper mainly focuses on SERS substrate fabricated by self-assembled nanoparticles.

2.4 The Application of SERS Active Substrate

SERS has been evaluated as one of the most powerful analytical tool in terms of identifying chemical compounds, drugs and molecular structures. With the sensitivity, accuracy, reliability and speed of analysis, SERS could become very valuable in real-world appli-

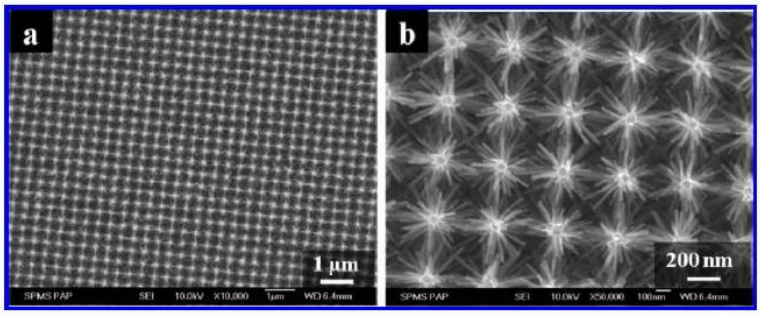

Figure 2.19: Arrays of Si/ZnO nanotreebranches.[9]

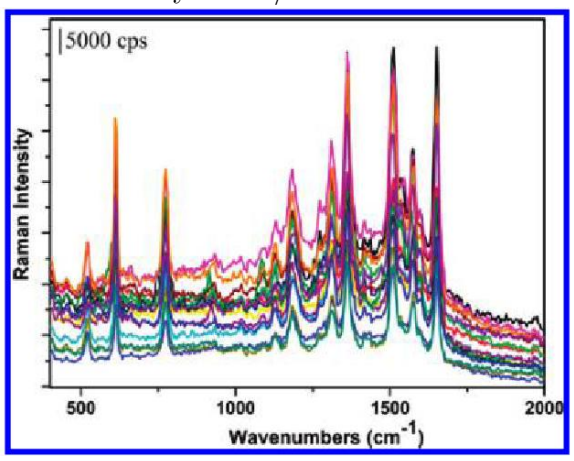

Figure 2.20: SERS spectra of R6G from 15 random points from the substrate under identical experiment conditions.[9]

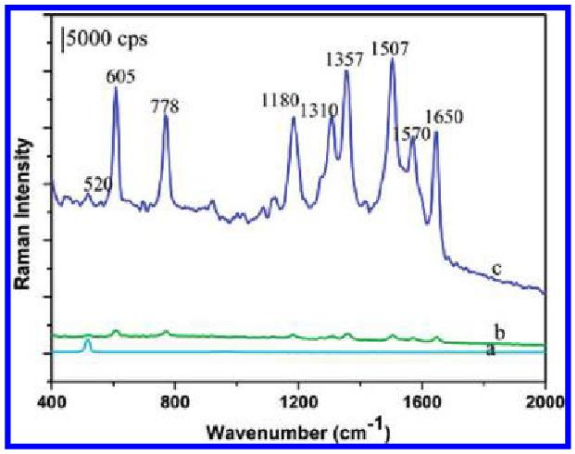

Figure 2.21: SERS intensities of a)plain Si/ZnO nanotree arrays, b)sputtering fabricated silver nanoparticle substrate and c)silver nanoparticle decorated with Si/ZnO nanotrees.[9]

cations; for instance, it has the potential to be facilitated in roadside tests, diagnostics and security measures, particularly aiming for the detection of illegal drugs, explosives and toxic substances in body fluids. If the conditions are satisfied, SERS not only can identify the substances in a sample but also trace the concentration level of that particular substance.[61][3] The application of SERS also has a great potential value in the field of pharmaceuticals and often it is used in combination with metallic surfaces. One example is to analyze the process of drug delivery, since delivering drugs to a specific human organ requires the design of drug adsorption on some functional centers. The utilization of silver and gold surfaces can be seen as artificial biological interfaces that are capable of mimicking these adsorption process.[2] Many research groups are also focusing on improving the application value of metallic nanoparticle and SERS as a combo design to serve as diagnostic probe, where the recognition of labeling chemistry and molecular structures of the drugs can be achieved *in situ.* The key to the success is to generate multifunctionl nanomaterials that can be integrated into standard clinical imaging and therapy to enable real-time visualization of biodistributions in patients, but the biomedical research community has recently recognized that the application cannot be achieved without solving the issue that no single targeting agent is capable of providing sufficient information when tracing and characterizing a specific disease process.[92][82] Therefore, efforts have been made into discovering suitable biomarkers for achieving multiplexing tasks and developing strategies to attach multiple biolabels onto nanostructured-based platforms in hoping to achieve the earliest simultaneous detection of multiple targets.

Until recently, Schlucker et al. demonstrated simultaneous SERS detection of 80 nm gold nanoparticles with multiplexing Raman label molecules, which consists of 5,5'-dithiobis(2-nitrobenzoic acid)(DTNB), 2-bromo-4-mercaptobenzoic acid (BMBA), and 4-mercaptobenzoic acid (MBA). Figure 2.22 shows the illustration of the molecular structure of the three labels and the possible labeling combination where DTNB, BMBA and MBA are denoted as blue circle, red square and green pentagon in respective order and the numbers are represented as the stoichiometric ratio. The resulting SERS measurement in respective to the combinations are shown Figure 2.24, but for the three component measurements, the stoichiometry ratio has been modified to show only 1:1:1 on the top and 1:2:2 at the bottom. From their results, it can be seen that an infinite number of bar code combinations can be generated by not only by increasing the number of labeling molecules but also changing the stoichiometric ratio of the Raman labels mixed within.[20]

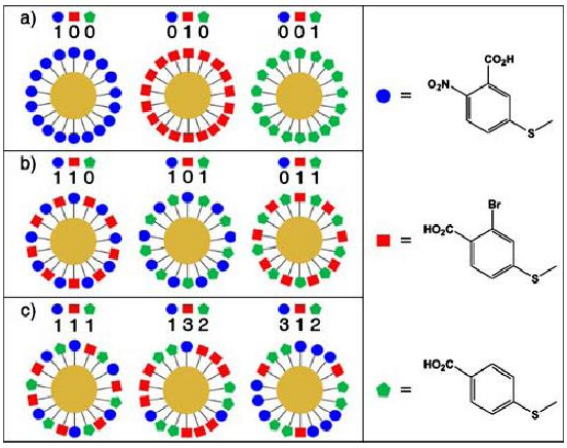

Figure 2.22: Labeling molecules and possible multiplexing combinations.[20]

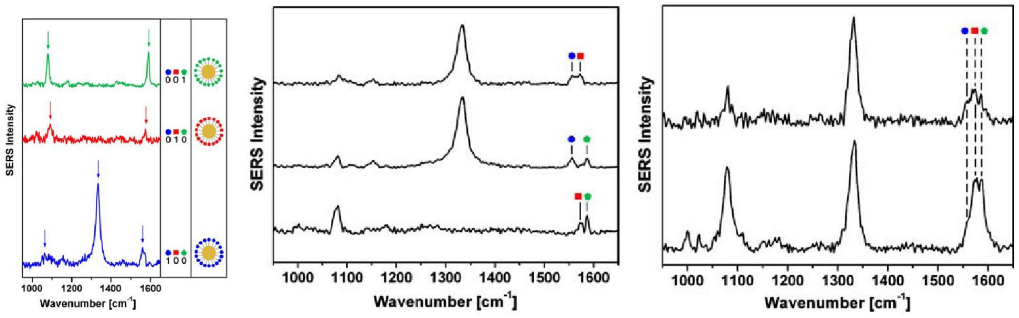

Figure 2.23: SERS intensity with a combination of one, two and three labels.[20]

The work done by Schlucker et al. is a good example to follow for preliminary multiplexing experiments. In order to picture the real potential application of multiplexing SERS labels, Gambhir et al. has done a preclinical experiment obtaining multiplexed imaging of surface enhanced Raman nanotags in living mice using noninvasive Raman spectroscopy. In their study, they identified and compared the SERS signals from ten different Raman nanotags attached to silica covered 60 nm gold nanoparticles *in vivo* from a living mouse. On the left in Figure 2.24 is a representation of tagged nanoparticles, the Raman code assigned with different colours and the corresponding Raman signals from each tagged nanoparticles; on the right is the Raman mapping of the mice after SERS particle injection and using postprocessing software, the ten different SERS nanoparticles can be identified *in vivo*. The scale bar for the intensity strength is also included where

white is the maximum and black is the minimum. In the next section of the experiment, five labeled nanoparticles that had the least amount of overlapping outputs were selected and in equal volume, the particles were injected into the tail vein of the mice. Due to the particle size, the particles have a tendency to be engulfed by the Kupffer cells of the reticuloendothelial system and become accumulated in the liver where deep tissue SERS imaging can be executed. Figure 2.25 shows the deep-tissue multiplexed Raman imaging of the nanoparticles 24 hours after injection and the postprocessing software can correctly identify all five SERS tags accumulated in the liver. Although all five tagged nanoparticles are injected with the same concentration, the analysis identified that the tags are inconsistently accumulated in the liver. This may have been due to the variability Raman intensity among each tags. The group has further investigated the effect on the SERS enhancement by varying the concentration of the tagged nanoparticles. They have chosen Raman labels S420, S440, S421 and S481 for the investigation since they have the least overlap and can output uniform intensity at the same concentration. The labels are injected into the mouse with an incremented concentration of 70 pM, 140 pM, 210 pM and 280 pM, respectively. A fifth injection is a mixture of the four Raman labels at different concentrations. Figure 2.26 shows the Raman intensity and Raman mapping of each individual labels. A graph indicating that the Raman intensity has a linear relationship with respect to the concentration of labeled nanoparticles is also shown in this figure.[92]

A study done by Bhatia et al. provided a strategy to produce SERS coded nanorods with multiplexing capability. They have used dialysis membranes to retain thiol-PEG polymers and gold nanorods in tubing that is submerged into large baths of a reporter molecule. This allows reporter molecules to replace the surfactant, CTAB, on the rod surface. Among all the reporter molecules that they have investigated, IR-792 perchlorate (IR-792), 3,3'-diethylthiadicarbocyanine iodide (DTDC-655) and 3,3'-diethylthiatricarbocyanine iodide (DTTC-765) are the three that have the highest ratio of the most intense peak height to peak height of internal ethanol standard vibration at 879 cm^{-1}. Figure 2.27 shown is A)the *in vitro* SERS spectra gold nanorods encoded with DTDC 655, DTDC 765 and IR-792 and the grey area highlights the encoding pattern, B)the *in vitroo* qualitative analysis for the fraction of each labeling signals with respect to the change of mixture composition and C)the *in vivo* identification of the Raman labeled nanorode from an athymic mouse after subcutaneous injection. [82]

From the studies of Schlucker et al., Gambhir et al. and Bhatia et al., it can be seen

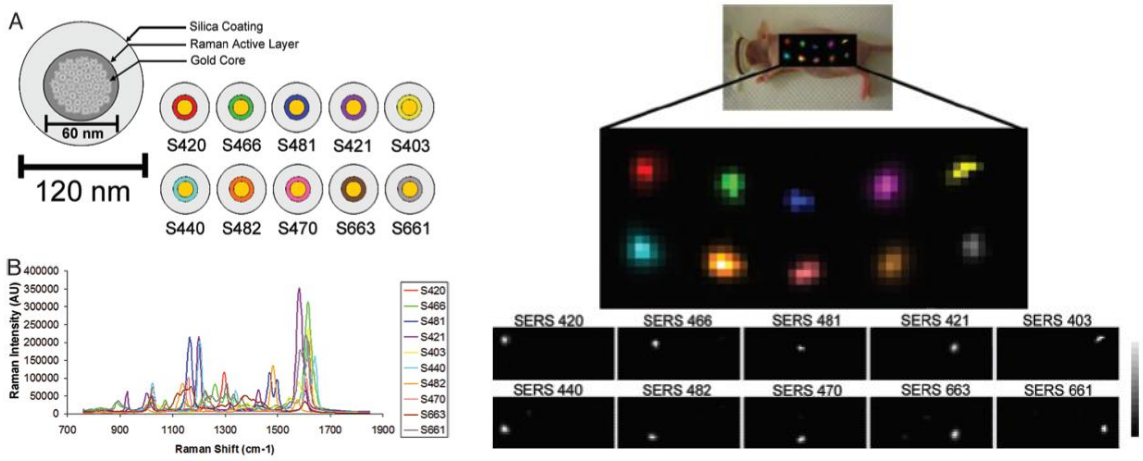

Figure 2.24: SERS spectra of the ten tags and the respective detection *in vivo*.[92]

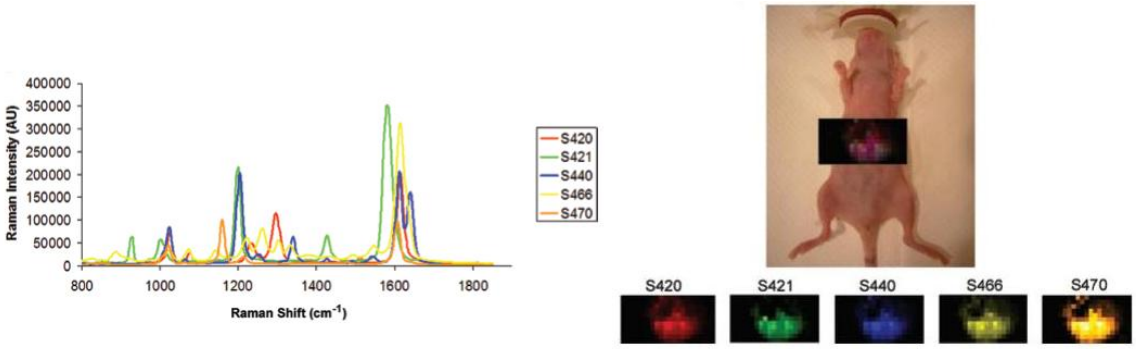

Figure 2.25: Successful detection and identification of all five tags after the injection of mixed labels.[92]

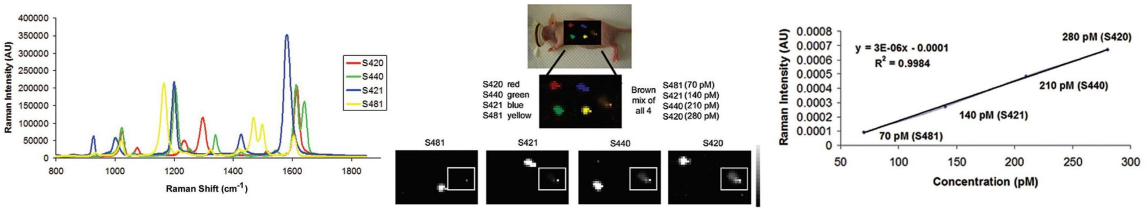

Figure 2.26: Relationship of SERS intensity increases with respect to the concentration of the multiplexed labels.[92]

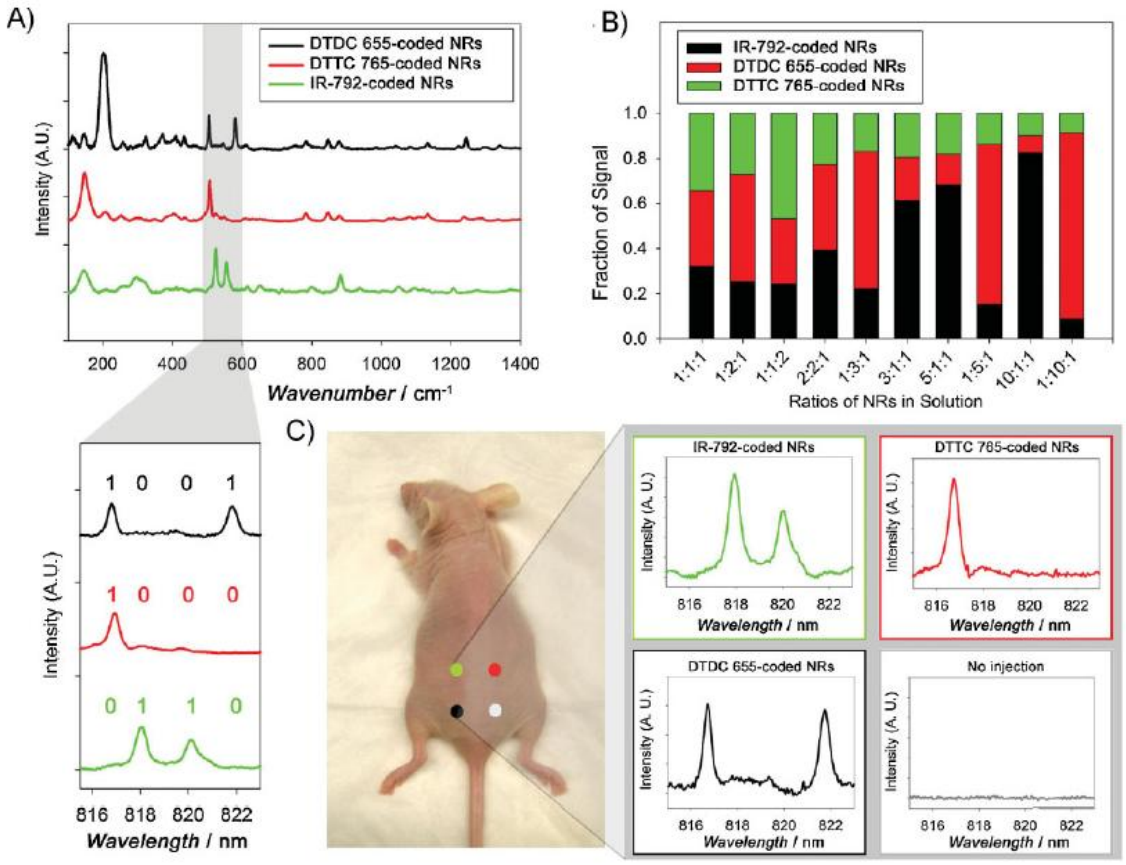

Figure 2.27: Illustration of A)SERS spectra of DTDC 655, DTDC 765 and IR-792, B)qualitative analysis of each labeling signals for each labeling with respect to the change of mixture composition and C)the *in vivo* identification of the Raman labeled nanorode from an athymic mouse.[82]

that gold nanoparticles are great candidates for the investigation of encoding multiplexed Raman labels. The *in vivo* detection not only can identify the location of nanoparticles, but also distinguish the type of labels that have been injected. In addition, all groups have indicated that multiplexing Raman labels with different concentrations can be observed from SERS outputs and this can be a strategic method of implementing additional information to Raman bar codes. However, excessively modifying the composition of the labeling molecules on the particle surface should be avoided since it may also influence the stability and functionality of the nanoparticles. Thus, it is desired to fully observe the characteristics of each labeling molecule and to understand its effect when used in combination with other molecules in order to achieve the best Raman output while maintaining the functionailty of nanoparticles.

2.5 Synthesis Gold Nanoparticles with Functionality

Since metallic nanoparticles are usually being used as the backbones for SERS active substrates, it is important that they are synthesized to the desired size and morphology. In the last decade, extensive research efforts have focused on the synthesis of nanoparticles. The synthesized products made to date evolved from simple monomaterial nanostructures to complex multimaterial heterostructures. In general, the growth of nanocrystals is driven by the interplay between thermodynamic factors and interfacial kinetics, where several experimental conditions may come into play; for instance, suitable precursors, catalysts, templates, stabilizer molecules, concentration ratio of each species and temperature modulation. Recent studies have shown that nanoparticles can be synthesized into various morphologies, such as rods, wires, prisms, disklets, cubes, dog bones, multi branches and other unusual shape objects.[12][11] Surfactants are amphiphilic molecules consisting of a polar head group that is hydrophilic and a non-polar tail that is hydrophilic. The use of surfactancts usually plays a key role in nanoparticle synthesis in liquid solutions since they are able to modify the solubility and stability of nanoparticles. In some cases, they even serve as physical constraints to nanoparticle formation, where the surfactant micelles layers surrounding nanoparticles can control the direction of growth, inhibit growth rate, prevent aggregation or provide functional masks to the resulting nanoparticles. The surfactants that have been widely reported in nanoparticle synthesis studies are alkyl thiols, amines, carboxylic and phosphonic acids, phosphines, phosphine oxides, phosphates, phos-

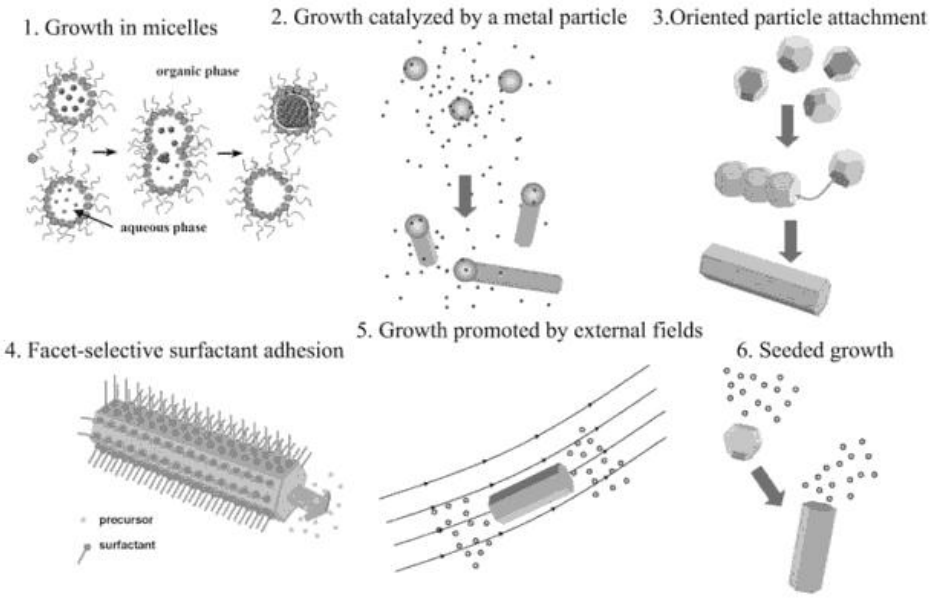

Figure 2.28: Anisotropic nanoparticles synthesis methodologies.[12][11]

phonates, and various coordinating or noncordinating solvents. The choice of surfactants is largely dependent on the application, since surfactant molecules with strong binding to nanoparticle surfaces may prohibit nanoparticle growing to the desire size and morphology, whereas weak binding surfactants may result in less uniform growth or aggregate formation in extreme cases.[12][11]

The most effective strategies in synthesizing naoparticles with anistropic shapes can be organized into the following categories: growth confined in micelles, growth in the presence of catalysts, seeded growth, oriented attachment mechanisms, surfactant or solvent induced anisotropy and anistropic growth with external fields. Schematics of each of the methodologies is shown in Figure 2.28.[12][11] The synthesis of nanoparticles encapsulated in micellar layers, provides a certain degree of control to the growth of nanoparticle shapes, and a success synthesis of various nanoparticle morphologies, such as rods, wires and platelets has been reported. The growth of the particles can be affected by the reaction and formation conditions inside the micellar bilayers and the morphology of particles are also likely to be confined by the micelle structures. However, this synthesis method is not suitable for materials that require annealing crystal defects in high temperature. Recent

studies have shown that anisotropic nanoparticles have been synthesized in the presence of catalyst particles in solution-liquid-solid phases and the synthesis of CdSe, InAs, InP, Si, Ge and branched CdSe composite colloidal nanorods and nanowires has been reported. The growth mechanism involves a solution of nanocrystal molecular precursors that are surrounded by layers of metal catalyst nanoparticles. Once saturated, the metal catalysts may exhibit preferential sites for molecular deposition and this deposition mechanism can cause an interruption to the particles' symmetrical growth, promoting the crystals' elongating growth. Oriented attachment nanoparticle growth begins by preparing a solution of isotropic nanocrystals where the particles are then synthetically fused along the axis defined by crystallography, where high energy facets are eliminated to achieve the minimal overall surface energy. The formation of wires, rings, rods and branched nanocrystals are a result of the connection of nanocrystals that are weakly passivated by organic ligands. The attachment process is encouraged by the dipole-induced interparticle attraction forces, so that the crystal growth in a particular direction is spontaneously promoted. The advantage of applying oriented attachment process is the ability to form anisotropic structures from symmetrical shaped particles, such as nanospheres, without using additional catalysts or additives. Surfactant directed growth mechanism can promote materials that crystallize in symmetric phases, but lead to anistropic shapes, such as discs, rods, wires. With different bonding strengths, the surfactants adhering onto the facets of the nanocrystals can lead to heterogeneous growth rates along the crystallographic directions where the final morphology of the nanocrystal is kinetically controlled by the equilibrium of thermodynamic and the concentration of monomers. The effects on the growth rate can usually be observed from facets that are protected less efficiently by organic ligands but overall, the growth mechanism evolves toward shapes that have a minimum overall surface energy. The best example to demonstrate anisotropic growth induced by external biases is the synthesis of magnetic materials in the presence of external magnetic field. In such configuration, the growth of the nanorods is preferably elongated along the magnetization axis. The advantage of this one-dimensional growth scheme is the positioning of the nanocrystals, for instance, between two electrodes where the growth can be directed along the field line. The seeded growth mechanism is often adapted to synthesize anisotropic nanoparticles from noble metals, such as silver, gold and platinum. The process consists of preparing nanocrystal seeds and mixing them with metal ion-surfactant complexes, where the seeds can serve as redox catalysts to promote metal ion reduction, enhancing heterogeneous nucleation along

with faster monomer addition to their surfaces. With the assistance of surface-selective adhesion of surfactants, nanorods, nanowires, and banched nanostructures formation has been observed using this synthesis. With a few modifications, the seeded growth process is capable of extending its control over the sizes and shapes of other materials.[12][11]

2.5.1 Implementing functional Nanoparticles

Once the particles have been synthesized to the desired size and morphology, they can go through an additional surface modification process by adhering to functional chemical groups and thus further increasing the application value of particles. One of the most widespread surface modifying processes is the formation of self-assembled monolayer (SAM) of functionalized molecules onto the surface of the particles and some examples of surface function groups often reported in literature are alkylsiloxane monolayers, fatty-acids on oxidic materials and alkanethiolate monolayers. The formation of self-assembled monolayers of alkanethiloates on gold surfaces is a spontaneous process, and the phenomenon has been extensively investigated, because of the potential to be applied in several areas, such as molecular recognition, biomembrane mimetic studies, selective binding of enzymes to surfaces, chemical force microscopy, metalization of organic materials, corrosion protection, molecular crystal growth, alignment of liquid crystals, pH sensing devices, patterned surfaces and conductive molecular wires, and photoresists.[15] In addition, the fabrication of gold SERS active substrate via the SAM-based technique has proven to be effective, since they can benefit from maximum coverage of Raman labels for high sensitivity, uniform molecular orientation within SAM for uniform signal recognition and selective label adsorption to particle surfaces for minimal noise signals.[20]

Typically, the thiol head group from an alkanethiol chain has a strong affinity to gold surfaces and when the head group is attached to the surfaces, the chain's tail group would point outwards from the surface to exhibit its designated functionality. The functionality of surfaces can be modified simply by changing the tail groups of the alkanethiol chain. By applying a molecule with multiple tail groups, a greater diversity of the functionality for the surfaces can be made. In addition, it is possible to modify of the tail groups after the SAM is formed on the gold surfaces, providing even more application versatility to the platforms.[15] Figure 2.29 is an illustration of a typical preparation procedure for SAM-based SERS active substrate. The process involves a silicon or glass support that is first

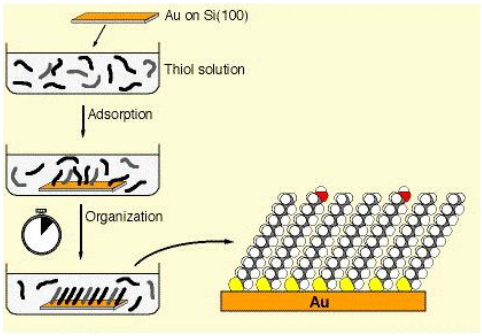

Figure 2.29: Formation of thiolate SAM on gold surface.[15]

coated with a thin layer of gold film and is immersed into a thiol containing solution for spontaneous assembly of the thiol groups onto gold surfaces. The initial adsorption process of the thiolates is usually random, but fast, then followed by an organized adhering phase where the intermolecular van der Waals forces allow thiol molecules to form rugged and highly ordered structures.[45][15] It is possible to produce a substrate with multi functional SAMs by immersing a piece of blank gold substrate into a solution containing a mixture of thiol groups. Nevertheless, the balance of the functionality exhibited by each thiol group depends on several factors, such as the mixing ratio in solution, alkane thiol chain length, solubility of the thiol groups, and the properties of the chain-terminating group.[15]

2.5.2 Novel Application of Functionalized Nanoparticles

Many of the current biomedical developments have shown that the attachment of thiol molecules to nanoparticle surfaces can be strategically implemented to modify the properties or the structures of nanoparticles; for instance, a study by Zubarev et al. demonstrated a two step surfactant replacement and thiol modification process that can make nanorods self assemble and form rings like structures. Figure 2.30 shows nanorods structures when the solvent is dried in air at room temperature.[42] Their synthetic process is one great real application examples to show that the thiol molecules can directly replace cetyltrimethylammonium bromide (CTAB), a strong capping agent, on the surface of nanorods. Following the replacement, the terminating group of the thiol chains can further be modified into polystyrene chains that can serve as expendable arms linking the nanorods with covalent forces. Franchini et al. also reported a study that directly replaces

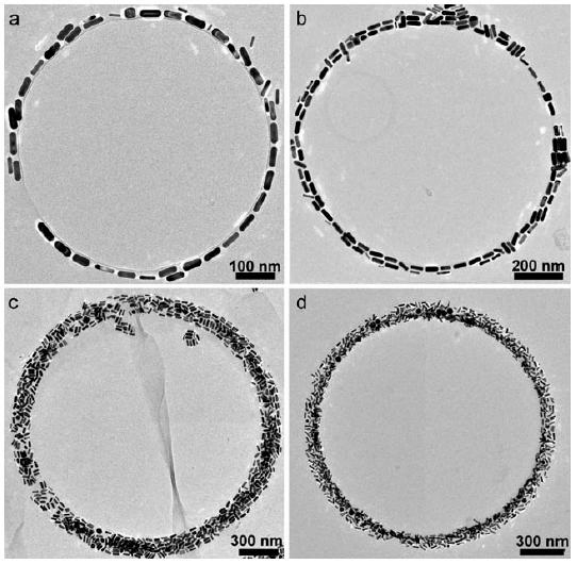

Figure 2.30: TEM of nanorods self-forming into ring like structures.[42]

CTAB on nanorods in water/alcohol mixture with thiol and polyethyleneglycol (PEG) terminal groups. They observed that with the replacement of CTAB, nanorods with ethyl 12-(4-mercaptobenzamido)dodecanoate (Number 2) ligand capping can be dispersed from a polar to a nonpolar phase. In the second phase exchange process, the ligand is reacted with PLGA-*b*-PEG-COOH groups to form PEG based polymeric nanoparticles, where the particles regain their ability to be dispersed in aqueous solution. Figure 2.31 shows the dispersion of the a)CTAB capped nanorods,b)ethyl 12-(4-mercaptobenzamido)dodecanoate capped nanorods and c)rods capped with polymer blocks in polar and nonpolar mixture, where the top phase is water and a chlofrom phase is in the bottom. The UV-Vis spectra of each rod solution is represented in black, red and green, respectively.[21] From a practical point of view, the surfactant replacement process in the two phase systems ensures that the rods are functional in the required phase and that it also prevents particle aggregation once the CTAB is removed. CTAB is a well known cationic surfactant that is commonly used as an anisotropic growth and aggregation protective substance for nanorod synthesis. However, as pointed out by Niddome et al., free CTAB molecules in nanorod solutions are cytotoxic and not removable by traditional centrifugal methods. They made a comparison study on the *in vitro* effect of PEG-SH protected nanorods with the traditional CTAB

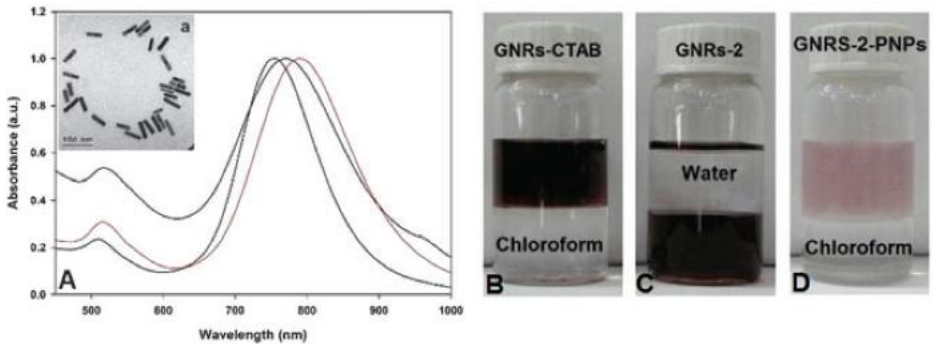

Figure 2.31: The UV spectra of CTAB capped nanorods, ethyl 12-(4-mercaptobenzamido)dodecanoate capped nanorods and rods capped with polymer blocks in polar and nonpolar mixture are shown in A) with corresponding mixture images shown in B), C) and D).[21]

protected nanordos. Their results showed that after the intravenous injection into a mice, 54% of the PEG-modified gold particles are found in blood at 0.5 h, where as almost all the CTAB coated gold nanorods are detected in the liver.[63]

Based on the modification of functional groups on the surface of nanoparticles, a number of studies have developed new methodologies in fabricating SERS substrates. One application ready substrate that has been developed is the assembly of spherical gold nanoparticles with functionalized gold nanoplates, as shown in Figure 2.32. The nanoparticles can be readily assembled onto the plate using dithiol linker molecules that attach to gold surfaces with two ends. This enables the self formation of SERS "hot-spots" on site on the nanoplates. On the other hand, Kim et al. developed novel SERS substrate consisting of gold nanoapricles on nanowires that also produced high SERS intensity.[39] With features such as multiplexing enabling, high portability, and function-modification ready, the design of these SERS substrates are a new class of nanomaterial that can be easily employed into many of the current pharmaceutical and security applications. The synthesis strategies from these studies provided valuable insight for the fabrication of SERS substrates used in this study.

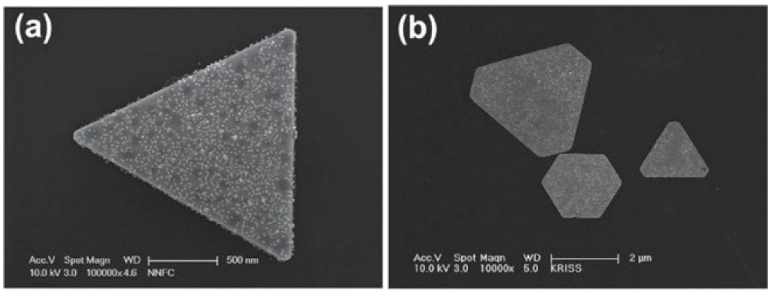

Figure 2.32: Gold Nanoparticles assembled on gold microplates.[29]

Chapter 3

Experimental Methods

3.1 Materials

Hexadecyltrimethylammonium bromide(CTAB, 98.0%), L-ascrobic acid(99.0%), trisodium citrate dihydrate(99.9%), poly(vinylpyrrolidone)(PVP10), sodium borohydride($NaBH_4$, 99%) tetrachloroauric(III) acid($HAuCl_4 \cdot 3\,H_2O$, 99.9%), N,N-dimethylformamide(DMF, 98.0%) were purchased from Sigma-Aldrich. Tetrahydrofuran(THF, 99.0%) was purchased from Caledron. All the chemicals are used as received from the suppliers. Deionized water was used in all solution preparations and experiments. The labeling molecules are 1,4-benzenedithiol, 4-nitrobenzenethiol, 2-naphthalenethiol, 4-aminobenzenethiol, benzenethiol and 4-quinolinethiol; these were also purchased from Sigma-Aldrich.

3.2 Nanoparticle Synthesis

The Frens method was adopted for the synthesis of gold nanoparticles.[18]. In brief, a 50 mL of 2.5x10^{-4}M of aqueous gold solution was prepared and heated to boiling while stirring. To synthesize small particles, 1.0 mL of 34x10^{-3}M trisodium citrate was added to the gold ion solution and, after boiling for three minutes, the solution was removed from the heating plate. The solution color changed from pale yellow to red, indicating the formation of gold nanoparticles . To synthesize large particles, 0.21 mL of 34x10^{-3}M of trisodium citrate was added to the hot gold solution and stirred for eight minutes. The

colour of the resulting solution appeared to be darker than the nanoparticle solution of smaller particles. These solutions were used within a month of their preparation.

3.3 Nanoplate Synthesis

Gold nanoplates were synthesized from the protocols of Huang.[10, 34] Large platelets were synthesized by first preheating 30 mL of 8.33x10^{-4}M trisodium citrate solution and an aqueous solution containing 1.25x10^{-3}M $HAuCl_4$ and 7.5x10^{-3}M CTAB. Once they had both reached 50°C, the gold and CTAB solution were injected into the hot trisodium citrate solution with moderate heating and stirring. In 30 minutes, the solution temperature was gradually increased to a final temperature of 82°C and maintained at this temperature for a further 10 more minutes to complete the reaction. During this process, the colour of the mixture would turn from orange yellow to transparent and then finally into goldish colour with flaky appearance. Once the reaction is completed, the mixture was removed from the heating mantle and left to cool for future use. The gold colour indicates the formation of large gold crystal structure. The plates would precipitate and settle at the bottom. Small plates were synthesized by similar procedures; first, 15 mL of 1.67x10^{-3}M trisodium citrate was heated to 68°C with stirring. Then, 10 mL of $HAuCl_4$ and 7.5x10^{-3}M CTAB mixture was preheated to 50°C and injected into the trisodium citrate solution with rapid heating. An indication that a reaction occurred is that the orange solution would turn into navy blue, indicating the formation of small nanoplates. After five minutes, the temperature reached 82°C. The solution was then removed from the heating plate.

3.4 Nanostar Synthesis

Nanostars were synthesized according to Liz-Marzan et al. method with some modification.[51] To prepare the nanostars, the seed solution was first prepared. Citrate coated small nanoparticles were used as the seeds for the star growth but before they were injected into the growth solution, they were treated with a PVP coating.[24] To coat the citrate seeds with PVP, 3.45 mL of 25.6 g/L PVP10 aqueous solution was first mixed into 40 mL of the small nanoparticle solution, then stirred overnight at room condition. 15 mL of the PVP coated particle solution drawn from stock was then centrifuged at 2500 rpm

for 10 minutes. After centrifugation, the supernatant was removed and the precipitate was redispersed in 5 mL of ethanol for another round of centrifugation. Once again, the supernatant was removed and the remaining seeds were redispersed in 1 mL of ethanol to be used for nanostar growth. The growth solution was prepared by adding 82 μL of 50 mM $HAuCl_4$ into 15 mL of DMF containing 10 mM of PVP10. Once the growth solution was prepared, 43 μL of PVP coated gold seeds in ethanol was injected into the growth solution and left undisturbed overnight at room temperature. The colour of the growth solution would turn from pink to grayish blue, indicating gold nanostar growth.

3.5 Nanorod Synthesis

Gold nanorods were prepared by using the seed growth method developed by Murphy et al.[36, 19] To synthesize the seeds, 20 mL of an aqueous solution containing 2.5x10^{-4}M $HAuCl_4$ and 2.5x10^{-4}M trisodium citrate was first prepared. Then, 0.6 mL of 0.1M $NaBH_4$ was injected into the mixture while stirring at room temperature. Upon the addition of the reducing agent, $NaBH_4$, nanoparticles formed as indicated by a colour change of the solution from pale yellow to orange red. The $NaBH_4$ reduced seeds were used within five days of preparation. The growth solution for the nanorods, which consists of 2.5x10^{-4}M $HAuCl_4$ and 0.1M CTAB, was then prepared, usually in 50 mL portions. The solution was then transferred into three test tubes, labeled A, B and C, each containing 9 mL of the growth solution. Before the seeds were added to the growth solution, 0.05 mL of 0.1M ascrobic acid was added into each of the test tubes and the solution colour would change from yellow to clear, indicating the change of gold ionic state, from Au^{3+} to Au^{+}. 1mL of the seed solution was then added to test tube A and and was gently mixed by inversion. After 15 seconds, 1 mL of solution A was added to test tube B and was gently mixed. 30 seconds later, 1 mL of solution B was transferred to test tube C. Test tube C was then left undisturbed overnight to complete nanorod growth. During the growth process, the colour of the solution would turn from red to purple, which is a typical sign for nanorod growth.

3.6 Particle Characterization

The nanostars, nanoplates and nanorods were centrifuged at 2500 rpm for 10 minutes and the supernatant was discarded. The remaining material was redispersed in water; in the case of nanostars, ethanol was used. The centrifugation was repeated until the supernatant appeared to be clear to ensure that excess surfactants were removed before they were analyzed by the UV-vis spectrometer and transmitted electron microscope (TEM). No further treatments were done on the nanoparticles. All the sample solutions were handled by a syringe during the transfer to carbon-Formvar-coated 400 mesh copper grid and quartz cuvettes. The UV-vis absorption spectra was obtained from an Ocean Optics USB4000 Spectrometer with ISS-UV-VIS Integrated Sampling System. The TEM images were obtained from a Philips CM10 microscope. ImageJ software was used to measure the average dimensions of the nanoparticles.

3.7 Preparation for SERS Detection

The substrates of gold chromed on silica were obtained from Dr. Tsui, fabricated on-site at the University of Waterloo. The gold substrates were cut into multiple 0.5 cm^2 pieces by a glass cutter. The surfaces of each gold pieces were marked with multiple dent spots to serve as markers for on-spot SEM analysis and SERS detection. The substrates were initially cleaned by soaking them into a highly corrosive piranha solution, and rinsed by deionized water to remove residual. Then, to attach the substrates with labeling molecules, the labeling molecule solutions were first prepared. Using ethanol as the solvent, 40 mL of $5x10^3$ M 4-nitrobenzenethiol, 2-naphthalenethiol, 4-aminobenzenethiol, benzenethiol and 4-quinolinethiol solutions were prepared in separate test tubes. The architecture of the sandwiched SERS substrates, as shown in Figure 3.1 provides more uniform binding of the analyte molecules throughout the surface of the substrates. This structure has been adopted in several preliminary SERS studies.[65][46] To make sandwiched structured substrates, once the labeling molecule solutions were prepared, the small gold platform piece were submerged into a petri dish filled with labeling molecule solution and left undisturbed overnight to ensure full monolayer coverage of molecules on substrate surface. The tagged gold substrates were taken out of the petri dish and rinsed with ethanol to remove any excess PVP and displaced molecules. Once rinsed and dried, the gold pieces were submerged

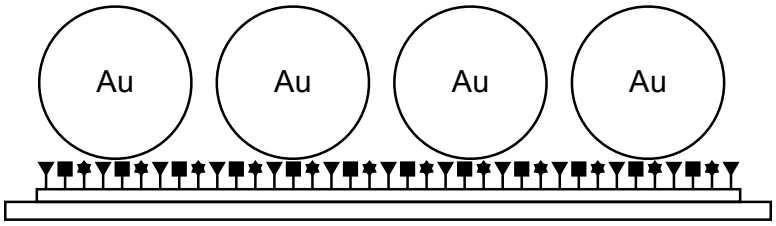

Figure 3.1: Schematic of a sandwiched structure.

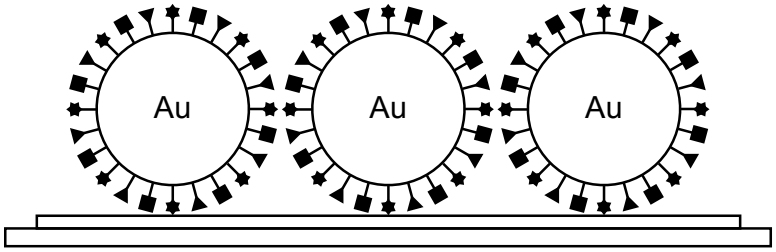

Figure 3.2: Schematic of an aggregated structure.

into the nanoparticle solutions for eight hours and left undisturbed for at least 4 hours. The samples were taken out of the gold particle solution, dried in air, and then taken to the SEM and SERS analysis. The aggregated structure, as shown in Figure 3.2, is a the traditional method of preparing SERS substrates. Since the labeling species are directly binded to the nanoparticles surfaces, sometimes more analyte molecules can be filled in a space confined in between particles depending on the surface structure of nearby particles. To make aggregated structure substrates, test tubes containing freshly prepared nanoparticles are centrifuged and the supernatant discarded. The nanoparticle residue was then redispersed with the labeling molecule solution with the assist of sonication. The resulting solutions were left disturbed overnight. To remove the excess labeling molecules, the labeled nanoparticle solutions were again centrifuged and the supernantant was removed, but this time the particles were redispersed in a clean ethanol solution. This process is repeated again to ensure complete removal of the labeling molecules. The resulting samples are dip dropped on to the gold surface substrate and, once dried, it is then sent to be analyzed by a SEM and SERS analysis. The SEM is a LEO FESEM 1530 high-resolution SEM with Carl Zeiss lenses and the SERS used to conduct the study is a Horiba Jobin Yvon LabRAM HR Raman spectroscopy system. SERS measurements were taken with

a 633 nm laser using the D1 filter, a 50x objective lens, a 250 μm confocal hole and a 1800 nm^{-1} grating. The acquisition time was set at one second with two average repeated readings to reduce the CCD transistor discharge. In order to ensure reproducibility of SERS measurements, efforts were made to find a dark spot or an assumed aggregated area on the substrates to take the SERS measurement readings.

3.8 Preparation for Particles-Thiol-Plates Substrate

The preparation of the particle-thiol-plate substrate follows a modified version of the protocols reported by Han et al..[29] First, 50 mL of the 15 nm gold nanoparticles were prepared by the citrate synthesis method and 50 mL of the microplates are prepared from the CTAB assisted nucleation growth under heating, as described previously. The freshly made microplates were then separated into 20 mL vials, each containing 10 mL of solution, and set ready to be used for the surfactant-thiol exchange process. Then, two 40 mL of 10 mM of benzendithiol and benzenethiol solutions were prepared by adding 0.046 mL of benzenedithiol and 0.041 mL of benzenethiol into 40 mL of THF solvents, respectively. Since the formation of thiolate SAM is a slow process, the rest of the process must be carried under a fumehood to prevent the organic solvent from escaping. To do a direct exchange of CTAB with benzenedithiol, the 10 mL of plate solution under rapid mixing was added to the benzenedithiol/THF solution. Drop by drop, the addition of the thiol solution takes approximately 20 minutes, until the final amount of 10 mL is reached and the mixture is left stirring overnight for the completion of the exchange process. The exchange process is then repeated for the preparation of benzenethiol-plate substrate. To make the final particles-thiol-plate substrate, 1 mL of the nanoparticle solution was added to the thiol-exchanged plates with thorough overnight mixing. Finally, the particle-thiol-plate solution transferred from the fumehood to prepare the SEM sample. The solution is dip dropped onto a piece of silicon wafer with an area of 1 cm x 1 cm and left to dry at room condition.

Chapter 4

Result and Discussion

4.1 Nanoparticle Characterization

4.1.1 Spherical Nanoparticles

The resulting spherical nanoparticles produced from the Frens method using 1 mL and 0.4 mL of sodium citrate capping are shown in Figure 4.1 and the respective TEM images of the nanoparticles are shown in Figure 4.2. The images reveal that the synthesis of nanoparticles are successful by the observation of colour changes of the nanoparticle solution since the solutions show a typical reddish and purplish colour that is emitted in nanoscale form.. Unless the appearance of the solution is blackish or else the nanoparticles are well protected by citrate from forming aggregates. The TEM images shown are the magnified physical view of the nanoparticles and it can be seen that with more citrate added, smaller and rounder nanoparticles are produces since the particles' nucleation and growing process is confined to stronger micellar structures. The growing in nanoparticle sizes have resulted in a change in color due to the deviation of the particles' surface plasmon, leading to a change in their optical properties, such as absorbance and scattering. From the TEM images, it can also be observated that the nanoparticles are well spaced from each other, ensuring that aggregates are unlikely and the particles can be redispersed into solvents. Checking for aggregation ensures that the particles are more stable to handle and have a much longer shelf life.

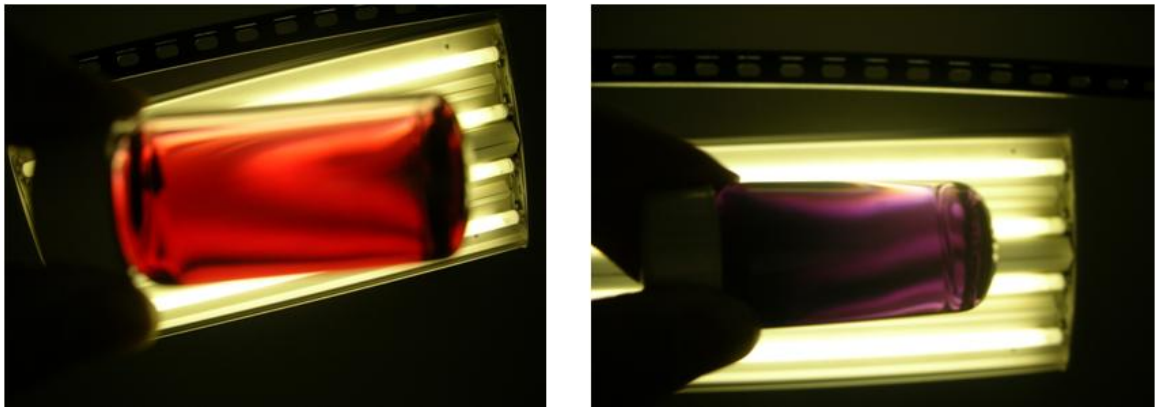

Figure 4.1: Appearance of 1 mL(left) and 0.4 mL(right) citrate capped gold nanoparticles.

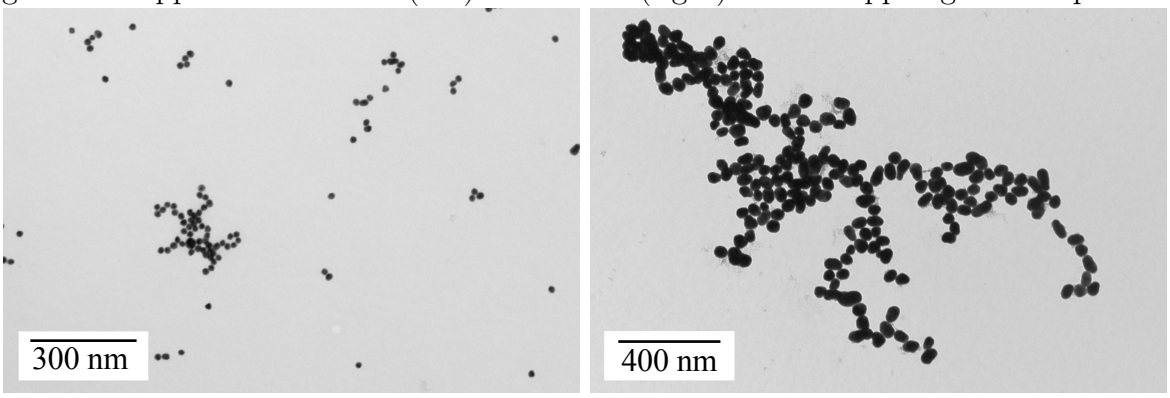

Figure 4.2: TEM of 1 mL(left) and 0.4mL(right) citrate capped gold nanoparticles.

Spherical nanoparticle are then synthesized with 1, 0.8, 0.6, 0.4, 0.3 and 0.2 mL of citrate capping in order to observe the relationship of the particle sizes with the amount of citrate added. With the TEM images of nanoparticles in digital form, ImageJ software is able to analyze the sizes of the particles by a length comparison of the on screen object and to the TEM image scale via the means of pixel values. The tabular and graphical relationship shown in Table 4.1 and Figure 4.3 summarize the effect of citrate concentrate on particle diameter sizes and the shift of absorbance maximum respective to each solution. It is observed that as the particles' diameters are in a reciprocal relationship respect to the particle citrate concentrations. Although the average particle diameter can be increased as the amount of citrate is decreased, overall the particles' sizes and shapes may gradually deviate from uniformity with increase in sizes where as indicated by the

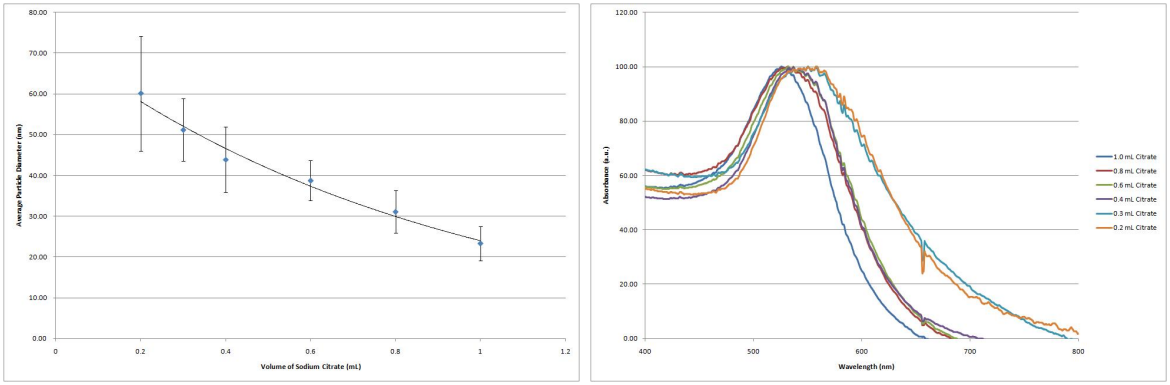

Figure 4.3: Graphical relationship of citrate volume and particle sizes and their respective absorbance spectra.

error bars. The absorption spectra of the nanoparticles shows that when the nanoparticle sizes are increased, the maximum abosrbance are more red-shifted and the findings are in agreement with the study reported by El-Sayed et al..[53]

Table 4.1: Summary of citrate volume effect on gold nanoparticles.

Citrate Volume(mL)	Particle Diameter(nm)	Diameter Variance(nm)	Lamda at Maximum(nm)
1.0	23.32	4.23	525.985
0.8	31.07	5.21	531.915
0.6	38.72	4.92	532.410
0.4	43.86	8.01	536.850
0.3	51.16	7.65	550.535
0.2	60.15	14.11	558.280

4.1.2 Nanorod Characterization

Pure gold nanorods are prepared from the seed-mediated growth developed by Murphy et al. where the quality of nanoparticle seeds have a great impact on the nanorod growth. The seeds are prepared by another protocol where the nucleation process is initiated by the addition of NaBH and CTAB is used as the capping agents. Using this particular method, small nanoparticle seeds can be produced without using heat and the sizes usually fall in the range of 5 nm. In addition, the stability of the seeds are better than the ones with citrate capping since CTAB can produce a much stronger cap.[36] For a typical nanorod growth, once the seeds are injected into the growth solution, CTAB in solution would form

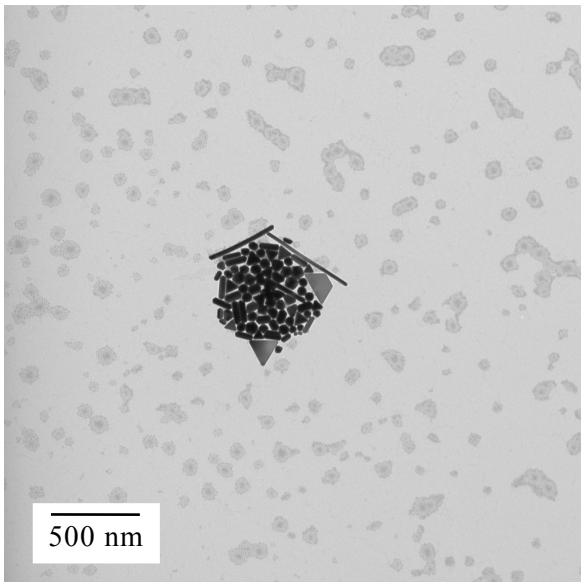

Figure 4.4: Nanorods synthesized using seed-mediated growth method.

elongated bilayer structures over the growing seeds surfaces and the nearby gold ions are fused to the seeds to form the rod structure. To be more specific, due to the reduction of $AuCl_4^-$ to $AuCl_2^-$ by ascorbate and bromide ions, the resulting $AuCl_2^-$ absorbed CTAB micelles has a controlled kinetics where the collision is more abrupt at the elongated tips of the seeds, leading to rod formation.[32] After the CTAB capped seed have been injected into the growth solutions, they are left undisturbed overnight for the remainder of the rest of growing process; the final form of the samples are purplish with sparkling white flakes and they are prepared for the examination by the TEM, as shown in Figure 4.4. The image reveals that the samples are a mixture of platelets, sphere and rods, where the majority are spheres and this result may not be the most desirable for application use. However, with repeated experimenting, the synthesis results show no signs of improvement and thus, a continuing effort have been put to synthesis gold nanorods with high yield.

Not surprisingly, many research groups also have encountered a similar problem of producing low yield high aspect ratio nanorods and therefore, various kinds of strategies have been proposed to improve the yield. The second set of the nanorod synthesis performed in this study follows the protocol described by Huang et al. and it is a modified synthesis based on Murphy's version.[33][32] The difference in the protocol is that it has

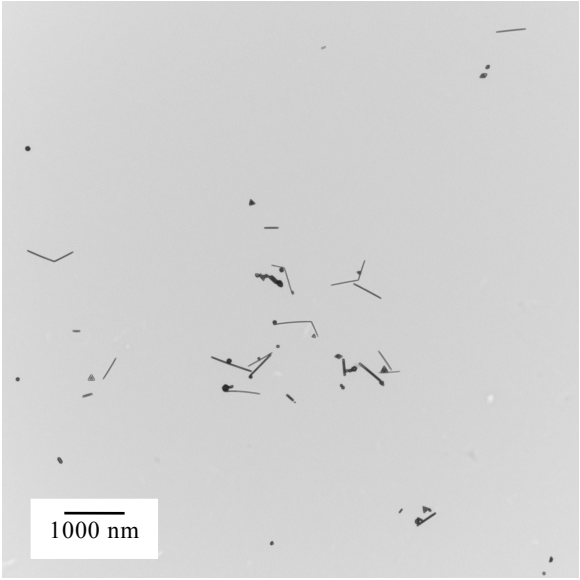

Figure 4.5: Nanorods synthesized using seed-mediated growth method with nitric acid.

an additional step where various amount of nitric acid is added into the growth solution to assist the formation of nanorods, achieving high magnitude in both aspect ratio and yield. Huang's group has shown that their high aspect ratio nanorod synthesis can achieve a high yield as high as over 90%. The group has observed that the nitrate ions play a key role in the growth of long rods because they can react to form cetyltrimethylammonium nitrate(CTAN) CTAN is a surfactant that has a lager aggregation property and micellar sizes compared to the ones formed by CTAB and at high concentrations, the CTAN micelles also has a stronger tendency of forming ellipsoidal or rod-like structures. Nevertheless, since the replacement of bromide ions with chloride ions has an impact on the overall nanorod growth by reducing micellar sizes and forming more spherical particles, it is desired that an appropriate amount of nitrate ions are added to the growth solution to significantly assist the yield of the long nanorods. They also have claimed that using CTAB cappings allows a strong inhibition to the growth of nanoplates compared to citrate ions which may undesirably modify the crystal growth direction. Nevertheless, despite the high yield synthesis reported by Huang et al., the actual synthesis result obtained from using their protocol are shown in Figure 4.5. The experiment has been conducted repeatedly and all of them have shown consistent result. Typically, the yield of rods have increased

but not to the potential point of 90% as claimed by Huang et al.. Another protocol by Kim et al. was shortly followed and they have claimed that nanorods with aspect ratio of 200 have been synthesized in acidic solutions.[44] Their procedure is similar with the ones claimed by Huang's group but they have used less seeds to initiate the rod growth and a higher volume of nitric acid in the growth solution to. They also have mentioned that low pH is the main driving force to favor the growth of nanorods, as they also have observed long rod growth by substituting HNO_3 with HCl and H_2SO_4. However, the substitution of the acid with $NaNO_3$ salt has generated products that are similar to the ones obtained without acid and this result is in disagreement with the mechanism claimed by Huang et al.. By following the protocol described by Kim's group, nitric acid in the volume of 200 μL, 100 μL and 50 μL are added into the growth solutions for each trial. However, when excess nitric acid are added to the growth solution, the growth solution quickly forms gel like substance and this gel formation makes the growth solution much harder to handle; for instance, the seeds can not be mixed throughly with gentle shaking and since a substantial amount of dilution is required to prepare the sample for TEM analysis, the resulting particles are scarce to find under the microscope. Even if the particles were found, they are mostly composed of spheres and thus, the synthesis is considered to have no significant improvement in production of long rods with high yield. An extensive experiment have been repeated by adjusting the concentration of HNO_3 but the maximum tolerance for the amount of acid to be added to the growth solution without forming gel is similar to the amount claimed by Huang's protocol and therefore, the addition of acids has already revealed its potential in producing high yield nanorods. The investigation of the producing high yield nanorods has been continued with a strategy reported by Murphy et al., whom have tried using strong base, NaOH, in the rod growth solution and their results show that the rods have higher aspect ratio than the ones obtained from HNO_3.[5] They have explained that the increase in the proportion of the gold rods are due to the increase in the pH value since the condition favors the formation of ascorbate monoanions, an effective reductant in the presence of CTAB and also adsorbs better to the end faces of the growing nanorods while can effectively reduce Au(III) and Au(I) intermediates. Rather than the combination of ascorbic acid and hydroxide, the use of sodium ascorbate as the reducing agent to promote the growth of nanorods is much more effective than ascorbic acid itself. Nevertheless, balancing the ratio of CTAB/ascorbate/intermediate Au(I) complex ions is not straight forward, as further increasing in the pH value to 5.6 not only can lead to

higher proportion of rods but also higher polydispersity. The study from Murphy et al. has suggested the use of NaOH in nanorods synthesis, but the results obtained from actual experiment are similar to the ones obtained from acidic condition.

The nanorod synthesis has been continued with the change of surfactants since many research groups have emphasized the importance of surfactants to nanopartilce synthesis and a majority of surfactant studies have been based on the three step growing protocol with CTAB. Mulvaney et al. has organized a review work in connection with nanorod production with aqueous solution and they have drawn out the important characteristics of surfactant used in the nanorods growth.[69] For instance, CTAB is better than CTAC, Cl^- and DTAB in terms of rod reducing ability. Although surfactants with longer chain length has lower solubility, they can be offseted by using higher temperatures. The critical micelles concentration for CTAB is 0.8 mM while the optimal CTAB:$HAuCl_4$ concentration ratio is in a narrow range that the precipitation can happen at ratio of <10:1, while higher CTAB concentrations can lead to a reduced in aspect ratio. In addition, although the bromide ions alone do not form nanorods in the growth solution, they are better rod-inducing agent than Cl^- in the presence of CTA^+ ions. The effect on the rod growth with addition of ionic salts, such as NaCl, $NaNO_3$ and NaBr, are similiar to each other, reducing the aspect ratio of the rods but an increase in ionic strength can reduce the overall rod yield. They also pointed out that the existence of CTAB not only can direct gold ions to the particle tips, but also can retard the growth of other types metallic structure. Lastly, $AgNO_3$ is not required to control the aspect ratio of rods but it can stablize the seeds and thus increase the rod yield. The inconsistency of the rods synthesis from lab to lab have actually concerned Korgel et al. and they have done interesting study to addressed the issue that the low reproducibility is actually affected by the impurities in the CTAB.[76] In the study, they have performed a controlled set of experiment using the same nanorod synthesis protocol but using CTAB surfactants produced by different manufactures and the resulting rods are analyzed with UV-Vis spectrometer, TEM and SEM. Despite that all of the surfactants have been specified with high purity, they have found that some of them actually did not form rods. Although in the initial report they are not able to identify the substance even with analysis by size exclusion chromatography, XRD, NMR, and mass spectrometry initially, it is later revealed by an inductive coupled plasma mass spectroscopy that iodine is what prevents the formation of the rods. The CTAB surfacatants that failed to form rods in the samples are identified with relative high

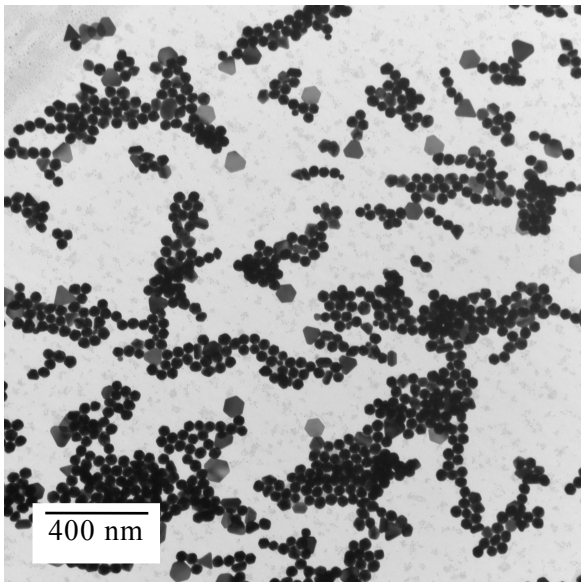

Figure 4.6: Nanorods synthesized using seed-mediated growth method with C_{12}TAB.

impurities concentrations compared to the ones that formed rods, with the lowest impurity value of less than 2.75 ppm up to a value of 839.27 ppm. From what the group has learnt, the iodine can possible effect the growth of nanorods by etching the gold seed surfaces, acting as a redox agent that can effect the reduction of Au(III) to Au^0 and binding to Au {111} surfaces that prevents further Au deposition of the facet. [13] Another study done by Murphy et al. has examined the effect of alkyltrimetylammonium bromides, particularly C_{10}TAB, C_{12}TAB, C_{14}TAB, C_{16}TAB, have on the growth of nanorods.[19] They have found that as the lengths of the alkyl chains are increased, higher-aspect-ratio nanorods are formed and the respective absorption maximum are extended from 520 nm to beyond 2000 nm. The effect that longer chain length can result in higher aspect ratio have been explained by the mass-action model using empirical data which concludes that the dynamic formation of a zipping bilayer on gold surfaces via hydrocarbon tail length promotes the stabilization to the growth of longer nanorods. In response of their findings, an actual synthesis has been performed using the same three step rod growing protocol by switching to C_{12}TAB in order to observe the effect of using different surfactant and a TEM image of the result is shown in Figure 4.6. From the image, it can be observed that the particle formed are mostly spherical with a few platelets and some short rods

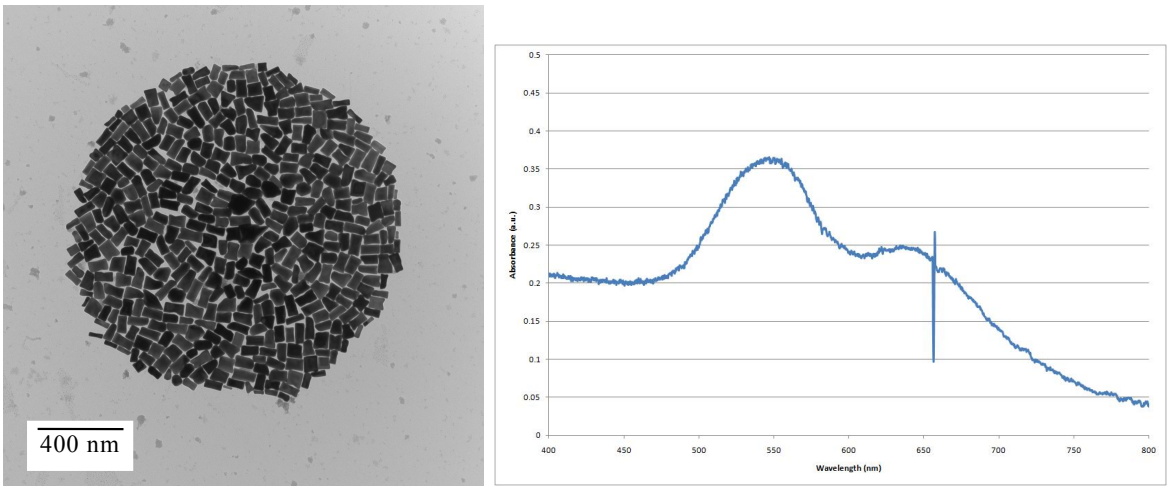

Figure 4.7: Nanorods synthesized using seed-mediated growth method with $AgNO_3$.

and if observed more closely, some of the particles are actually forming hexagonal and pentagonal like edges. This result is comparable to Murphy's rods using C_{10}TAB and it showed distinctive contrast to the original rods synthesized from CTAB, shown Figure 4.4. The distinctive comparison hints that the modification of surfactants can definitely be the solution of producing high rod yield. High yield rod synthesis are commonly reported with emphasizing on the addition of silver nitrate as additives in the synthesis solution and the reason that it is not desirable for the purpose of this project is because of the biocompatibility properties of silver. Nevertheless, to understand the possible effect of additives on the surfactants and more importantly, to verify that the stock chemicals are viable to produce nanorods, a small sample of rods with the addition of silver nitrate are produced, as shown in Figure 4.7. From the samples' TEM image, it can be seen that the particle are in rod like structures with low uniformity but they are self-assembled into a circular pattern. The sample does exhibit some rod characteristics since the absorbance spectra for the sample shows both distinctive longitudinal and transverse peaks and these observations have made an indication that the quality of stock chemicals are not a major concern in the project. The findings from the rod synthesis are in good agreement with the study by Murphy et al. whom have concluded that nanorods synthesized without silver ions as additives are in relative low yield but are much longer, with aspect ratio of roughly 20. In contrast, with the presence of silver ions, the nanorod formation can be

easily quantified but with highest aspect ratio of being roughly five and the reason the rod lengths are restrained is due to the differences in crystallography compared to the ones made without silver ions. In the synthesis without silver nitrate, rods are formed in pentatetrahedral twins with five {111} triangular facets on the ends of the rods and {100} facets on the long sides of rods. From the preliminary HRTEM analysis of the rods synthesized with silver nitrate, the short rods are made into single crystalline, with a possible {111} facets on the long side of the rods. The radical change in the growth structure is likely due to the formation of silver bromide which can adhere onto the surface of the gold seeds, slowing the kinetics of the rod growth to from into a single crystalline structure. The rest of rod formation is due to the silver bromide laying on the {111} plane of the crystals which makes the reduction available on other faces and thus producing rods with {111} facets on the long side.[72]

Some studies have proposed strategies that can be implemented into the three step synthesis with or without silver nitrate to assists the rod yield. For instance, several reports have indicated the concerns over the mixtures of sizes and shapes of the synthesized nanoparticles and elaborated the importance of post-synthesis treatment to classify nanoparticles accordingly. Several methodologies to separate the nanoparticles in suspension to produce the narrowest distributions have been proposed, such as size exclusion chromatography, electrophoresis methodology and centrifugation.[84][27] Centrifugation process can be simply adapted to provide efficient separation of nanorods from a typical synthesized mixture consisting of colloidal rods, spheres and plates.[73][42] In the most ideal condition, the purification process begins with rods that are synthesized with silver nitrate to produce high yield nanorods and therefore, only one or two repeated steps of centrifugation, precipitation and redispersion process is required for the purification of rods. The separated supernatant are usually collected and treated using a similar set of separation process, until a single size of nanorods are collected. The separation is possible based on the hydrodynamic behavior of the nanoparticles of various shapes since the drag forces leading to sedimentation are shape-dependent. Nevertheless, the methodology has a drawback of not able to archive its effectiveness with particles that are similar in sizes and a duration of the centrifugation has to be precise for each sample since over centrifuging may result in all particles going to the bottom. From the literature, the centrifugation process are usually carried under high speed, ranging from 5600 to 13000 rpm, and the higher the rotating speed, the less time are used. As for the separation processes that are carried out

through this report, the efficiency is much lower due to the inconsistency of the synthesized nanorods, making the estimation of the speed and time of centrifugation setting difficult. Under centrifuging the samples usually has no effect on the sample but over centrifuging can cause samples to form precipitation of rod aggregation and whitish, flaky CTAB that are not fully dissolved at the bottom of the centrifugation tube. A set of experiments has also been done by centrifuging tubes of heated nanorod solution where the CTAB are fully dissolved but after the centrifugation process, it is observed that the CTAB forms a transparent gel like substance and is precipitate at the bottom of the test tube along with the nanoparticles, making the particle retrieving process much harder. Another strategy that can be implemented into the nanorod synthesis to improve the yield without adding silver nitrate is to grow the rods in low temperatures. The strategy is simple yet the most effective compared to other techniques that have been tested. Yun et al. has explained that temperature changes influences the critical micellization concentration which can also effect the surfactant structural formation behavior and the characteristics of the micellar template. From a cryogenic-TEM study, the shape of the micelles structure are observed to deviate from spherical to cylindrical structures as the temperature is decreased.[68][4] In addition, lowing the temperature slows the reduction rate of gold and surface diffusion, where the interactions of the CTAB and gold on the stabilized surfaces may lead the crystal growth to a preferential direction.[8] However, lowering the temperature of decreases the solubility of the CTAB and can cause more precipitation and therefore more difficulties for post synthesis purification.

A little success is finally achieved in producing high yield long rods following a trial and error scheme by implementing different modifying elements in the three step synthesis protocol. A TEM image of the sample and its respective aborbance spectra is shown in Figure 4.8. In this synthesis, the growing procedure is reduced from three to two steps because when a three step process is used, usually no rods are formed and it is suspected with over diluting the seeds which leads to not enough nucleation sites. The second change to the synthesis is that 50 μL of 0.1M of NaOH has been added into every 10 mL of the original growth solution and once the growth solution is added with the seeds, test tubes are inserted into a water bath set at 4°C. The test tubes are left undisturbed overnight and the separation by centrifuge is carried out at 3000 rpm for 10 minutes where precipitation is treated with dilution for TEM analysis. As seen from the TEM image, the particles are mostly long rods with some unreacted seed particles and a few fraction of plates.

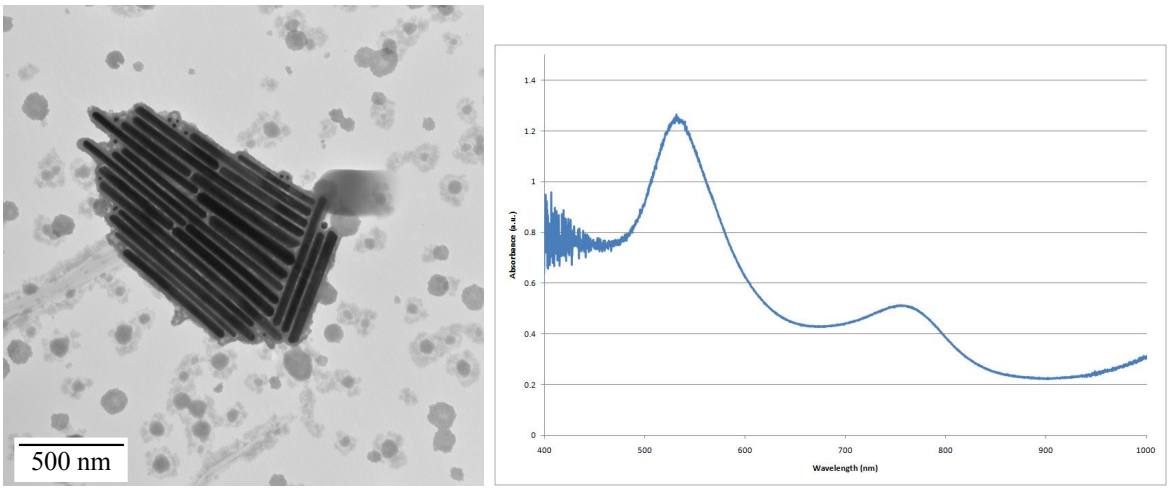

Figure 4.8: Nanorods synthesized using seed-mediated growth method with NaOH at 4°C.

These rods are comparable to the rods synthesized by Jana, who reported the rods in high surfactant concentrate would self-assembled and form into organized packs.[35] However, the rods synthesized in low temperature are contained with much more excess CTAB due to the their low solubility and they are much more difficulty to separate from the rods but it does indicate that the rod formation are closely related to the strong binding of the surfactants. The absorbance spectra of the long rod solution shows both distinctive peaks referring to the transverse and latitudinal maximum and in comparison with Figure 4.7, the long rods has a wider latitudinal shift than the shorter rods. However, the absorbtion spectra of the long rod over the range of 900 nm does show an upward increase trend but is cut off by the limitation of the instrument and this may have indicated that a spectra with wider detection range is necessary to obtain the full spectra of the much longer rods.

4.2 Nanoplate Characterization

The gold microplates are synthesized following the protocol by Huang et al. where $HAuCl_4$ is thermally reduced in aqueous solution with the presence of trisodium citrate and CTAB. Although the plate synthesis is simple to perform, to reproduce the result of the plate synthesis, however, demands a strict control in a set of parameters, such as the stirring rate, heating rate and heating time. Appropriate amount of CTAB and trisodium citrate

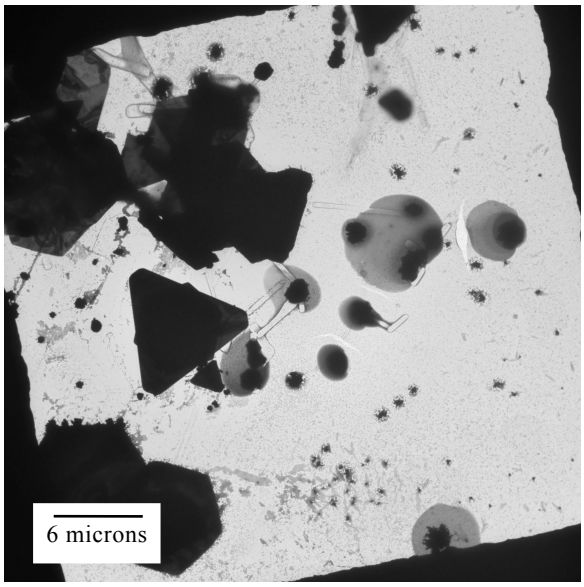

Figure 4.9: A TEM image of gold microplates.

is can also effect the facilitation of plate growth. The variance in such parameters may result in plates with various size and shape compositions, mainly hexagons, triangles, truncated triangles and occasionally some unusual shapes. The final appearance of the plates solution is golden, filled with sparkling flakes and Figure 4.9 shown is an actual TEM of the resulting synthesized microplates where the size of the plates are roughly one micron to five microns. From Huang's observation, the growth of the microplates is a result of rapid nanostructure formation, aggregating towards a center of fused mass. The formation of plate is carried on as the center mass, a gold polycrystalline continues to incorporate nearby blossoming gold nanostructures, eventually forming into a plate morphology. The SEM of another plates sample in Figure 4.10 and in this sample, the edges of plates are rough and this may indicate the intermediate plate product. From the literature, such structural characteristic also found from plates produced even after 30 minutes of reaction but products with sharper edges can be obtained formed from further reaction. Huang's group has also proposed a strategy of synthesizing smaller nanoplates using the same thermal aqueous solution approach and the resulting small nanoplate solution appears to be purplish. The synthesis is carried under higher temperature but short heating time interval; in consequence, using more heat promotes faster nucleation and where the crystal

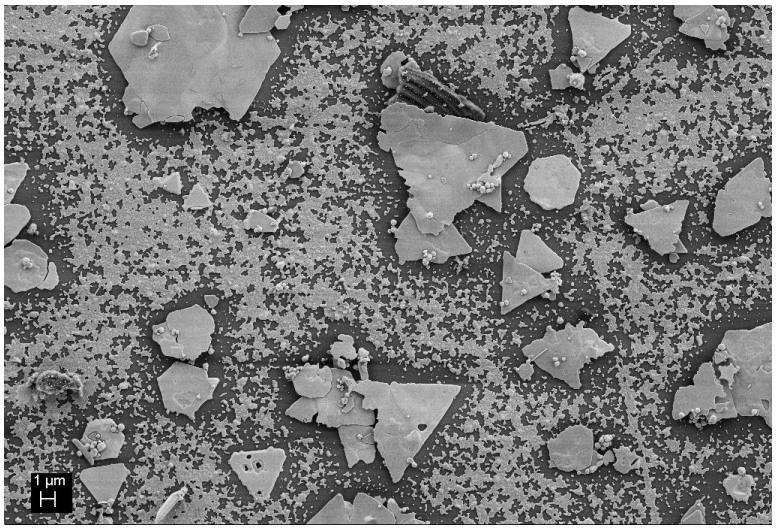

Figure 4.10: A SEM image of gold microplates.

size growth is limited by the amount of ions presented. Since the making of the smaller nanoplate requires less temperature control and growth time, the reproducibility is much higher than the larger plates. Nevertheless, due to the small volume of growth solution is heated at such a high temperature, the sample can be easily overheated and the resulting plate solution may consist of larger spheres and aggregated structures. The TEM image and the absorbance spectra of a sample is shown in Figure 4.11 and the SEM images from the respective sample is shown in 4.12. The images confirms the formation of small nanoplates, mainly consisting of small triangles crystallines and other sharp edge particles, and the the particle are ranged from 20 to 60 nanometers which is in a good agreement with the ones in Huang's report. The absorbance spectra is also similarity where the maximum peak can be observed at around 600 nm but the peak is much boarder, indicating a broader size range and anisotropic shapes of the particles compared to the sphere's spectra.

4.3 Nanostar Characterization

The very preliminary nanostar samples are synthesized according to the portocol from Liz-Marzan et al. but under high heat and therefore, the resulting nanoparticles are formed with rough surface features, as shown in Figure 4.13. The rough surfaces may have been

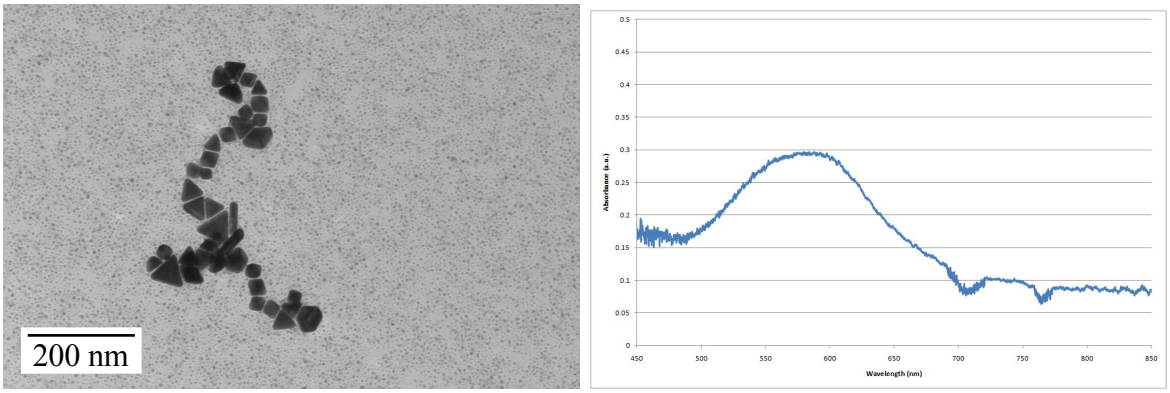

Figure 4.11: TEM image and absorbance spectra of small nanoplates.

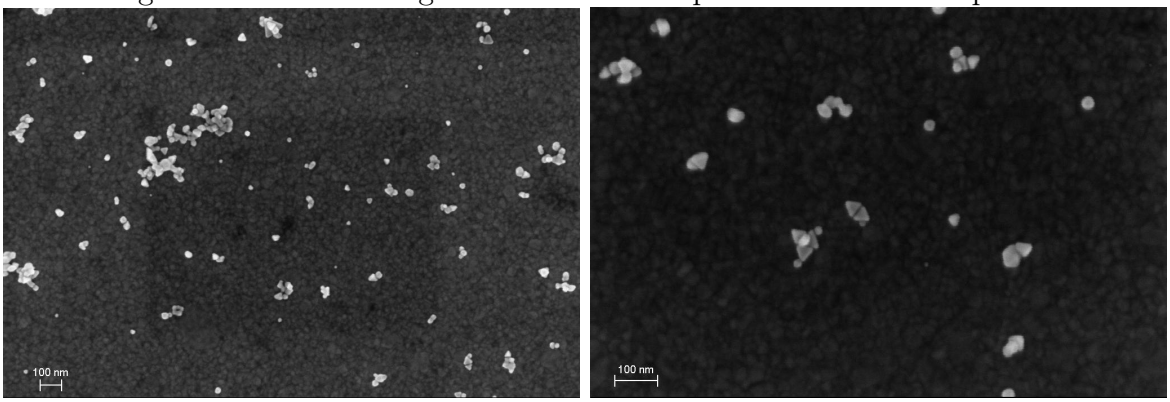

Figure 4.12: SEM images of small nanoplates

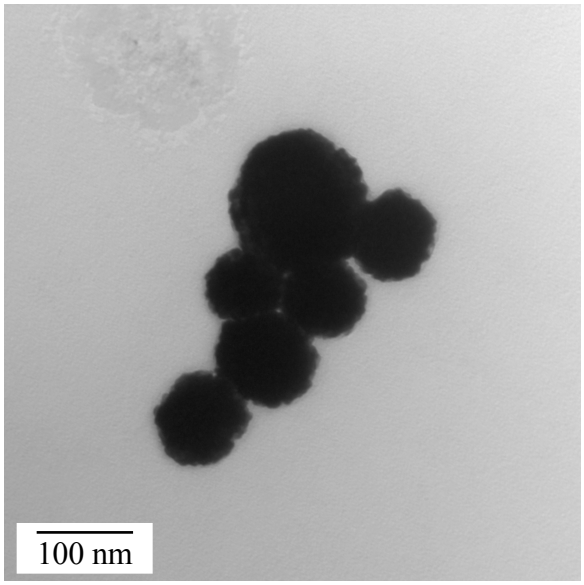

Figure 4.13: Size distribution of synthesized nanostars

caused by the heating of the capping PVP, a water soluble polymer, which may have resulted in a softened shell for the reduction of gold. The result from this synthesis is another good example to show how heating can influence the growth of a nanoparticle. The nanostars are successfully synthesized in later trials without any external energy source applied and the stars in DMF appears to be grayish. A TEM and absorbance spectra of a sample is shown in Figure 4.14 and an addition SEM image of the nanostars is shown in Figure 4.15. From the TEM image, the nanostars are in high yield and appear to be in the size range of 50 to 150 nm in diameter with random length and orientation of branches pointing outwards. The consistent observation has been foun from the SEM image but more surprisingly, the stars are self-assembled into packs which may have been caused by the affinity of excess PVP surfactants. The key factor to the growth of the stars is the reducing effect of PVP in DMF where it is reported that using higher concentration of PVP in the synthesis can result in longer branches. With the analysis using HRTEM, Liz-Marzan et al. has reported that the tips of nanostars have a {011} growth direction, suggesting higher surface energy for {110} facets in comparison with {111} and {100} facets, as commonly observed from an fcc lattice. Although the absorbance spectra of the nanostars can only be observed from 450 to 850 nm due to the limitation of the instrument, it can still be

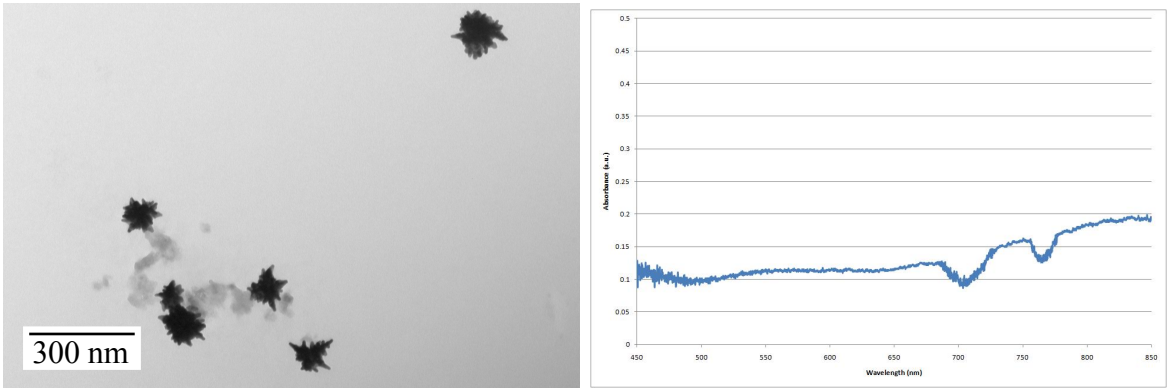

Figure 4.14: Nanostars

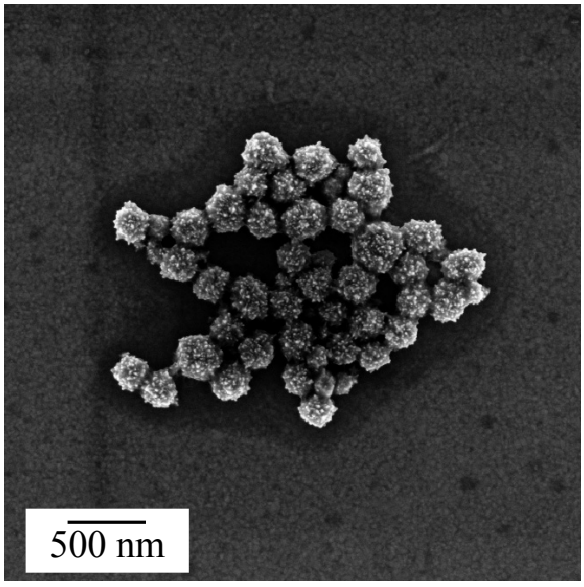

Figure 4.15: SEM nanostars

observed that the maximum peaks at around 840 nm. The absorbance is attributed to the dipolar resonance localized either at the tips or the center core of the particles. To precisely quantify the optical response of the gold nanostar structure, Liz-Marzan et al. has carried out an optical model study with boundary element method which can be applied to objects with rational shapes and axial symmetry. Their result shows that the number of tips on the nanostars is irrelevant to the positioning of longitudinal resonance wavelength but aperture angles and the roundness of the tips are effective factors. A study by Norlander et al. has used a numerical approach to describe the origin of the plasmon effect from gold nanostars but it is not discussed due to the scope of this report.[23]

4.4 Multiplexing on Flat Gold Substrates

In the preliminary multiplexing experiment, five molecules consisted of 4-nitrobenzenethiol (NBT), 2-naphthalenethiol (NPT), 4-aminobenzenethiol (ABT), benzenethiol (BT) and 4-quinolinethiol (QT) are all being tested for the Raman multiplexing capability. It is observed from multiplexing results with sandwiched structure using nanospheres to conclude that the combination that has the most types of analyte with the least amount of overlapping and the most stable response is by using BT, QT and NBT. The molecules are shown in Figure 4.16 with their respective pure Raman spectra obtained from Aldrich FT-NMR, FT-IR and FT-Raman Libraries, shown in Figure 4.17. From the observation of the molecule structures, it can be seen that all three molecules have at least one aromatic ring with an sulfur bond adhesive to the gold surfaces and it is expected that the benzenethiol would have taken up the least bonding space compared to quinolinethiol which would have taken the most due to the structural size of the two connected aromatic rings. With dif-

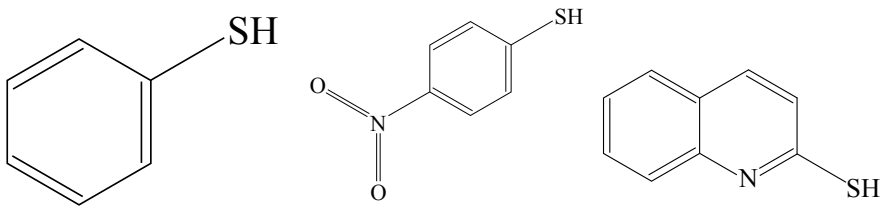

Figure 4.16: Benzenethiol(BT), 4-quinolinethiol(QT) and 4-nitrobenzenethiol(NBT) molecules.

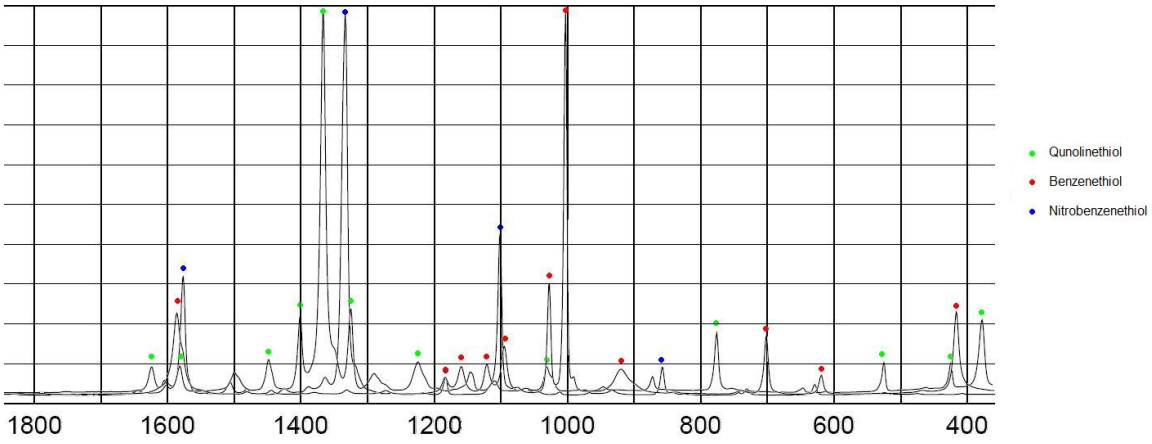

Figure 4.17: Reference Raman spectra of pure BT, QT and NBT molecules.

ferent molecular structures, the Raman spectra for each molecule features different signal pattern; for instance, the major peaks for BT in the reference Raman spectra are found to be located at 993, 1015, 1066, 1563 cm^{-1}. For QT, the peaks are at 1084, 1317, 1365, 1431, 1466 and 1578 cm^{-1} and for NBT, they are 845, 996, 1069, 1099, 1135, 1324, 1420 and 1562 cm^{-1}. By overlapping all three spectra into one forms a reference multiplexed spectra where the unique peaks for each molecule are assigned for easier identification. The overlapping of the actual SERS spectra of each molecule and the multiplexed spectra obtained using small nanoparticles aggregates are shown in Figure 4.18. The three spectra of each molecule are in good agreement with the ones from the reference spectra but some peaks in the multiplexed spectra are missing. The remaining peaks in the multiplexed spectra are often the result of the similar peaks form each molecule that are overlapping each other but there are peaks that are uniquely featured from each of the labeling molecules. For BT, the unique labels are assigned to be 994 and 1017 cm^{-1}, QT label is assigned with 1360 cm^{-1} and NBT is with 1324 cm^{-1}. In addition, the intensity of the peaks attributed by each molecule may appear to be different depending on the multiplexing combination since the surface plasmon phenomenon can be complexed by factors such as the localized density of the molecules contributing to the intensity, localized particle configuration, the nature of the bonds and the attachment configuration of the molecule. Figure 4.19 shown is the actual microscopical view taken from from SERS instrument at 50x magnification from a preliminary sample consisting of labeled aggregated nanospheres self assembled on to the

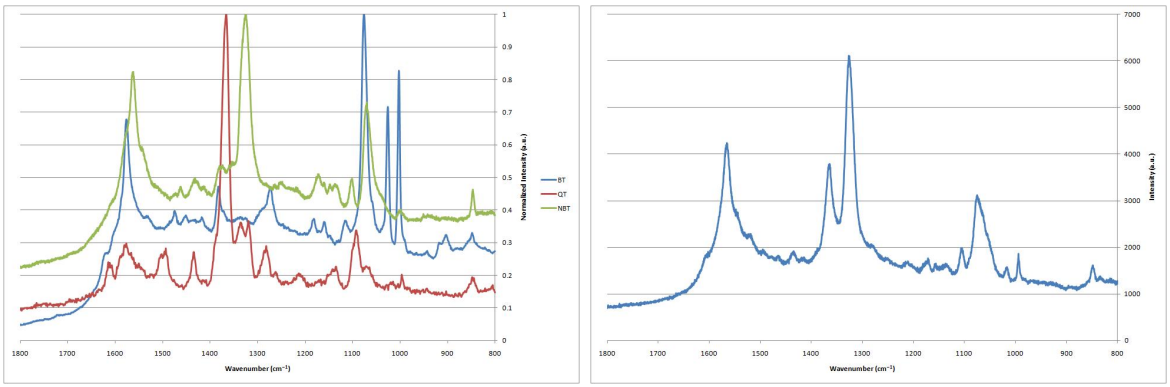

Figure 4.18: Actual SERS spectra of BT, QT and NBT molecules.

gold film that is approximately 25μm in diameter chromed on glass. The nanoparticle are formed into a few large islands appearing as black clumps and with distorted smaller dots covering the rest of the gold surface; the detailed formation of the nanoparticle structure cannot be determined. Figure 4.20 are the SEM images taken from the same sample. Although the SEM imaging is expected to be able to examine the nanoparticle structure on the film surface, the images highlights the troublesome in relocating the SERS measurement spots since the particles are randomly packed and distributed on the platform surfaces. Applying physical markers on the surface of the substrates merely can assist the process of relocating the spot and it also has a high risk of damaging the particles and the substrates. The difficulty applies to both the aggregated and sandwiched structures of the SERS substrates since the main issue is that the SERS instrument can only observe the substrates' surface using a 50x magnitude lens so only the larger particle aggregates can be observed. Nevertheless, even though a majority of the measurements are taken at the aggregated spots, the signals are often consisted of random noises or no peaks at all. In addition, fabricated at the nanoscale magnitude, the sample is quite sensitive to any movement and positioning so it becomes very difficult to readjust to the exact location where the SERS measurement is taken for examination, not even mentioning to correctly observing the localized molecules on the particles surfaces that are contributing to the SERS measurement. Therefore, as for a preliminary experiment analyzing the construction of the SERS substrate with different particle morphologies, repeated measurements are taken from random spots on each substrate and only the ones that appear to have the correct peaks are recorded. Four spectra are recorded for each sample and only three are

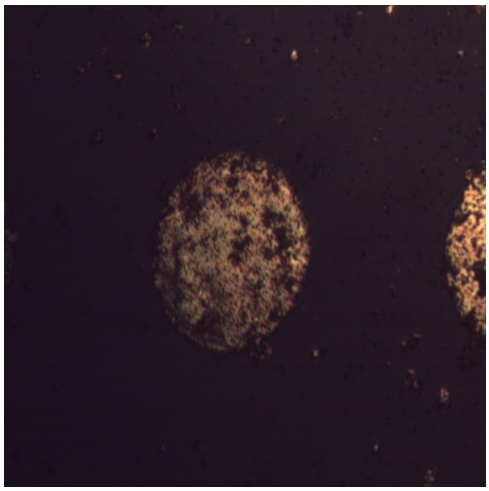

Figure 4.19: SEM image of the SERS substrate reveals random nanoparticle packing.

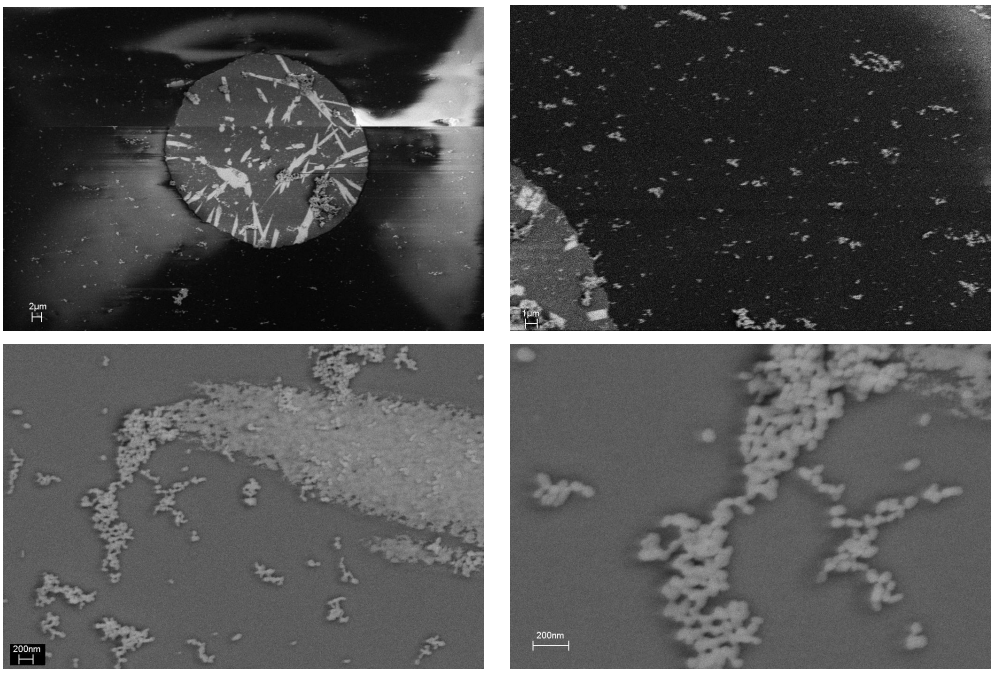

Figure 4.20: SEM image of the SERS substrate reveals random nanoparticle packing.

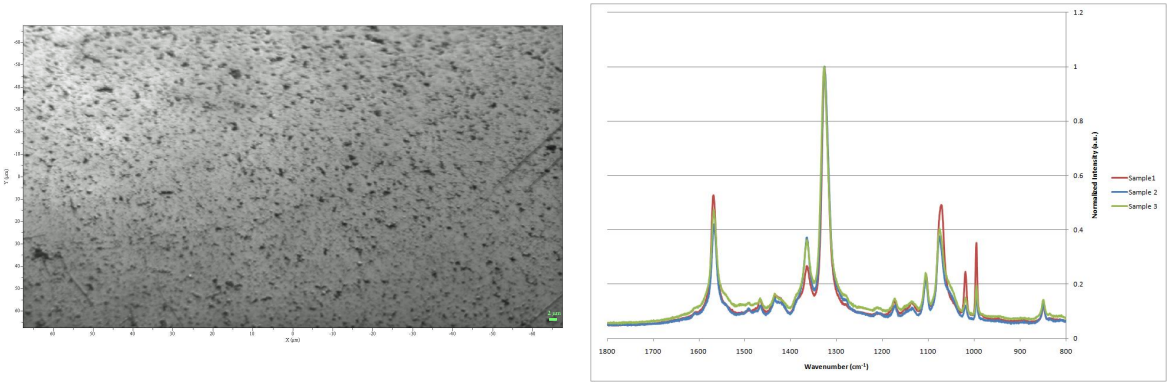

Figure 4.21: Multiplexing results from small spheres with sandwiched construction.

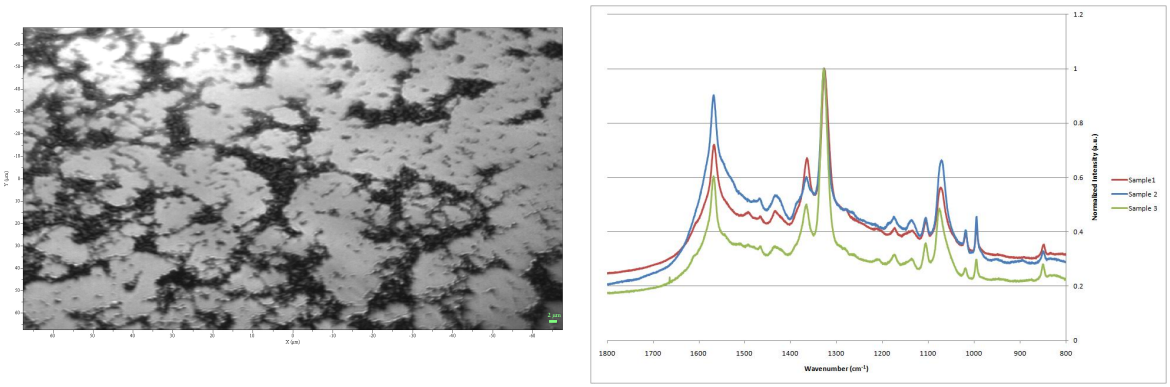

Figure 4.22: Multiplexing results from large spheres with sandwiched construction.

shown.

4.4.1 Sandwiched Structures

A 50x microscopical view of the substrate constructed of using sandwiched structure with small spheres and the respective multiplexed spectra obtained from the substrate is shown in Figure 4.21. With this spectra, the unique peaks for BT at 994 and 1017 cm^{-1}, QT at 1360 cm^{-1} and NBT at 1324 cm^{-1} can be clearly identified and the intensity of the peaks are consistent within the three measurements. Figure 4.22 shown the multiplexed spectra observed from the large spheres fabricated with sandwiched structure. Compared to the

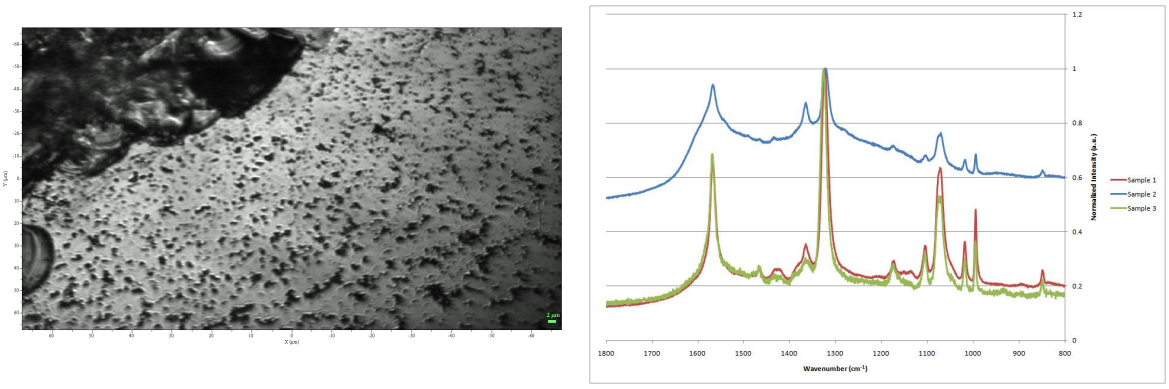

Figure 4.23: Multiplexing results from small nanoplates with sandwiched construction.

spectra of the small spheres, the spectra has a small deviation in the intensities and the broadness of the peaks and this can be a result of the differences in packing density and increase of particle sizes featuring broader size ranges. The background signal may also play a role in the deviation but despite the variations, the spectra from the large particles can also clearly identify the three molecules' unique peaks.

The multiplexed spectra obtained from the small nanoplates with the sandwiched structure is shown in Figure 4.21. The spectra features are generally similar to the ones obtained from small spheres and perhaps this is due to the similarity in sizes and the plasmon resonance properties are less affected. Nevertheless, except for one of the spectra where the peaks are substantially shorter and wider than the others and the primary explanation to the observation is the differences in the shapes of the nanoparticles. As for the results obtained from large nanoplates constructed with the sandwiched structure shown in Figure 4.24, the multiplexed spectra are less meaningful due to the poor ability of identifying the three molecules. The reason that there are no spectra features is because the size of large plate is much larger than the light source amplitude so that the resonance effect can not be created. The orientation of the plates may also play a role since a plate laying flat to the surface can cover up the molecule underneath and therefore, the actual detection is located at the top of the lying plate. Nevertheless, the result does provide an insight to how the SERS measurement is responding to the recognition of different shape configuration.

The sandwiched rod substrate is fabricated with rods synthesized following the original three step recipe since they require less time to produce and is much easier to handle. The

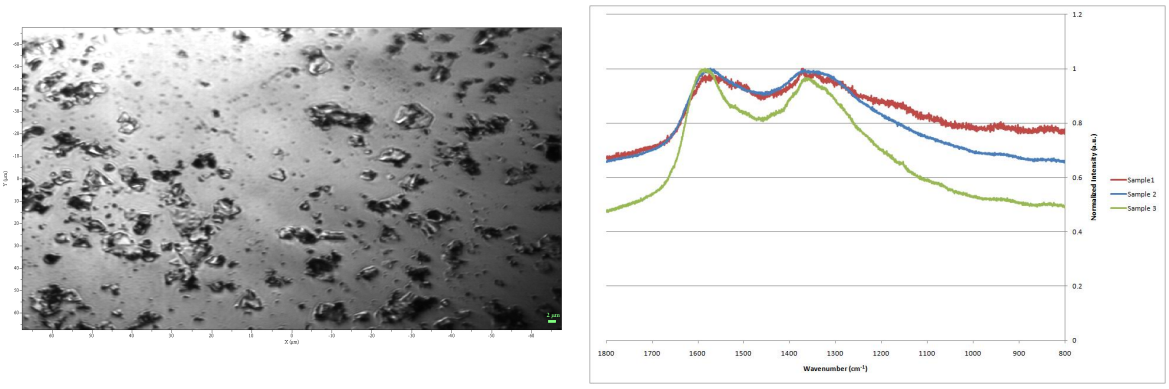

Figure 4.24: Multiplexing results from big nanoplates with sandwiched construction.

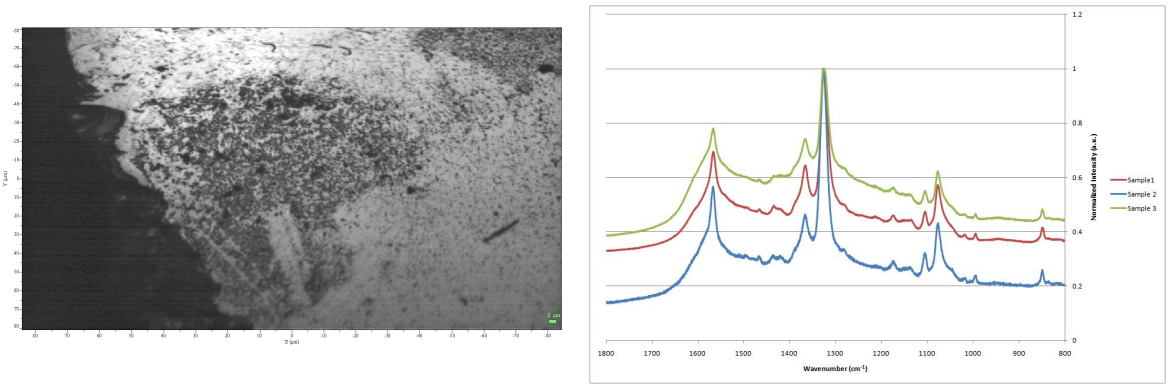

Figure 4.25: Multiplexing results from nanorods with sandwiched construction.

microscopical image and the spectra of the resulting rod substrate is shown in Figure 4.25. The spectra is comparable to the spectra obtained from the large spheres and this can be due to the poor quality of rods. Instead of forming into rods, the majority of the seeds added into the growth solution are forming into large particles and even platelets and this may also be the reason that the effect of rod features on the SERS measurement less noticeable. Nevertheless, the multiplexing detection ability for this substrate is pleasing since it can be seen that all the unique peaks from the three molecules can be identified and the signals produced from the rods are fairly consistent except for the deviation in the background reference signals. Figure 4.26 shown is the multiplexing spectra of the sandwiched nanostar substrate. The peaks from this spectra is observed to be shorter and wider compared to

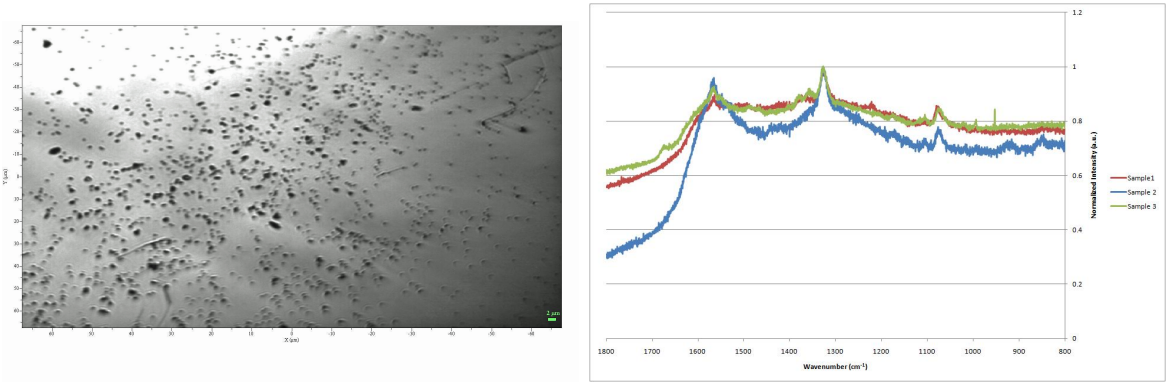

Figure 4.26: Multiplexing results from nanostars with sandwiched construction.

those obtained from the large spheres and small nanoplates and even less appealing, the main unique peak of the QT molecule is not showing on the spectra. Since SERS is based on the resonance effect of the molecules confined within a space between two particles, the concentration of BT and NBT must be condensed within the space of the nanostars. One of the hypothesis is that due to special structure of the nanostar spikes, there is a higher chance for the smaller sizes molecules, BT and NBT, to adhered on the spike surfaces since they can adhere more freely and require less space. Another hypothesis is that due to the dense packing of the polymer coating on the nanostars, the bigger labeling molecule is prevented from adhering to the gold surface but this is less likely, since similar effect is not seen on the particles coated with CTAB, which also offers dense packing to nanoparticle surfaces. The study by Vo-Dinh et al. has mentioned that the intensity of SERS among stars is related to the ratio number of labeling molecules to the branch tips, and the larger the fraction, the grater the anticipated intensity.[43] Nevertheless, due to the complexity morphology of nanostars, modeling and quantifying the enhancement factor are extremely hard to attain.

4.4.2 Aggregated Structures

The microscopical view of the substrate fabricated with small spheres employing aggregated structure and the respective multiplexed spectra is shown in Figure 4.27. From the microscopic observation, the aggregated nanoparticles are forming into a big black spot on the gold surface, suggesting a dense, populated packing within the region. The multiplexed

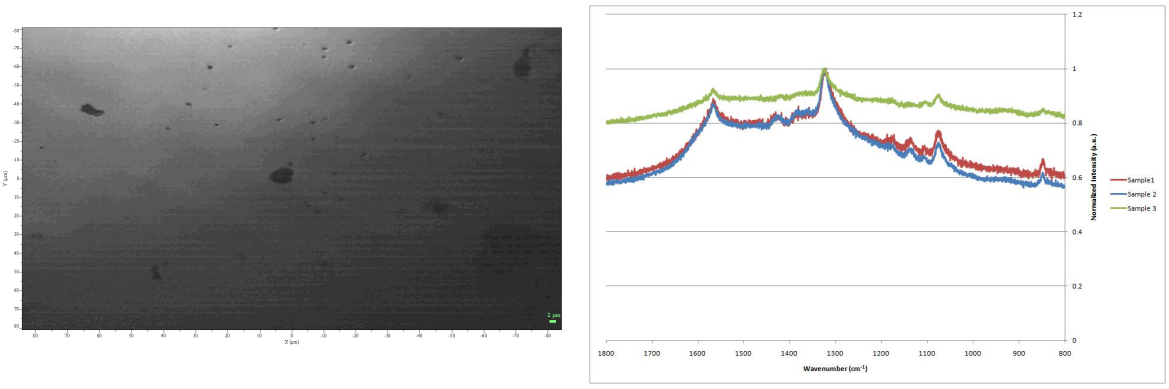

Figure 4.27: Multiplexing results from small spheres with aggregated construction.

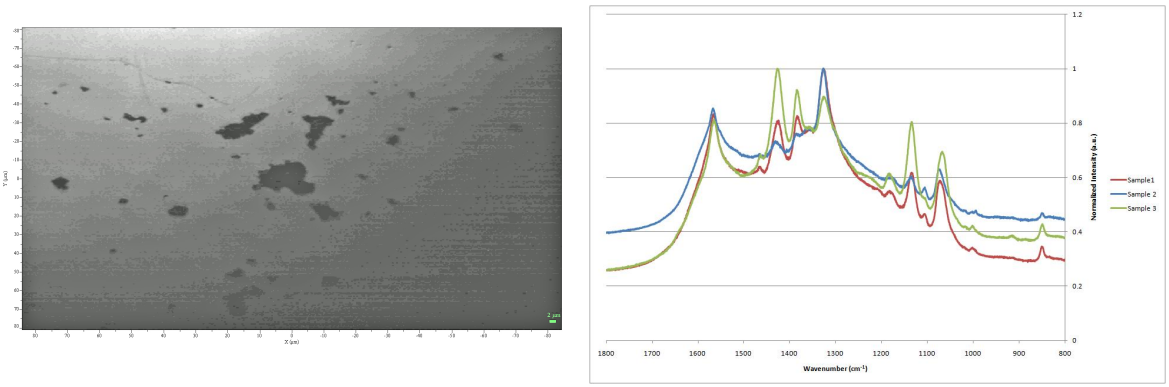

Figure 4.28: Multiplexing results from large spheres with aggregated construction.

spectra shown is very similar to the ones produced by the nanostars substrate fabricated with the sandwiched structure where short and wide peaks are observed and yet again, the unique peak for QT is not identified. These similarities in the findings is in agreement with the hypothesis that BT and NBT molecules can be more densely confined within smaller particle spaces, such as gaps in between nanosphere aggregates. On the other hand, Figure 4.27 shown is the multiplexing spectra from large spheres employing the aggregated structure and it can be seen from the spectra that the unique peaks of the three molecules can be identified with greater details. Nevertheless, when the spectra is compare to the one obtained from the large sphere substrate fabricrated with sandwiched structure, the peak at 1426 cm^{-1} appears to be more intense and this could be a result of the aggregated

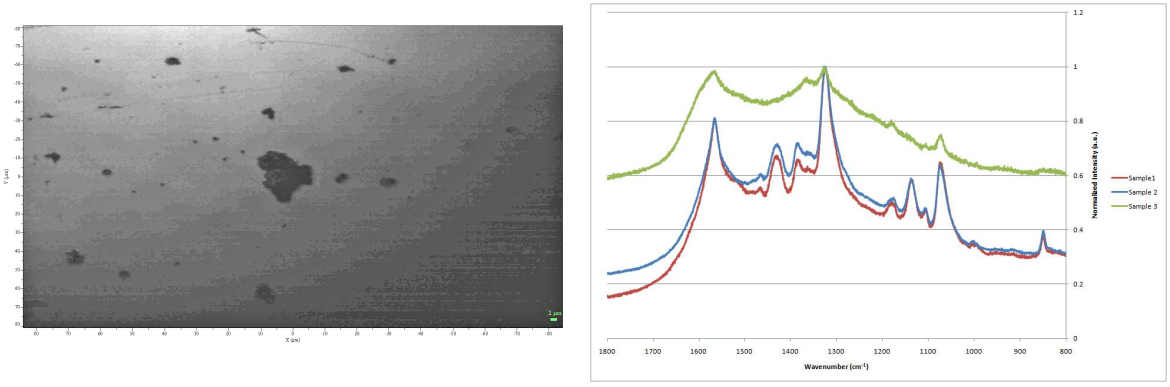

Figure 4.29: Multiplexing results from small plates with aggregated construction.

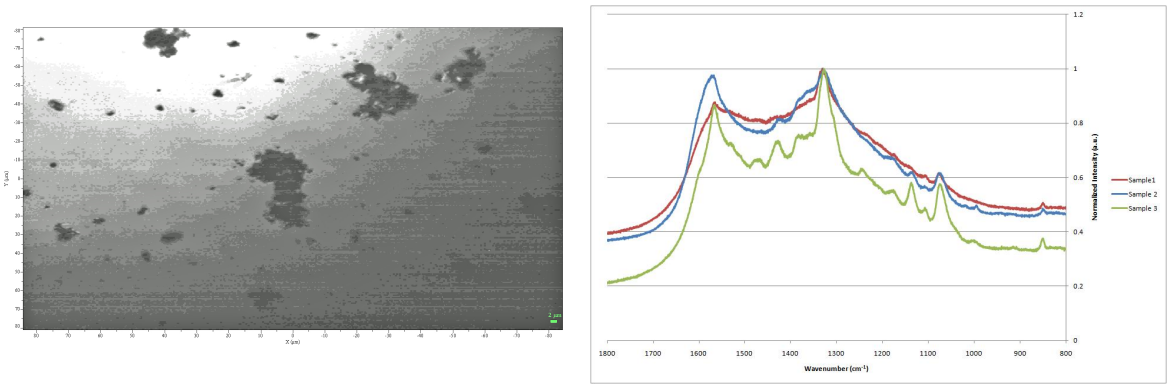

Figure 4.30: Multiplexing results from large plates with aggregated construction.

structure, where the geometry or alignment of the molecule attachment are effected.

The substrate consisting of small nanoplates aggregates is then examined and the results are shown in Figure 4.29. Since these two types of particles also have similar spectra from the substrate fabricated with the sandwiched structure, it is not a surprise that the spectra observed from the small nanoplates are showing similar attributes to ones observe from the large particles. However, due to the effect of aggregation, the substrate sometimes produces a spectra with intensity so strong that most of the peak details are covered up and hence making the overall spectra features less significant. Figure 4.30 is a microscopical view of the substrate fabricated with large plates aggregates and the substrate's respective multiplexed spectra. Unlike the result observed from the sandwiched structure, the spectra

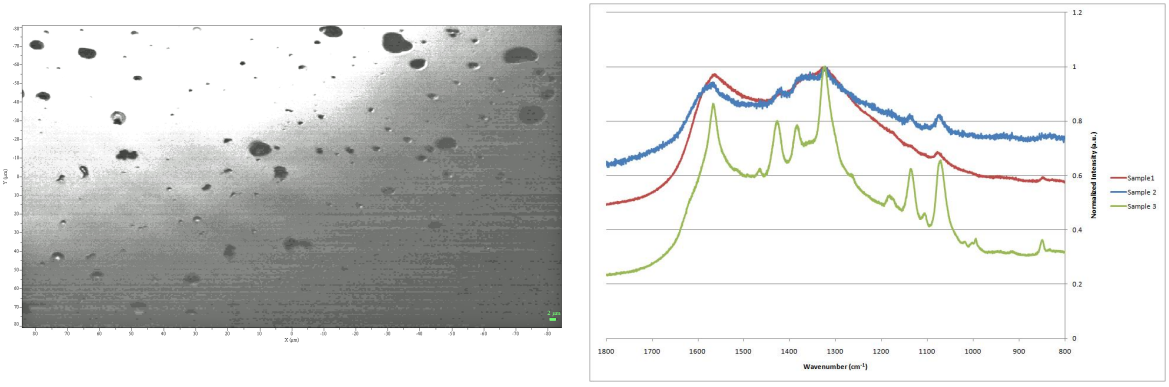

Figure 4.31: Multiplexing results from nanorods with aggregated construction.

does show the traits of the unique peaks of the labeling molecules and overall spectra features are similar to the ones obtained from the aggregated small plates. This is probably due to the fact that the aggregated structures have caused the packed into a random orientation; for instance, instead of laying flat to the gold substrates, the plates may be tilting sideways, standing straight up on the surface or experiencing deformation due to the random packing. Because of all these spacings in between particles and surface roughness that have been created from the plates's aggregated packing, better SERS characteristics can be generated.

The results obtained from the aggregated nanorods substrate are shown in Figure 4.31. The resulting spectra have shown that the attributes of peaks are comaprible with the large nanospheres, which is also the case in the sandwiched structure. Restating the fact that this could be due to the nanorods are synthesized in poor quality and may consists of high portion of large spheres and small plates and thus, resulting in the similar aggregated particle packings and similar spectra attributes. However, when compared directly to the rod substrate with sandwiched structure, the spectra are less detailed and consistent like other aggregated substrates and perhaps it is due to the disordered packing of the particles. As for the case of nanostars, where the resulting spectra are shown in Figure 4.32, the spectra result is similar to the sandwiched structure substrate. From this spectra, the QT peak is missing once again and this also agrees with the corresponding sandwiched sample that the nanostars in less viable in recognizing full multiplexed spectra features.

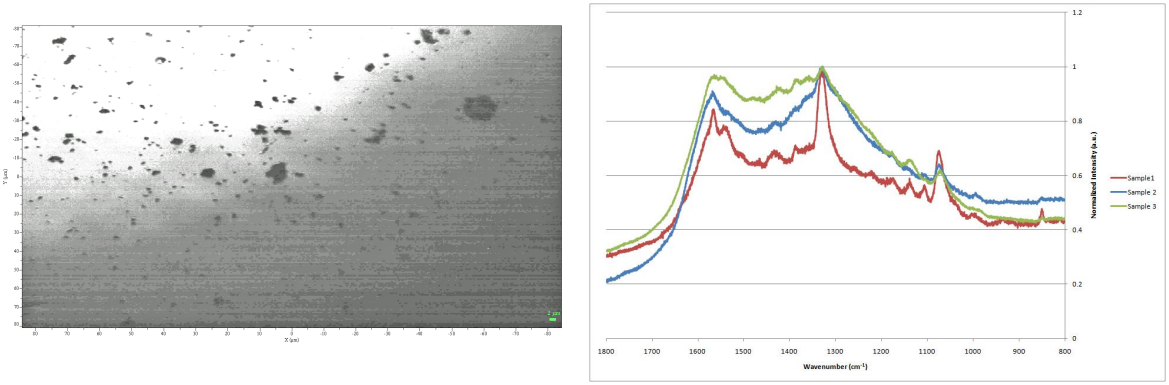

Figure 4.32: Multiplexing results from nanostars with aggregated construction.

4.5 Multiplexing Remarks

The SERS multiplexing effect has been observed from substrates fabricated with small nanospheres, large nanospheres, small nanoplates, large nanoplates, nanorods and nanostars using sandwiched and aggregated structures and it has been observed that the multiplexing effects can be effected by the sizes and the shapes of the nanoparticles. The best observation for the size effect can seen from the multiplexing spectra of the small and large nanoplates fabricated from the sandwiched structure. Although the small plates is capable of producing clearly showing all the attributes from the labeling molecule, the large plates have a poor ability to even generate a signal from the labeling molecules. Due to sizes of the plate particles and their orientation laying flat to the substrate surface, restricting the light in resonance with the particle's surface plasmon resonance oscillation and hence, inability to generate any SERS signals. The other example to observe the size effect on SERS measurement is the small and large nanoparticles fabricated from the aggregated structure. The large aggregated particles is capable of reproducing spectra that can distinguish the three labeling molecules but the smaller nanoparticle can only generate the spectra in a limited detail. The reasons for the lack of signals in this case might be opposing to effect observed from the large plates, where the wavelength of the light might be much greater than the sizes of the small nanoparticles so the interaction with the particles are merely insignificant. Another reason that may have caused a reduction in signal strength is the aggregated structure of the smaller nanoparticle since the amount of free spaces in between particles may be reduced, also affecting the surface's plasmon resonance ability.

The shape of the nanoparticles is also an important factor in determining the SERS multiplexing capabilities. For instance, regardless whether the substrate is fabricated with the sandwiched or aggregated methodology, the nanospheres can generally produce more consistent multiplexing spectra showing all labeling attributes than the anisotropic nanoparticles and this can be explained by the differences in surface geometry configuration such as sharper edges and pointy spikes, causing the surface's electric field density to shift and hence, resulting in less consistency. The nanostars have produced the least promising multiplexing results among all the particles since that the QT molecules cannot be identified from any of the multiplexing spectra from nanostars. This can be due to the their own special morphology features where the smaller molecules are more likely to be retained on the surface of the pointing branches and the larger molecule adhering on the particle's ground surface. Therefore, when the nanostar particles are piled together, the gaps in between the nanostars will be retained by the length of the branches, forming hot spots from their branch spaces and the labeling molecules trapped in the branch spaces have a high tendency to generate SERS effects.

In this report, sandwiched and aggregated structures have been employed to fabricate SERS substrates and the differences in structure have been another major factor for the quality of the outputs. It has been mentioned previously that one of the general concerns for the SERS measurement is that the reproducibility may vary from substrate to substrate. Even though the substrate fabricated with nanospheres in sandwiched configuration has the most highest reproducibility among all substrates, there are still times that signals cannot be obtained from another sample made from using the same fabrication process. The situation is even worse for substrates fabricated with the aggregated structure, where the SERS signals are saturated most of the time, making it extremely difficult to recognize the unique peaks from the labeling molecules. In addition to the smaller gap found in between aggregated particles, many factors may also have caused the inability for SERS measurements; for instance, the deformation of particle shapes during the aggregation structures, reorienting surface geometry configuration and causing the surface's electric field density to shift. Another finding that is specifically from the aggregated structures is that the change of molecular characteristics responded from the SERS spectra since the peak at 1426 cm^{-1} has become much strengthened for some substrates with aggregated structure. The transformation could be a result of adjusted molecule orientation evolved from randomly packed structures. Since it has been a major concern that the aggregated

substrates have been reproducing saturated SERS signals, attempts have been made to change the SERS reading parameters in oder to find the most desirable setting that improve the spectra outputs. For instance, shorter acquisition time, a higher magnification objective lens, laser filters and spectrum filters have been employed in the measurement and they do not deliver much improvements in the measurements. The multiplexing spectra with much higher resolution from the same aggregated structure substrates are then produced by employing a 785 nm laser excitation. The spectra excited with 785 nm laser from aggregated structure of small and large nanospheres and nanoplates are shown in Figure 4.33 and 4.34; the spectra for the nanorods and nanostars are shown in Figure 4.35. With higher wavelength excitation is used for the SERS measurements, the spectra from the smaller nanospheres still appears to be less detailed than the large nanospheres, but the spectra from the large nanospheres clearly has less damping from the background and has a much more detailed SERS signals. The reduction of damping is also observed similarly from the aggregated nanoplate, nanorod and nanostar substrates where the unique peaks of all three molecules can be easily seen. A report by Culha et al. has discussed that the excitation of the surface plasmon for aggregated nanoparticles are shifted into the longer wavelengths due to the deformation and dampening electron clouds around the nanoparticles. The group has further explained that a higher wavelength excitation is more appropriate for bulkier samples since it has a greater penetration depth that can excite more molecules such as the ones trapped underneath the surface nanoparticlesand.[40][41] in this report, it has been been verified by switching the excitation from the 633 nm to the 785 nm is capable of producing multiplexing spectra with much more details for the aggregated substrates but the reproducibility of the spectra still have room for improvement and a further investigation is required.

Measurements of multiplexing SERS labels have been obtained from the substrates consisting of nanospheres, nanoplates, nanorods, and nanostars using the sandwiched and aggregated fabrication methods. Among all the resulting spectra of each substrate, the spectra of the small spheres is by far the most consistent and has the greatest detail. The low reproducibility of the other substrates may have been caused by the mixing of particles with different morphologies, uneven distribution of particle spacings on the substrate surfaces, and formation of particle aggregates leading into random sizes and packing. Another factor which should also be exclusively evaluated is the efficiency of surfactant replacement with the labeling molecules since weaker surfactants can be replaced by more

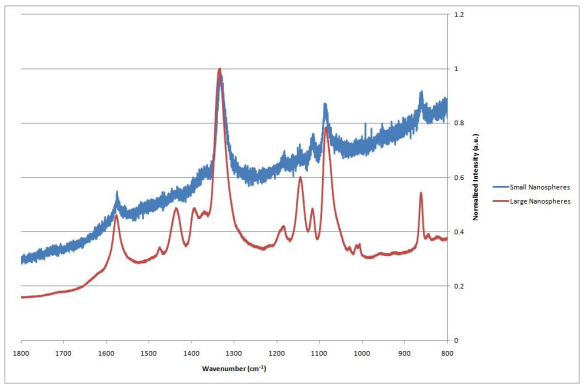

Figure 4.33: 785 nm excited multiplexing results of nanospheres with aggregated construction.

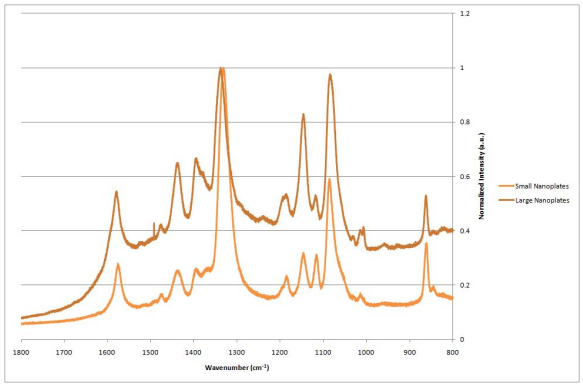

Figure 4.34: 785 nm excited multiplexing results from nanoplates with aggregated construction.

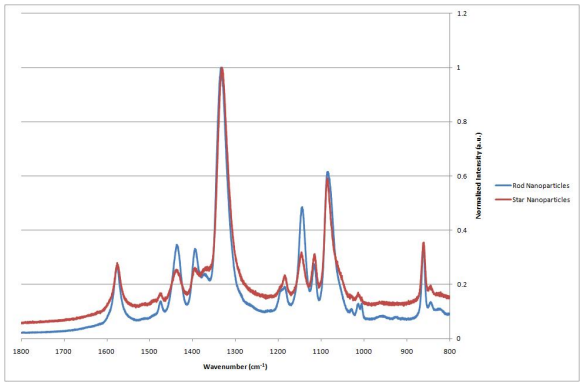

Figure 4.35: 785 nm excited multiplexing results from nanorods and nanostars with aggregated construction.

molecule labels on the particles surfaces and resulting in much higher intensity. Overall, the most consistent spectra has been obtained from the small spheres and this can be due to the narrow size distribution, uniformity in morphology and weak capping surfactants that allows a highly efficient replacement of reporter molecules. In addition, from the observation of the microscopic images of the substrate, they have shown a even spread on the gold substrates and have much smaller black spots indicating less aggregates are formed. Therefore, among all the particles with different morphologies, citrate synthesized small spheres are considered to be a best choice to be further employed into the particle-thiol-plate sandwiched structure.

4.6 Gold Particles-Thiol-Gold Plate Substrate

The particle-thiol-plate configuration is an attractive substrate structure to be constructed since it has a potential of being further developed into ultra portable SERS active substrates and substrates with such configuration can be generated from what is already being available, such as the small nanoparticles with citrate capping and the CTAB assisted microplates that have been utilized throughout this report. Nevertheless, instead of using benzenethiols, benzenedithiol molecules are utilized as the labeling molecules since the molecules have two sulfur ends that are capable of providing the functionality of holding the gold nanospheres and the plates together. Figure 4.36 shown is an SEM image of a freshly synthesized gold blank plate and from the image, it can be seen that the plate is well formed into a hexagon with flat surface and sharp edges that are in symmetry with each other. However, there is a spot on the plate surface that appears to be darker than the other area and presumably, it is the residue from the CTAB capping. Since excessive CTAB is required to assist the anisotropic growth and enhance the particle stability, the replacement of the CTAB on the surface of the plates with the benzenedithiol molecules has become relatively important for the SERS substrate fabrication. From the protocol of Han et al., the removal of CTAB has been by drying the large nanoplates on a silicon wafer and then is immersed into the Piranha solution. However, the substrate can become extremely difficult to handle since the Piranha is highly corrosive and may washed away or dissolve the gold pieces on the silicon. Therefore, the replacement of CTAB with the labeling molecule is only implemented by the direct replacement method where the 10mM of the labeling solution is added in equal volume with the plate solution and is stirred

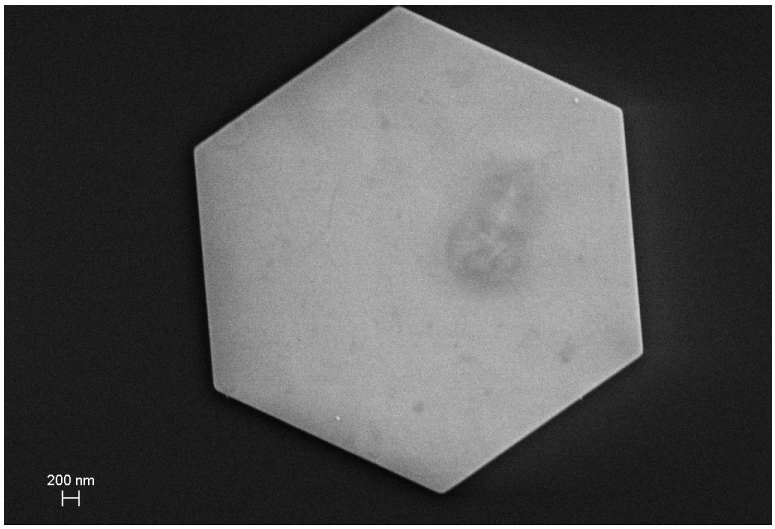

Figure 4.36: A SEM image of a blank gold microplate.

overnight. The plates solution are then centrifuged and with supernatant removed, the residue is added with 10 mL of the nanoparticle solution to allow the particles to adhere onto the plate and the solution is also left disturbed for overnight stirring. Then, the resulting particle-thiol-plate solution is dip dropped onto a silicon wafer and left dry in room condition for SERS and SEM analysis.

Figure 4.37 shown is an SEM image of the particle-thiol-plate substrate on a silicon wafer. From the image, it can be seen that the most of the gold microplate surface is covered with nanoparticles but unlike the results obtained from Han et al., they are packed in an aggregated structure. This is likely due to the characteristics of the non-polar solvent used that can cause particle aggregation as well as the the differences in the method of removing the CTAB, resulting in a less uniform replacement with the labeling molecule. It may also be likely due to the positioning geometry of the benzenedithiol molecules where they are laying flat against the plate surface so their free sulfur ends are unable to reach out to the particle surface; thus, lowering the probability of particle attachment.

The reference SERS measurements are taken on flat gold surfaces with large nanospheres to obtain the spectra of BT, BDT and the combination of the two molecules and their respective spectra are shown in Figure 4.38,4.39 and 4.40. The SERS obtained from BT and BDT are very similar to each other where the peaks have almost identical positions

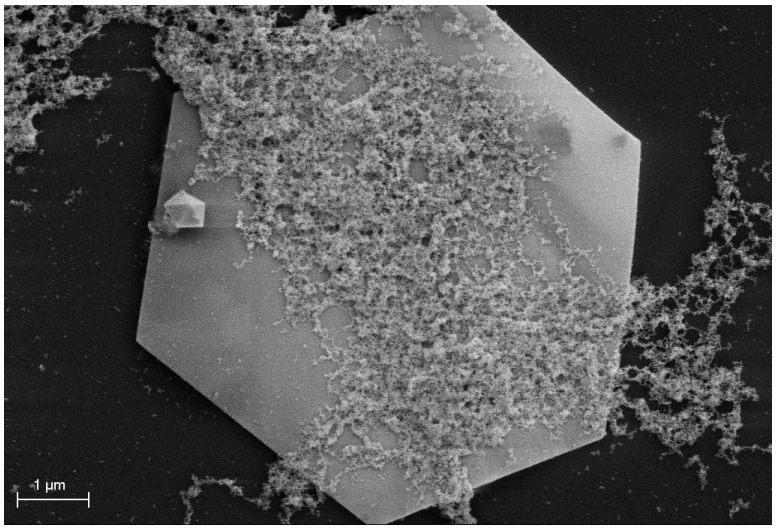

Figure 4.37: A SEM image revealing the construction of Au nanoparticle-thiol-Au microplate.

and the close proximity in the peak positions can be due to the similarity in the molecular structure. Therefore, it is no surprise that the spectra obtained from the multiplexed substrate also have similar appearance to the spectra obtained from each molecule. The spectra obtained from the particle-thiol-plate substrate on silicon wafer are similar to of those obtained from the gold substrate with large spheres. However, the reproducibility is relatively low and this could be due to the uneven distribution of the particle aggregates on the microplate surfaces. Nevertheless, a major issue that may also have lowered the reproducibility is because of the overpowering of the light source since the microplates often appear to be melted and evaporated once they have been exposed to the radiation from the SERS measurement. A lower passive light filters have been utilized in order to reduce the laser intensity exposure on the microplates; however, the measurement can only obtain noise like signals from the substrate. A further investigation is required to adjust the SERS instrument settings so that the particle-thiol-plate substrate can prove to be fully functional. In addition, the strategies of replacing the two ended thiol molecules on the plate surfaces still requires a lot of improvement so that the particles can be more evenly distributed on the plate surfaces and improve on the reproduciblity of the signals.

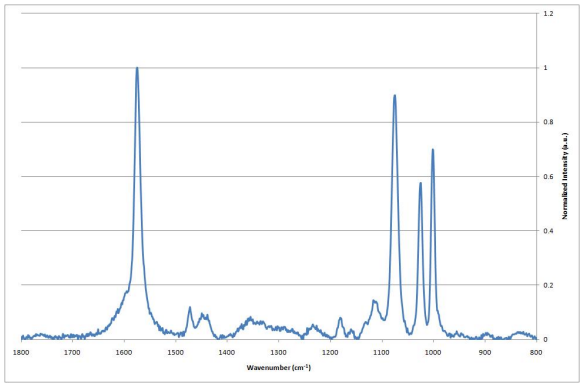

Figure 4.38: Benzenethiol spectra obtained from gold surface substrate.

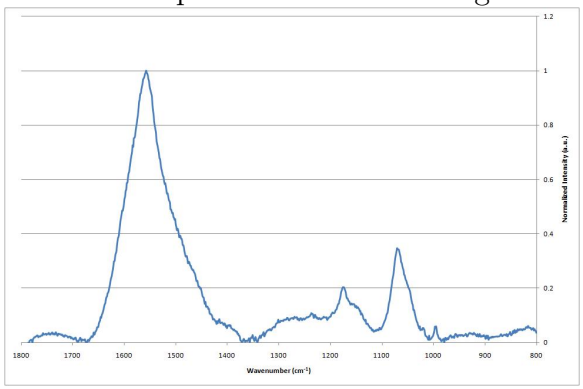

Figure 4.39: Benzenedithiol spectra obtained from gold surface substrate.

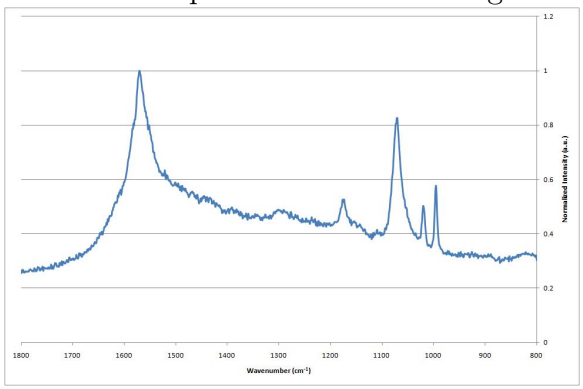

Figure 4.40: A mixed benzenethiol and benzenedithiol spectra obtained from gold surface substrate.

Chapter 5

Conclusion and Recommendation

5.1 Conclusions

In this study, several synthesis procedures have been adopted to synthesizing nanoparticles with various sizes and morphologies in order to observe the their surface plasmon properties. Particularly, large and small nanospheres, large and small nanoplates, nanorods and nanostars have been synthesized and characterized by the UV-vis spectroscopy and the electron microscopes. It has been observed that nanoparticles with more uniform shapes and size distribution exhibit narrower absorbance peaks and as the nanoparticle sizes are increased, the absorbance peaks are shifted towards the NIR region. The shift of these absorbance peaks may also be the cause for the change in colours for the nanoparticle solution. For the rod-like nanoparticles, they usually have two absorbance peaks representing the transverse and longitudinal resonance modes along the width and length of the rods respectively. However, the actual production of the nanoparticles are limited to low yield and the resulting absorance peaks have much weaker longitudinal features compared to the results found else where. The absorbance peaks of the large plates generally appear to be random and cannot be identified and this may be due to their sizes and particle orientation in the solution. The optical properties of the nanostars are reported to be corresponding not only to their bulk body sizes but also their tip lengths; the boardened absorbance peaks may have been caused by the special morphology due to the spikes and also the aggregated packing that may have been induced by the PVP surfactants and the solvent used.

Multiplexed SERS measurements using 633 nm excitation have been conducted on substrates fabricated with large and small nanospheres, large and small nanoplates, nanorods and nanostarsthe with aggregated and sandwiched structures. Individual SERS spectra of each labeling molecules, benzenethiol, 4-nitrobenzenethiol and 4-quinolinethiol, have been successfully obtained and the combination of these three molecules have the least amount of overlapping and can all be identified from the reference multiplexed spectra. Among all the substrates that have analyzed, the substrate made from nanospheres with sandwiched structure is able to produce multiplexed SERS spectra with more details and higher reproducibility. Although multiplexed SERS spectra can also be observed from substrates made from small nanoplates, nanostars and nanorods substrates with sandwiched structures, the unique peaks representing the labeling molecules are less consistent in their intensity. In addition, substrates with micro sized plates in sandwiched configuration are found to exhibit much lower SERS activities and this can be due to the size of the plate being much greater than the light source, restraining the surface plasmon resonance effect. Most of the substrates fabricated with aggregated nanoparticles have very low reproducibilities and saturated signals with 633 nm excitation. The spectra peaks are much easier to identify and are much more reproducible when 785 nm excitation have been adopted. This can be due to the size of the aggregated nanoparticles are much bulkier which a deeper penetrating light source is required to induce more molecules labels to exhibit SERS activities. A novel SERS substrate has been fabricated with nanoparticle-thiol-microplate sandwiched configuration by using a double ended thiol molecules, benzenedithiol, to strongly connect nanospheres and the plates together. However, the measurement of the SERS activity is limited by the overpowering of the light source, which has frequently melted and evaporated the plate samples once they have been exposed to the excitation radiation. In addition, instead of spreading evenly on the microplate surfaces, the nanoparticles have appeared to be aggregated which may have further increased the difficulty in obtaining SERS activity by using a even more powerful light source.

Even though the quality of the SERS substrate produced in this report did not meet our expectation, the fundamentals of the gold nanoparticle synthesis and SERS phenomenon have been studied. The sandwiched particle-thiol-plate SERS substrates is believed to have a tremendous application potential in the field of pharmaceuticals; nevertheless, the data in this report have suggested that a lot of improvements is still need to be made in order for the reproducibility of the substrate to increase.

5.2 Recommendations

Many synthesis routes have been explored in this study to fabricate nanoparticles with different sizes and morphologies and these particles have been used in the preliminary design of SERS substrate. However, the signals measured from the SERS substrates have a low reproducibility and there are a few improvements can be made for future studies.

- In order to produce a higher yield nanorods, the right ratio of the surfactants and the gold ions in the growth solution may benefit the capping and directing the nanorod growth and a reduced temperature is necessary to stabilized the growth. In addition, prior adding the freshly made CTAB capped seeds to the rod growing solution, it is important to ensured that the seeds are in a stable condition by making the excess $NaBH_4$ completely decomposed. Once the rods are synthesized, the resulting growth solution should be added with excess amount of deionized and inserted into warm water to dissolve the excess CTAB and then separated by the centrifugal method.

- The composition of the plate solution is a mixture anisotropic particles mainly consisting of hexagons, triangles and truncated triangular particles and the size and composition of the plates are varied from batch to batch which can be caused by the uneven heating distribution and difficulty in controlling the temperature from using the heating plate. Implementing an oil bath or an oven with digital timing and temperature ramping control may give a more precise heating profile for each batch of growing solution, reducing the amount of radicals such as variation of room temperatures, leftover heat from the last sample, uneven contact surface area from the glassware to the heating plate and inconsistent temperature profile control over time.

- One of the major issues that have made the SERS substrate to exhibit low reproducibility is the uneven distribution of nanoparticles on the gold substrates. The measurement may become more reporducibile from substrates made with controlled assembly, such as lithographical method so substrates can have evenly distribute nanoparticles on the surfaces or a group nanoparticles forming aggregates in a defined area. In addition, lithography assembly is also capable of controlling the orientations of the nanoparticles and therefore, the substrate's roughness features can be more precisely controlled in order to reproduce the signals at higher intensity.

- The reproducibility of the SERS measurements can also be caused by the limitation of the instrumentation since using an optical microscope along is not able to observe the structure of the nanoparticles within the SERS measurement spot. Due to the size of substrate samples, by applying physical markers on the substrates and analyzed them with higher resolution microscope can highly increase the risk of damaging the substrate. The risk can be avoided by using a commercially available system that is integrated with both SERS and AFM so that the physical structure and the SERS can be observed from the identical spot. Employing the instrument is strongly recommended since it allows the user to have a better understanding of the particle structure on the substrate surface and the areas with similar structures can be selected to be analyzed with SERS.

Bibliography

[1] M. Grant Albrecht and J. Alan Creighton. Anomalously intense raman spectra of pyridine at a silver electrode. *Journal of the American Chemical Society*, 99:5215–5219, 1977. 18

[2] Monica Baia, Traian Iliescu, and Simion Astilean. *Raman and SERS Investigations of Pharmaceuticals*. Springer-Verlag, Berlin, Germany, 2008. 19, 25, 36

[3] Gary A. Baker and David S. Moore. Progress in plasmonic engineering of surface-enhanced raman-scattering substrates toward ultra-trace analysis. *Anal. Bioanal. Chem.*, 382:1751–1770, 2005. 25, 26, 32, 36

[4] Roderich Bott, Thomas Wolff, and Karl Zierold. Temperature-induced transitions from rodlike to globular micellar aggregates in aqueous cetyltrimethylammonium bromide in the presence of 9-anthrylalkanols. *Langmuir*, 18:2004–2014, 2002. 65

[5] Brantley D. Busbee, Sherine O. Obare, and Catherine J. Murphy. An improved synthesis of high-aspect-ratio gold nanorods. *Adv. Mater.*, 15(5):414–416, 2003. 60

[6] Alan Campion and Patanjali Kambhampati. Surface-enhanced raman scttering. *Chemical Society Reviews*, 27:241–250, 1998. x, 19, 21, 22, 23, 24

[7] D. Chakravorty and A.K. Giri. *Chemstry of Advanced Materials*. Blackwell Scientific Publications, Oxford, UK, 1993. 5

[8] Hao Ming Chen, Ru Shi Liu, and Din Ping Tsai. A versatile route to the controlled syntheis of gold nanostructures. *Crystal Growth & Design*, 9(5):2079–2087, 2009. 65

[9] Chuanwei Cheng, Bin Yan, She Mein Wong, Xianglin Li, Weiwei Zhou, Ting Yu, Zexiang Shen, Hongyu Yu, and Hong Jin Fan. Fabrication and sers performance of silver-nanoparticle-decorated si/zno nanotrees in ordered arrays. *ACS Applied Materials and Interfaces*, pages A–E, 2010. xi, 34, 35

[10] Hsin-Cheng Chu, Chun-Hong Kuo, and Michael H. Huang. Thermal aqueous solution approach for the synthesis of triangular and hexagonal gold nanoplates with three different size ranges. *Inorg. Chem.*, 45:808–813, 2006. 50

[11] P. Davide Cozzoli and Liberato Manna. Synthetic strategies to size and shape controlled nanocrystals and nanocrystal heterostructures. In Warren C.W. Chan, editor, *Bio-Applications of Nanoparticles*, chapter 1, pages 1–17. Landes Bioscience and Springer Science+Business Media,LLC, Austin, Texas, 2007. xii, 41, 42, 44

[12] Pantaleo Davide Cozzoli, Teresa Pellegrino, and Liberato Manna. Synthesis, properties and perspectives of hybrid nanocrystal structures. *Chem. Soc. Rev.*, 35:1195–1208, 2006. xii, 41, 42, 44

[13] Nathan R. Miller Danielle K. Smith and Brian A. Korgel. Iodide in ctab prevents gold nanorod formation. *Langmuir*, 25(16):9518–9524, 2009. 62

[14] Steven R. Emory, William E. Haskins, and Shuming Nie. Direct observation of size-dependent optical enhancement in single metal nanoparticles. *J. Am. Phys. Chem. Soc.*, 120:8009–8010, 1998. 26

[15] Isak Engquist. Self-assembed monolayers. `http://www.ifm.liu.se/applphys/ftir/sams.html`, October 1996. xii, 44, 45

[16] E. Nalbant Esenturk and A.R. Hight Walker. Surface-enhanced raman-scattering spectroscopy via gold nanostars. *J. Raman Spectrosc.*, 40:86–91, 2009. 18

[17] Meikun Fan and Alexandre G. Brolo. Silver nanoparticle self assembly as sers substrates with near single moleucle detection limit. *Phys. Chem. Chem. Phys.*, 11:7381–7389, 2009. 34

[18] G. Frens. Controlled nucleation for the regulation of the particle size in monodisperse gold suspensions. *Nature*, 241:20–22, 1973. 49

[19] Jinxin Gao, Christopher M. Bender, and Catherine J. Murphy. Dependence of the gold nanorod aspect ratio on the nature of the directing surfactant in aqueous solution. *Langmuir*, 19:9065–9070, 2003. 51, 62

[20] Magdalena Gellner, Karsten Kompe, and Sebastian Schlucker. Multiplexing with sers labels using mixed sams of raman reporter molecules. *Anal. Bioanal. Chem.*, 2009. xi, 36, 37, 44

[21] Denis Gentili, Guido Ori, and Mauro Comes Franchini. Double phase transfer of gold nanorods for surface functionalization and entrapment into peg-based nanocarriers. *Chem. Commun.*, pages 5874–5876, 2009. xii, 46, 47

[22] Matthew A. Young George C. Schatz and Richard P. Van Duyne. Electromagnetic mechanism of sers. 24

[23] Anand Gole and Catherine J. Murphy. Seed-mediated synthesis of gold nanorods: role of the size and nature of the seed. *Chem. Mater.*, 6:3633–3640, 2004. 72

[24] Christina Graf, Dirk L.J. Vossen, Arnout Imhof, and Alfons van Blaaderen. A general method to coat colloidal particles with silica. *Langmuir*, 19(17):6693–6700, 2003. 50

[25] Geun Hoi Gu, Jurae Kim, Lily Kim, and Jung Sang Suh. Optimum length of silver nanorods for fabrication of hot spots. *J. Phys. Chem. C*, 111:7906–7909, 2007. 27

[26] David W. Hahn. Raman scattering theory. Tutorial Notes from Florida University Website, Feb 2007. 15

[27] Matthias Hanauer, Sebastien Pierrat, Inga Zins, Alexander Lotz, and Carsten Sonnichsen. Separation of nanoparticles by gel electrophoresis according to size and shape. *Nano Letters*, 7(9):2881–2885, 2007. 64

[28] Feng Hao, Colleen L. Nehl, Jason H. Hafner, and Peter Nordlander. Plasmon resonances of a gold nanostar. *Nano Letters*, 7(3):729–732, 2004.

[29] Jinhwa Heo, Young Wook Lee, Miniung Kim, Wan Soo Yun, and Sang Woo Han. Nanoparticle assembly on nanoplates. *Chem. Commun.*, pages 1981–1983, 2009. xii, 48, 54

[30] Gabor L. Hornyak, Harry F. Tibbals, Joydeep Dutta, and John J. Moore. *Introduction to Nanoscience and Nanotechnology*. CRC Press Taylor and Francis Group, New York, NY, 2009. ix, 2, 3, 4, 6, 10, 16

[31] Masuo Hosokawa, Kiyoshi Nogi, Makio Naito, and Toyokazu Yokoyama. *Nanoparticle Technology Handbook*. Elsevier, Oxford, UK, 2007. 4

[32] Hsin-Cheng Chu Hsiang-Yang Wu, Tz-Jun Kuo, Chi-Liang Kuo, and Michael H. Huang. Seed-mediated synthesis of high aspect ratio gold nanorods with nitric acid. *Chem. Mater.*, 17:6447–6451, 2005. 58

[33] Wan-Ling Huang Hsiang-Yang Wu and Michael H. Huang. Directed high-yield synthesis of high aspect ratio gold nanorods. *Crystal Growth & Design*, 7(4):831–835, 2007. 58

[34] Wan-Ling Huang, Chiu-Hua Chen, and Michael H. Huang. Investigation of the growth process of gold nanoplates formed by thermal aqueous solution approach and the synthesis of ultra-small gold nanoplates. *J. Phys. Chem. C*, 111(6):2533–2538, 2007. 50

[35] Nikhil R. Jana. Nanorod shape separation using surfactant assisted self-assembly. *Chem. Commun.*, pages 1950–1951, 2003. 66

[36] Nikhil R. Jana, Latha Gearheart, and Catherine J. Murphy. Wet chemical synthesis of high aspect ratio cylindrical gold nanorods. *J. Phys. Chem. B*, 105:4065–4067, 2001. xi, 28, 30, 51, 57

[37] David L. Jeanmaire and Richard P. Van Duyne. Surface raman electrochemistry part i. heterocyclic, aromatic and aliphatic amines adsorbed on the anodized silver electrode. *Journal of Electroanalytical Chemistry*, 84:1–20, 1977. 18

[38] C. Jehn, B. Kustner, P. Adam, A. Marx, P. Strobel, C. Schmuck, and S. Schlucker. Water soluble sers labels comprising a sam with dual spacers for controlled bioconjugation. *Phys. Chem. Chem. Phys.*, 11:7499–7504, 2009.

[39] Hye Young Jung, Yong-Kyun Park, Sungho Park, and Seong Kyu Kim. Surface enhanced raman scattering from layered assemblies of closed-packed gold nanoparticles. *Analytica Chimica Acta*, 602:236–243, 2007. 28, 47

[40] Mehmet Kahraman, Omer Aydin, and Mustafa Culha. Size effect of 3d aggregates assembed from silver nanoparticles on surface-enhanced raman scattering. *Chem. Phys. Chem.*, 10:537–542, 2009. 85

[41] Mehmet Kahraman, M. Muge Yazici, Fikrettin Sahin, Omer F. Bayrak, Emine Topcu, and Mustafa Culha. Towards single-microorganism detection using surface-enhanced raman spectroscopy. *Intern. J. Environ. Anal. Chem.*, 87(10–11):763–770, 2007. 85

[42] Bishnu P. Khanal and Eugene R. Zubarev. Rings of nanorods. *Angew. Chem. Int. Ed.*, 46:2195–2198, 2007. xii, 45, 46, 64

[43] Christopher G. Khoury and Tuan Vo-Dinh. Gold nanostars for surface-enhanced raman scattering: synthesis, characterization and optimization. *J. Phys. Chem. C*, 112:18849–18859, 2008. 79

[44] Franklin Kim, Kwonnam Sohn, Jinsong Wu, and Jiaxing Huang. Chemical synthesis of gold nanowires in acidic solutions. *J. Am. Chem. Soc.*, 130:14442–14443, 2008. 60

[45] Ji Eun Kim, Hyung Jun Kim, and Sangwoon Yoon. Influence of surface functionalities of self-assembeld monolayers on the adsorption of gold nanoparticles. *Bull. Korean Chem. Soc.*, 30(5):999–1000, 2009. 45

[46] Kwan Kim and Jae Keun Yun. Raman scattering of 4-aminobenzenethiol sandwiched between ag/au nanoparticle and macroscopically smooth au substrate. *J. Phys. Chem.*, 109:20731–20736, 2005. 52

[47] Katrin Kneipp, Harald Kneipp, Irving Itzkan, Ramachandra R. Dasari, and Michael S. Feld. Surface-enhanced raman scattering and biophysics. *J. Phys.: Condens. Matter*, 14:R597–R624, 2002. x, 19, 20, 21, 23

[48] Katrin Kneipp, Yang Wang, Harald Kneipp, Irving Itzkan, Ramachandra R. Dasari, and Michael S. Feld. Population pumping of excited vibrational states by spontaneous surface-enhanced raman scattering. *Physical Review Letters*, 76(14):2444–2447, 1996. 17, 25

[49] Katrin Kneipp, Yang Wang, Harald Kneipp, Lev T. Perelman, Irving Itzkan, R. R. Dasari, and M. S. Feld. Single molecule detection using surface-enhanced raman scattering(sers). *Physical Review Letters*, 78(9):1667–1670, 1997. 25

[50] Hyunhyub Ko, Srikanth Singamaneni, and Vladimir V. Tsukruk. Nanostructured surfaces and assemblies as sers media. *Small*, 4(10):1576–1599, 2008. 26

[51] Pandian Senthil Kumar, Isabel Pastoriza-Santos, Benito Rodriguez-Gonzalez, F Javier de Abajo, and Luis M Liz-Marzan. High-yield synthesis and optical response of gold nanostars. *Nanotechnology*, 19(1):015606, 2008. 50

[52] Seung Joon Lee, Zhiqiang Guan, Hongxing Xu, and Martin Moskovits. Surface-enhanced raman spectroscopy and nanogeometry: The plasmonic origin of sers. *J. Phys. Chem. C*, 111(49):17985–17988, 2007. 31

[53] Stephan Link and Mostafa A. El-Sayed. Size and temperature dependence of the plasmon absorption of colloidal gold nanoparticles. *J. Phys. Chem. B*, 103:4212–4217, 1999. 57

[54] Adam D. McFarland, Matthew A. Young, Jon A. Dieringer, and Richard P. Van Duyne. Wavelength-scanned surface-enhanced raman excitation spectroscopy. *J. Phys. Chem. B*, 109:11279–11285, 2005. 28

[55] Joseph M. McLellan, Andrew Siekkinen, Jingyi Chen, and Younan Xia. Comparison of the surface-enhanced raman scattering on sharp and truncated silver nanocubes. *Chemical Physics Letters*, 427:122–126, 2006. 27

[56] James E. Morris. Nanoparticle properties. In James E. Morris, editor, *Nanopackaging: Nanotechnologies and Electronics Packaging*, chapter 5, pages 93–107. Springer Science+Business Media, LLC, New York, NY, 2008. 4

[57] M. Moskovits and J. S. Suh. Surface selection rules for surface-enhanced raman spectroscopy: Calculations and application to the surface-enhanced raman spectrum of phthalzine on silver. *J. Phys. Chem.*, 88:5526–5530, 1982. 23

[58] Martin Moskovits. Surface-enhanced spectroscopy. *Review of Modern Physics*, 57(3):783–826, 1982.

[59] Inc. Nanosphere. Nanoparticles. `http://www.nanosphere.us/Nanoparticles_4516.aspx`, 2010. x, 7

[60] Caterina Netti, John Lincoln, and Gregory Flinn. Reliable substrate technology for surface enhanced raman spectroscopy. *Raman Technology for Today's Spectroscopists*, pages 3–8, 2005. 24

[61] Caterina Netti and Helen Stanford. Applications of reproducible sers substrates for trace level detection. *Spectroscopy*, 2006. 36

[62] Shuming Nie and Steven R. Emory. Probing single molecules and single nanoparticles by surface-enhanced raman scattering. *Science*, 275:1102–1106, 1997. x, xi, 24, 25, 31

[63] Takuro Niidome, Masato Yamagata, Yuri Okamoto, Yasuyuki Akiyama, Hironobu Takahashi, Takahito Kawano, Yoshiki Katayama, and Yasuro Niidome. Peg-modified gold nanorods with a stealth character for in vivo applications. *Journal of Controlled Release*, pages 343–347, 2006. 47

[64] Alain Nouailhat. *An Introduction to Nanoscience and Nanotechnology.* John Wiley and Sons, Inc., Hoboken, NJ, 2008. 1

[65] Christopher J. Orendorff, Anand Gole, Tapan K. Sau, and Catherine J. Murphy. Surface-enhanced raman spectroscopy of self-assembled monolayers: sandwich architecture and nanoparticle shape dependence. *Anal. Chem.*, 77:3261–3266, 2005. 52

[66] A. Otto, I. Mrozek, H. Grabhorn, and W. Akemann. Surface-enhanced raman-scattering. *J. Phys.: Condens. Matter*, 4:1143–1212, 1992. 20

[67] Yoshiharu Ozaki, Seiichiro Kashu, and Noboru Ichinose. *Superfine Particle Technology.* Springer-Verlag, New York, NY, 1988. 4

[68] Hyung Ju Park, Chil Seong Ah, Wan-Joong Kim, Insung S. Choi, Kwang-Pil Lee, and Wan Soo Yun. Temperature-induced control of aspect ratio of gold nanorods. *J. Vac. Sci. Technol. A*, 24(4):1323–1326, 2006. 65

[69] Jorge Perez-Juste, Luis M. Marzan, Steven Carnie, Derek Y. C. Chan, and Paul Mulvaney. Electric-field-directed growth of gold nanorods in aqueous surfactant solutions. *Adv. Funct. Mater.*, 14(6):571–579, 2004. 61

[70] Lidong Qin, Shengli Zou, Can Xue, Ariel Atkison, George C. Schatz, and Chad A. Mirkin. Designing, fabricating and imaging raman hot spots. *PNAS*, 103(36):13300–13303, 2006. xi, 33, 34

[71] E. C. Le Ru, C. Galloway, and P. G. Etchegoin. On the connection between optical absorption/extinction and sers enhancements. *Phys. Chem. Chem. Phys.*, 8:3083–3087, 2006. 27

[72] Tapan K. Sau and Catherine J. Murphy. Seeded high yield synthesis of short au nanorods in aqueous solution. *Langmuir*, 20(15):6414–6420, 2004. 64

[73] Vivek Sharma, Kyoungweon Park, and Mohan Srinivasarao. Shape separation of gold nanorods using centrifugation. *PNAS*, 106(13):4981–4985, 2009. 64

[74] Jian-Jun Sheng, Jian-Feng Li, Bing-Shen Yin, Bin Ren, and Zhong-Qun Tian. A preliminary study on surface-enhanced raman scattering from au and au@pd nanocubes for electrochemical applications. *Canadian Journal of Analytical Sciences and Spectroscopy*, 52(3):178–185, 2007. 27

[75] Patrick N. Sisco and Catherine J. Murphy. Surface-coverage dependence of surface-enhanced raman scattering from gold nanocubes on self-assembly monolayers of analyte. *J. Phys. Chem. A*, 113:3973–3978, 2009.

[76] Danielle K. Smith and Brian A. Korgel. The importance of the ctab surfactant on the colloidal seed-mediated synthesis of gold nanorods. *Langmuir*, 24:644–649, 2007. 61

[77] Ewen Smith and Geoffrey Dent. *Modern Raman Spectroscopy.* John Wiley and Sons, Inc., Hoboken, NJ, 2005. 17, 23

[78] W. Ewen Smith. Raman scattering. In *Kirk-Othmer Encyclopedia of Chemical Technology.* John Wiley and Sons, Inc., 2006. x, 10, 17

[79] Ujjal Kumar Sur. Surface-enhanced raman spectroscopy: Recent advancement of raman spectroscopy. *Resonance*, 15(2):154–164, 2010. 24

[80] Ratna Tantra, Richard J. C. Brown, and Martin J. T. Milton. Strategy to improve the reproducibility of colloidal sers. *Journal of Raman Spectroscopy*, 38:1476–1479, 2007. 32

[81] Z. Q. Tian. Surface-enhanced raman spectroscopy: It's present status. `http://www.ijvs.com/volume4/edition2/index.html`, 2000. x, 22, 24

[82] Geoffrey von Maltzahn, Andrea Centrone, Ji-Ho Park, Renuka Ramanathan, Michael J. Sailor, T. Alan Hatton, and Sangeeta N. Bhatia. Sers-coded gold nanorods as multifunctional platform for densely multiplexed near-infared imaging and photothermal heating. *Adv. Mater.*, 21:3175–3180, 2009. xii, 36, 38, 40

[83] Hui Wang, Carly S. Levin, and Naomi J. Halas. Nanosphere arrays with controlled sub-10-nm gaps as surface-enhanced raman spectroscopy substrates. *J. Am. Chem. Soc.*, 127:14992–14993, 2005. 31

[84] Guor-Tzo Wei, Fu-Ken Liu, and C.R. Chris Wang. Shape separation of nanometer gold particles by size-exclusion chromatography. *Anal. Chem.*, 71(11):2085–2091, 1999. 64

[85] D.A. Weitz, M. Moskovits, and J.A. Creighton. Surface-enhanced raman spectroscopy with emphasis on liquid-solid interface. In R.B. Hall and A.B. Ellis, editors, *Chemistry and Structral Interfaces, New Laser and Optical Techniques*, pages 197–243. VCH, New York, NY, 1986. 20

[86] UCDavis Chem Wiki. Harmonic oscillator. `http://chemwiki.ucdavis.edu/Physical_Chemistry/Quantum_Mechanics/Quantum_Theory/Trapped_Particles/Harmonic_Oscillator`, August 2010. x, 12

[87] Katherine A. Willets and Richard P. Van Duyne. Localized surface plasmon resonance spectroscopy and sensing. *Annu. Rev. Phys. Chem.*, 58:267–297, 2007. x, 6

[88] Curtis Woodford, Eric Jervis, Dale Hennenke, and Tim Chen. Multiplexing capacity of sers substrates depends on architecturally organized reporter molecules. Undergraduate research report, Sept 2009. 8

[89] D.Y. Wu, B. Ren, and Z.Q. Tian. Progress in the theory of surface enhanced raman scattering. `http://www.ijvs.com/volume4/edition2/index.html`, 2000. 21, 23

[90] Bo Yan, Anupama Thubagere, W. Ranjith Premasiri, Lawrence D. Ziegler, Luca Dal Negro, and Bjorn M. Reinhard. Engineered sers substrates with multiscale signal enhancement: Nanoparticle cluster arrays. *ACS Nano*, 3(5):1190–1202, 2009. xi, 24, 32, 33

[91] Yong Yang, Jianlin Shi, Taiki Tanaka, and Masayuki Nogami. Self-assembled silver nanochains for surface-enhanced raman scattering. *Langmuir*, 2007. x, xi, 28, 29

[92] Cristina L. Zavaleta, Bryan R. Smith, Ian Walton, William Doering, Glenn Davis, Borzoyeh Shojaei, Michael J. Natan, and Sanjiv S. Gambhir. Multiplexed imaging of surface enhanced raman scattering nanotags in living mice using noninvasive raman spectroscopy. *PNAS*, 106(32):13511–13516, 2009. xi, 36, 38, 39